NOAA Technical Memorandum OAR ARL-235

THE OVER-LAND ALONG-WIND DISPERSION (OLAD) FIELD EXPERIMENT

T.B. Watson
G.H. Crescenti
R.C. Johnson
B.R. Reese
R.G. Carter

Field Research Division
Idaho Falls, Idaho

S.D. Turley
B. Grim
C.A. Biltoft

Meteorology and Obscurants Division
West Desert Test Center
U.S. Army Dugway Proving Ground
Dugway, Utah

Air Resources Laboratory
Silver Spring, Maryland
June 2000

noaa NATIONAL OCEANIC AND ATMOSPHERIC ADMINISTRATION / Oceanic and Atmospheric Research Laboratories

NOAA Technical Memorandum OAR ARL-235

THE OVER-LAND ALONG-WIND DISPERSION (OLAD) FIELD EXPERIMENT

Thomas B. Watson
Gennaro H. Crescenti
Randall C. Johnson
Bradley R. Reese
Roger G. Carter

Field Research Division
Idaho Falls, Idaho

Shayes D. Turley
Bruce Grim
Christopher A. Biltoft

Meteorology and Obscurants Division
West Desert Test Center
U.S. Army Dugway Proving Ground
Dugway, Utah

Air Resources Laboratory
Silver Spring, Maryland
June 2000

UNITED STATES DEPARTMENT OF COMMERCE

William M. Daley
Secretary

NATIONAL OCEANIC AND ATMOSPHERIC ADMINISTRATION

D. JAMES BAKER
Under Secretary for Oceans and Atmosphere/Administrator

Oceanic and Atmospheric Research Laboratories

David L. Evans
Director

Notice

This document was prepared as an account of work sponsored by an agency of the United States Government. The views and opinions of the authors expressed herein do not necessarily state or reflect those of the United States Government. Neither the United States Government, nor any of their employees, makes any warranty, express or implied, or assumes any legal liability or responsibility for the accuracy, completeness, or usefulness of any information, product, or process disclosed, or represents that its use would not infringe privately owned rights. Mention of a commercial company or product does not constitute an endorsement by NOAA/OAR. Use of information from this publication concerning proprietary products or the tests of such products for publicity or advertising is not authorized.

Table of Contents

		Page
	Notice	ii
	List of Figures	vi
	List of Tables	xi
	Abstract	xv
1	Introduction	1
2	Theoretical and Empirical Treatments of Along-Wind Dispersion	3
3	Data	10
	3.1 Site Description	10
	3.2 Climatology	11
	3.3 Experimental Summary	11
	3.4 Dissemination Methods	13
	3.4.1 Aircraft Release	14
	3.4.2 Ground Release	16
	3.4.3 Quality Assurance	18
	3.5 SF_6 Sampling Methods	18
	3.5.1 Continuous Analyzers	18
	3.5.2 Whole Air Samplers	20
4	Methodology	27
	4.1 Meteorological Data	27
	4.2 Whole Air Sampler Data	27
	4.3 Continuous Analyzer Data	28
	4.3.1 Method 1: Center of Mass	29
	4.3.2 Method 2: Peak / Area Match	29
	4.3.3 Method 3: Width at 10%	29
	4.3.4 Method 4: Width at 2/3 Area	30
	4.4 Coordinate Transformation	30
	4.5 Transport Properties	31
5	Results and Discussion	33
	5.1 Individual Test Results	33
	5.1.1 Test 1	33
	5.1.2 Test 2	34

5.1.3 Test 3 35
5.1.4 Test 4 35
5.1.5 Test 5 36
5.1.6 Test 6 37
5.1.7 Test 9 38
5.1.8 Test 10 39
5.1.9 Test 11 40
5.1.10 Test 12 41
5.2 Summary Results: Whole Air Samplers 41
5.2.1 Ground Releases 42
5.2.2 Aircraft Releases 43
5.3 Summary Results: Continuous Analyzers 43
5.3.1 σ_x Versus x 44
5.3.2 Whole Air Samplers Versus Continuous Analyzers 47

6 Conclusions and Recommendations 50

Acknowledgments 51

References 52

Appendix A: Sampling Locations and Coordinates 55

Appendix B: Analysis of SF_6 Concentration Data for Test 1 58

Appendix C: Analysis of SF_6 Concentration Data for Test 2 65

Appendix D: Analysis of SF_6 Concentration Data for Test 4 74

Appendix E: Analysis of SF_6 Concentration Data for Test 5 83

Appendix F: Analysis of SF_6 Concentration Data for Test 6 93

Appendix G: Analysis of SF_6 Concentration Data for Test 9 106

Appendix H: Analysis of SF_6 Concentration Data for Test 10 116

Appendix I: Analysis of SF_6 Concentration Data for Test 11 126

Appendix J: Analysis of SF_6 Concentration Data for Test 12 132

Appendix K: Whole Air Sampling System 137
K.1 Operational Description 137

K.2 Component Descriptions 138
K.2.1 Sampler and Cartridges 138
K.2.2 TimeWand II 138
K.2.3 Gas Chromatographs 139
K.2.4 Relational Database 140

List of Figures

Page

Figure 1. Dugway Proving Ground and surrounding area (Shearer, 1956) 10

Figure 2. Dugway Proving Ground test area 11

Figure 3. Topography of test site with locations of release (red) and sampling (white) lines for ground release. Black dots represent meteorological towers. The area of the figure is 43 km (north-south) by 35 km (east-west) 13

Figure 4. Topography of test site with locations of release (red) and sampling (white) lines for aircraft release. Black dots represent meteorological towers. The area of the figure is 43 km (north-south) by 35 km (east-west) 14

Figure 5. Aircraft dissemination system mounting frame 15

Figure 6. Components of the aircraft dissemination system 15

Figure 7. Configuration of the SF_6 tank inlet and outlet plumbing 16

Figure 8. Components of the ground dissemination system 17

Figure 9. Comparison of reanalysis of samples. The solid line is a linear fit to the data: $y = (0.93 \pm 0.01)\,x + (9 \pm 10)$, $r^2 = 0.98$, N = 205. The dashed line is $y = x$ 21

Figure 10. Results of analysis of blank samples. The solid line is the mean. The dashed lines are one and two standard deviations about the mean. Mean = 4 ± 3.4 pptv, N = 159 23

Figure 11. Results of the analysis of 127 spiked samples versus the concentration of the standards. The solid line is a linear fit to the data: $y = (0.97 \pm 0.004)\,x + (13 \pm 7)$, $r^2 = 0.997$, N = 127. 24

Figure 12. The standard deviation of measurements of spiked samples versus the concentration of the standards. The solid line is a linear fit to the data: $y = (0.02 \pm 0.08)\,x + (24 \pm 15)$, $r^2 = 0.36$, N = 205. 25

Figure 13. Results of analysis of duplicate samples. The solid line is a linear fit to the data: $y = (0.94 \pm 0.006)\,x + (5 \pm 8)$, $r^2 = 0.99$, N = 205. The dashed line is $y = x$ 26

Figure 14. Analysis coordinate system for ground releases. The black line represents the ground release line and the red crosses represent the individual samplers that comprise each

sampling line 31

Figure 15. Analysis coordinate system for aircraft releases. The black line represents the aircraft releases line and the red crosses represent the individual samplers that comprise each sampling line 32

Figure 16. σ_x versus x. The data plotted are from ground-based continuous analyzers. The solid line is a linear fit to the data with the equation $\sigma_x = (0.105 \pm 0.01)\, x + (165 \pm 85)$, $r^2 = 0.7$, N = 57 46

Figure 17. σ_x versus x. The data plotted are from the aircraft-based continuous analyzer. The solid line is a linear fit to the data with the equation $\sigma_x = (0.05 \pm 0.006)\, x + (670 \pm 85)$, $r^2 = 0.3$, N = 157 46

Figure 18. σ_x versus x. The data plotted are from the aircraft-based continuous analyzer recorded during ground releases. The solid line is a linear fit to the data with the equation $\sigma_x = (0.09 \pm 0.008)\, x + (430 \pm 90)$, $r^2 = 0.6$, N = 82 47

Figure 19. SF_6 transport speed versus mean 2-m wind speed from ground continuous analyzer data. The line is a fit to the data with an equation of $y = (1.7 \pm 0.01)\, x + (0.3 \pm 0.3)$, N = 57. 48

Figure 20. Integrated SF_6 concentration from continuous analyzers versus sample concentration from whole air samplers for all tests. The line is a fit to the data $y = (0.99 \pm 0.05)\, x + (112 \pm 135)$, $r^2 = 0.64$, N = 189 48

Figure B1. Whole air sampler data for Test 1, Line 1 58

Figure B2. Whole air sampler data for Test 1, Line 2 59

Figure B3. Test 1 continuous analyzer data. Altitude versus downwind distance. The red crosses are aircraft measurements. The black crosses are ground measurements at sampling Lines 1 and 2. The width is $\pm 1\sigma$ from the position of peak concentration 60

Figure B4. Test 1 continuous analyzer data. Altitude versus time after release. The red crosses are aircraft measurements. The black crosses are ground measurements at sampling Lines 1 and 2 61

Figure C1. Whole air sampler data for Test 2, Line 1 65

Figure C2. Whole air sampler data for Test 2, Line 2 66

Figure C3. Test 2 continuous analyzer data. Altitude versus downwind distance. The red crosses are aircraft measurements. The black crosses are ground measurements at sampling

Lines 1, 2, and 3. The width is ± 1σ from the position of peak concentration 67

Figure C4. Test 2 continuous analyzer data. Altitude versus time after release. The red crosses are aircraft measurements. The black crosses are ground measurements at sampling Lines 1, 2 and 3 68

Figure C5. Test 2 σ_x versus downwind distance from aircraft continuous analyzer measurements. The blue line is a linear fit to the data with the equation $\sigma_x = (0{:}13 \pm 0.02)\,x + (130 \pm 40)$, $r^2 = 0.8$ 69

Figure D1. Whole air sampler data for Test 4, Line 1 74

Figure D2. Whole air sampler data for Test 4, Line 2 75

Figure D3. Whole air sampler data for Test 4, Line 3 76

Figure D4. Test 4 continuous analyzer data. Altitude versus downwind distance. The red crosses are aircraft measurements. The black crosses are ground measurements at sampling Lines 1, 2, and 3. The width is ± 1σ from the position of peak concentration 77

Figure D5. Test 4 continuous analyzer data. Altitude versus time after release. The red crosses are aircraft measurements. The black crosses are ground measurements at sampling Lines 1, 2 and 3 78

Figure E1. Whole air sampler data for Test 5, Line 1 83

Figure E2. Whole air sampler data for Test 5, Line 2 84

Figure E3. Test 5 continuous analyzer data. Altitude versus downwind distance. The red crosses are aircraft measurements. The black crosses are ground measurements at sampling Lines 1 and 2. The width is ± 1σ from the position of peak concentration 85

Figure E4. Test 5 continuous analyzer data. Altitude versus time after release. The red crosses are aircraft measurements. The black crosses are ground measurements at sampling Lines 1 and 2 86

Figure F1. Whole air sampler data for Test 6, Line 1 93

Figure F2. Whole air sampler data for Test 6, Line 2 94

Figure F3. Whole air sampler data for Test 6, Line 3 95

Figure F4. Test 6 continuous analyzer data. Altitude versus downwind distance. The red

crosses are aircraft measurements. The black crosses are ground measurements at sampling Lines 1, 2, and 3. The width is ± 1σ from the position of peak concentration 96

Figure F5. Test 6 continuous analyzer data. Altitude versus time after release. The red crosses are aircraft measurements. The black crosses are ground measurements at sampling Lines 1, 2, and 3 97

Figure F6. Test 6 σ_x versus downwind distance from aircraft continuous analyzer measurements. The blue line is a linear fit to the data with the equation $\sigma_x = (0.08 \pm 0.01)\,x + (150 \pm 20)$, $r^2 = 0.7$ 98

Figure G1. Whole air sampler data for Test 9, Line 1 106

Figure G2. Whole air sampler data for Test 9, Line 2 107

Figure G3. Test 9 continuous analyzer data. Altitude versus downwind distance. The red crosses are aircraft measurements. The black crosses are ground measurements at sampling Lines 1, 2, and 3. The width is ± 1σ from the position of peak concentration 108

Figure G4. Test 9 continuous analyzer data. Altitude versus time after release. The red crosses are aircraft measurements. The black crosses are ground measurements at sampling Lines 1, 2 and 3 109

Figure H1. Whole air sampler data for Test 10, Line 1 116

Figure H2. Whole air sampler data for Test 10, Line 2 117

Figure H3. Test 10 continuous analyzer data. Altitude versus downwind distance. The red crosses are aircraft measurements. The black crosses are ground measurements at sampling Lines 1, 2, and 3. The width is ± 1σ from the position of peak concentration 118

Figure H4. Test 10 continuous analyzer data. Altitude versus time after release. The red crosses are aircraft measurements. The black crosses are ground measurements at sampling Lines 1, 2, and 3 119

Figure H5. Test 10 σ_x versus downwind distance from aircraft continuous analyzer measurements. Data is from all altitudes. The blue line is a linear fit to the data with the equation $\sigma_x = (0.11 \pm 0.02)\,x + (200 \pm 200)$, $r^2 = 0.7$ 120

Figure H6. Test 10 σ_x versus downwind distance from aircraft continuous analyzer measurements. Data is from altitudes less than 50 m. The blue line is a linear fit to the data with the equation $\sigma_x = (0.12 \pm 0.02)\,x + (300 \pm 140)$, $r^2 = 0.9$ 121

Figure I1. Test 11 continuous analyzer data. Altitude versus downwind distance. The red crosses are aircraft measurements. The black circles are the positions of sampling Lines 1, 2, and 3. The width is ± 1σ from the position of peak concentration 126

Figure I2. Test 11 continuous analyzer data. Altitude versus time after release. The red crosses are aircraft measurements 127

Figure J1. Whole air sampler data for Test 12, Line 1 132

Figure J2. Whole air sampler data for Test 12, Line 2 133

Figure J3. Whole air sampler data for Test 12, Line 3 134

List of Tables

Page

Table 1. OLAD test summary 12

Table 2. OLAD releases 17

Table 3. Performance statistics for TGA-4000 continuous analyzers during OLAD 19

Table 4. Performance statistics for TGA-4000 continuous analyzers from laboratory measurements 19

Table 5. Performance statistics from gas chromatographs estimated from calibration standards 21

Table 6. Performance statistics from gas chromatographs estimated from replicate analyses 22

Table 7. Results of analysis of spike samples 23

Table 8. Performance statistics for whole air sampling method over three concentration ranges estimated from duplicate samples 24

Table 9. Variation in cross-line SF_6 concentrations for all tests 41

Table 10. Variation in cross-line SF_6 concentrations for all ground release tests 42

Table 11. Mean distance of sampling lines from release line 43

Table 12. Variation in cross-line SF_6 concentrations for all aircraft releases 44

Table 13. Agreement between parameters calculated from data collected by two TGA-4000 continuous analyzers positioned on the ends of the sampling lines. O indicates agreement. X indicates not in agreement. 45

Table 14. Mean SF_6 velocity calculated from ground-based and aircraft continuous analyzer data 47

Table 15. Comparison of the whole air samplers against TGA-4000 continuous analyzers . 49

Table 16. Variation TGA-4000 integrated SF_6 concentrations and sampler results for all ground releases 49

Table 17. Variation TGA-4000 integrated SF_6 concentrations and sampler results for all aircraft releases 49

Table A1. Ground release sampling locations and coordinates 55

Table A2. Air release sampling locations and coordinates 56

Table A3. Perpendicular and trajectory distances from the ground release line to the sampling lines 57

Table A4. Perpendicular and trajectory distances from the aircraft release line to the sampling lines 57

Table B1. Test 1 sampling line SF_6 concentration variability. 62

Table B2. Test 1 sampling line SF_6 concentration variability by line for each sampling bag 62

Table B3. Test 1 SF_6 transport parameters from ground-based continuous analyzers 63

Table B4. Test 1 SF_6 transport parameters from aircraft continuous analyzer 64

Table C1. Test 2 sampling line SF_6 concentration variability. 70

Table C2. Test 2 sampling line SF_6 concentration variability by line for each sampling bag 70

Table C3. Test 2 SF_6 transport parameters from ground-based continuous analyzers 71

Table C4. Test 2 SF_6 transport parameters from aircraft continuous analyzer 72

Table D1. Test 4 sampling line SF_6 concentration variability. 79

Table D2. Test 4 sampling line SF_6 concentration variability by line for each sampling bag 79

Table D3. Test 4 SF_6 transport parameters from ground-based continuous analyzers 80

Table D4. Test 4 SF_6 transport parameters from aircraft continuous analyzer 81

Table E1. Test 5 sampling line SF_6 concentration variability. 87

Table E2. Test 5 sampling line SF_6 concentration variability by line for each sampling

bag 87

Table E3. Test 5 SF_6 transport parameters from ground-based continuous analyzers 88

Table E4. Test 5 SF_6 transport parameters from aircraft continuous analyzer 89

Table F1. Test 6 sampling line SF_6 concentration variability. 99

Table F2. Test 6 sampling line SF_6 concentration variability by line for each sampling bag 99

Table F3. Test 6 SF_6 transport parameters from ground-based continuous analyzers for plume #1 100

Table F4. Test 6 SF_6 transport parameters from ground-based continuous analyzers for plume #2 101

Table F5. Test 6 SF_6 transport parameters from ground-based continuous analyzers for plume #3 102

Table F6. Test 6 SF_6 transport parameters (release 1) from aircraft continuous analyzer .. 103

Table F7. Test 6 SF_6 transport parameters (release 2) from aircraft continuous analyzer .. 104

Table F8. Test 6 SF_6 transport parameters (release 3) from aircraft continuous analyzer .. 105

Table G1. Test 9 sampling line SF_6 concentration variability. 110

Table G2. Test 9 sampling line SF_6 concentration variability by line for each sampling bag 110

Table G3. Test 9 SF_6 transport parameters from ground-based continuous analyzers 111

Table G4. Test 9 SF_6 transport parameters from aircraft continuous analyzer 112

Table H1. Test 10 sampling line SF_6 concentration variability. 122

Table H2. Test 10 sampling line SF_6 concentration variability by line for each sampling bag 122

Table H3. Test 10 SF_6 transport parameters from ground-based continuous analyzers 123

Table H4. Test 10 SF_6 transport parameters from aircraft continuous analyzer 124

Table I1. Test 11 SF_6 transport parameters from aircraft continuous analyzer 128

Table J1. Test 12 sampling line SF_6 concentration variability. 135

Table J2. Test 12 sampling line SF_6 concentration variability by line for each sampling bag 135

Table J3. Test 12 SF_6 transport parameters from ground-based continuous analyzers 136

Abstract

The purpose of the Over-Land Along-Wind Dispersion (OLAD) field experiment was to measure along-wind dispersion over distances from 2 to 20 km. A gaseous, chemical tracer, sulfur hexafluoride (SF_6), was released in a line approximately perpendicular to the mean wind direction and similar in length to the downwind distance at which the tracer was measured. A line release was chosen to minimize the effects of cross wind processes on the dispersion of the cloud so that the along-wind dispersion could be more accurately measured. The experiment was designed with quality control procedures on all tracer measurements that allowed the measurement uncertainty to be accurately quantified. The sampling array and sampling protocols were designed to give a greater degree of spatial and temporal resolution to the tracer measurements than in any previous line source experiments.

OLAD was conducted during September 1997 at the West Desert Test Center, U. S. Army Dugway Proving Ground (DPG) in northwestern Utah. There were 14 tracer releases; ten releases from the ground, along a line approximately 10 km long. There were four releases from the air, along a line approximately 17 km long. There were three sampling lines at approximately 2, 5, and 10 km downwind of the ground release line and 10, 15, and 20 km downwind of the aircraft release line. Each sampling line consisted of fifteen whole air samplers spaced 100 m apart. These samplers collected twelve 15-min samples. Continuous analyzers were positioned at the sampler locations on the ends of each line. There was one continuous analyzer in an aircraft sampling at various altitudes.

Analysis of 205 duplicate samples showed that the error in the measurement method was 24% at the 95% (2σ) confidence level for the concentration range 100-500 pptv. Concentration differences between samples that were greater than this level could be unambiguously identified as the result of atmospheric processes.

Concentrations in contemporaneous samples on Line 1, both during ground and aircraft releases, always exhibited greater variability than could be attributed to measurement errors alone. Lines 2 and 3 also exhibited similar variability, although somewhat smaller in magnitude. From this we have concluded that the line source does not eliminate cross-wind variability from the concentration measurements, particularly over distances less than 10 km.

We determined that the SF_6 transport speeds are generally greater than the mean 2-m wind speed by a factor of 1.7. This suggests that wind shear coupled with vertical turbulence is important in transporting the cloud and that this coupling influences dispersion. We found that the tracer transport speed at the ground is not significantly different from the speed up to 250 m above the surface. We also found that when tracer is released at the surface and 2-m wind speeds are greater than 2 m s^{-1}, there is a correlation between along-wind diffusion σ_x and downwind distance x. This correlation is not evident for elevated releases. This effect cannot be quantified because of a lack of upper air and turbulence data.

1 Introduction

The military, chemical and energy industries, industrial and civil emergency response communities, and regulatory agencies have developed models to predict the transport and exposure levels resulting from releases of hazardous materials. These models rely on assumptions about the physics of atmospheric transport and dispersion that, at best, simplify a complex problem. At their worst, the models are based on assumptions that are invalid under some commonly occurring meteorological conditions. The purpose of the Over-Land Along-Wind Dispersion (OLAD) field experiment was to measure specific aspects of the process of atmospheric dispersion. The data gathered from this study are being used to improve and validate models designed to predict battlefield exposure to chemical and biological weapons and to provide an important resource for the study of atmospheric dispersion processes.

Many releases of hazardous gases are usually a few minutes in duration because they result from the breach of a vessel(s) containing a finite quantity of material. This results in a puff or cloud of material released into the atmosphere. The rate and duration of the release, the speed and direction of the mean wind, and the nature of the atmospheric turbulence in which the release takes place determine the initial dimensions and concentration profile of the cloud. The duration of the release determines the degree of the interaction between the release process and the atmospheric conditions. Short duration releases behave more like puffs than plumes and longer duration releases more like plumes than puffs.

The mean wind is accompanied by variations in speed and direction caused by turbulent eddies. These eddies occur on the scale of less than a meter to hundreds of meters. The scale of these turbulent fluctuations, relative to the initial dimensions of the cloud, determines their effect. If they are much larger than the dimensions of the cloud, they translate the entire mass of the released material. If they are on the same scale or smaller than the dimensions of the cloud, they disperse the material over a larger volume.

Once the material is released into the atmosphere, the concentration distribution of the resulting cloud at any point in time is usually considered to be the result of a finite number of discrete turbulent fluctuations (Draxler, 1984). These fluctuations expand the cloud in three dimensions as it is being transported by the mean wind. Vertical wind shear is a major contributor to transport and diffusion. As vertical turbulence transports material aloft, the increased wind speed moves this material ahead of the main body of the cloud. Vertical turbulence is still acting on the elevated material, this time transporting some of it back to lower levels. The size of the cloud in the along-wind dimension is increased by the combination of vertical turbulence and wind shear in addition to turbulence in the along-wind direction.

Little data exist to characterize along-wind diffusion, especially for distances of more than a few kilometers. While there is a wealth of information on cross-wind and vertical diffusion, relatively few studies have been specifically designed to measure the along-wind diffusion parameter, σ_x, and how it varies with distance or atmospheric stability. This is due, in part, to a greater interest in continuous sources of industrial air pollution in which along-wind dispersion can be neglected (Draxler, 1979). It has only been in recent years that sampling techniques capable of providing concentration time histories required to determine σ_x have

become readily available (Bowers, 1992). However, σ_x is an important parameter when considering instantaneous or near-instantaneous sources.

The lack of understanding of along-wind diffusion is a major concern in military operations in which ground forces and civilians may be subject to sudden point source releases of chemical and/or biological agents. Such releases can result from the detonation of missile warheads or exploding bunkers. The understanding of along-wind diffusion is also important in modeling accidental releases of toxic pollutants from stationary or mobile containment vessels (e.g., storage tank, tank car or tank trailer) which can pose an immediate threat to life and property. Many puff models apply the same expressions of cross-wind and vertical dispersion parameters, σ_y and σ_z, respectively, valid for continuous plumes, to an instantaneous release (Hanna, 1996). Many transport and diffusion models such as INPUFF (Petersen and Lavdas, 1986) commonly assume that σ_x and σ_y are the same. While these approaches may be useful as rough approximations for predicting downwind concentrations, they fail to recognize two fundamental problems. The dispersion coefficients σ_y and σ_z for an instantaneous puff are typically less than those for a continuous plume by a factor of two or more (Slade, 1968). In addition, σ_x is larger than σ_y because of the effects of wind shear (Pasquill, 1974). Both short-range diffusion experiments (Nikola, 1971) and theoretical analyses (Wilson, 1981) indicate that $\sigma_x = \sigma_y$ is a poor assumption.

A study of along-wind diffusion can be simplified if the effects of cross-wind processes can be minimized. In theory, this is accomplished using a line source. The assumption is that a more uniform concentration in the across-wind dimension (y) can be achieved by releasing tracer, at a constant rate, in a line perpendicular to the mean wind direction and similar in length to the distance over which the dispersion is to be measured. The along-wind diffusion can then be studied directly. During September 1997, a series of line releases was conducted at the West Desert Test Center, U. S. Army Dugway Proving Ground (DPG) in northwestern Utah to acquire data for validation of atmospheric transport and dispersion models. The specific objective of the OLAD field experiment was to acquire a database on along-wind diffusion over 2 to 20 km distances for verification and improvement of the Vapor, Liquid and Solid Tracking (VLSTRACK) model and the Second-Order Closure Integrated Puff (SCIPUFF) dispersion model. A series of trials was conducted in which sulfur hexafluoride (SF_6) was released by truck or aircraft along a line approximately perpendicular to the mean wind. Lines of whole-air samplers and continuous analyzers were used to measure the concentration of SF_6 downwind of the quasi-instantaneous line source. Tower-based and portable in situ sensors acquired surface-based meteorological measurements. Pilot balloon (PIBAL) and radiosondes acquired upper-air data. These trials were conducted in the early and late morning hours during September 1997. OLAD participants included DPG's West Desert Test Center (WDTC), the National Oceanic and Atmospheric Administration's (NOAA) Air Resource Laboratory Field Research Division (ARLFRD), and Alpine Aviation.

2 Theoretical and Empirical Treatments of Along-Wind Dispersion

As briefly summarized by Drivas and Shair (1974), there have been two largely successful, overlapping, analytical approaches to quantifying atmospheric dispersion: Semi-empirical diffusion equation (e.g. Monin and Yaglom, 1971) and a Gaussian representation (e.g., Pasquill, 1974). For the two-dimensional geometry of a line source, the semi-empirical equation is:

$$\frac{\partial \langle \chi \rangle}{\partial t} + u\frac{\partial \langle \chi \rangle}{\partial x} + w\frac{\partial \langle \chi \rangle}{\partial w} = \frac{\partial}{\partial x}\left(K_x \frac{\partial \langle \chi \rangle}{\partial x} \right) + \frac{\partial}{\partial z}\left(K_z \frac{\partial \langle \chi \rangle}{\partial z} \right) \qquad (1)$$

where $\langle \chi \rangle$ is the ensemble mean of the concentration $\chi(x,z,t)$, and K_x and K_z are the turbulent eddy diffusivities in the x and z directions, respectively. Since turbulence theory deals statistically rather than deterministically with atmospheric motions, it describes the ensemble mean behavior of puffs rather than the behavior of a specific puff (Bowers, 1992). The "semi-empirical" label derives from the parameterization of a turbulent eddy diffusivity K that is analogous to molecular diffusivity and from the neglect of off-diagonal tensor coefficients (e.g., K_{xz}, which may contribute if a positive correlation exists between u and w). This simple gradient transport analogy is not generally valid for atmospheric turbulence (Priestly, 1959; Calder, 1965) but has practical applications (Corrsin, 1959), most notably the widely-used Gaussian representations.

Solutions to the semi-empirical diffusion equation depend on boundary conditions and on the functional form of K. For Fickian diffusion (K = constant), one solution is a Gaussian concentration profile. Using the Gaussian model (Slade, 1968), the concentration χ downwind of an instantaneous cross-wind line source of height h is given by:

$$\chi(x, z, t, h) = \frac{Q_L}{2\pi\,\sigma_x \sigma_z} \exp\left(\frac{-(x - ut)^2}{2\sigma_x^2} \right) \left[\exp\left(\frac{-(z - h)^2}{2\sigma_z^2} \right) + \exp\left(\frac{-(z + h)^2}{2\sigma_z^2} \right) \right] \qquad (2)$$

where Q_L is the mass released per unit length, u is the mean along-wind velocity, and t is the time of transport.

There are fundamental differences in dispersion between an instantaneous puff and a continuous plume. To address these differences, Hanna (1996) defines a length scale as $u_c T_d$, where u_c is the advective speed of the cloud and T_d is the source release duration. Hanna (1996) also suggests a dimensionless ratio as a criterion for whether a release behaves more like a continuous plume or like an instantaneous puff:

$$\frac{u_c T_d}{\sigma_x} \gg 1 \quad \text{------} \rightarrow \quad \textit{continuous plume} \qquad (3)$$

$$\frac{u_c T_d}{\sigma_x} \ll 1 \qquad \text{------} \rightarrow \quad \textit{instantaneous puff} \tag{4}$$

Hanna et al. (1984) suggests that instantaneous dispersion parameters should be used when either the release time or sampling time is less than the transport time between the source and downwind receptor, while continuous dispersion parameters should be used when both the release and sampling times are greater then the transport time. Thus, instantaneous dispersion parameters are applicable at all downwind distances for instantaneous and quasi-instantaneous releases and may be applicable to continuous or quasi-continuous releases under some circumstances.

Boundary-layer similarity theories are used to develop simplified formulas for σ_x which are tested against data from laboratory and field experiments. Saffman (1962) theoretically derived expressions for σ_x by analyzing the moments of the diffusion equation for an instantaneous cross-wind line source assuming an unbounded upper atmosphere and power law profiles of velocity and eddy diffusivity. For a linear velocity profile and constant values assigned to K_x and K_z, he obtains:

$$\sigma_x^2 = \left(\frac{7}{30} - \frac{\pi}{16} \right) \alpha^2 K_z t^3 + 2 K_x t \tag{5}$$

where α is slope of the wind profile ($u = u_o + az$). The first term in this equation is the horizontal diffusion due to the interaction of wind shear and vertical transport. The second term gives the extra dispersion due to horizontal diffusion. When Saffman (1962) assumes that K_x/z = constant, he derives the following equation from (5):

$$\sigma_x^2 = \left(\frac{7}{30} - \frac{\pi}{16} \right) \alpha^2 K_z t^3 + \frac{K_x}{2z} \sqrt{\pi K_x t^3} \tag{6}$$

Saffman (1962) argues that along-wind diffusion can not be described by a constant diffusivity and is not a linear function of time. However, the horizontal fluctuations and the interaction of wind shear with vertical transport still contribute independently to the along-wind diffusion.

In a similar study, Chatwin (1968) derived an expression for σ_x assuming an instantaneous ground-level line source release in a neutral boundary layer, an unbounded atmosphere, a logarithmic wind profile, and a linear vertical eddy diffusivity profile neglecting the first term on the right-hand side of (1). In this case, the along-wind dispersion is parameterized by the simple expression:

$$\sigma_x = 0.596 \frac{u_* t}{k} \tag{7}$$

where u_* is the friction velocity and k is the von Karman constant (0.4). Note in this expression that σ_x is a linear function of time.

Csanady (1969) solved the diffusion equation with an effective diffusivity based on the wind shear of an Ekman profile. His results showed that along-wind diffusion was a combination of turbulent and shear induced components. Accordingly (Draxler, 1979; Van Ulden, 1992), σ_x can be expressed as the quadratic sum of a turbulent diffusion parameter σ_{xt} and a wind shear diffusion parameter σ_{xs} in the along-wind direction as:

$$\sigma_x^2 = \sigma_{xt}^2 + \sigma_{xs}^2 \tag{8}$$

There are a number of relationships defining the along-wind turbulent and wind shear parameter. The turbulent parameter is typically given (Smith and Hay, 1961; Draxler, 1979) as:

$$\sigma_{xt}^2 = 3 I_x^2 t \tag{9}$$

where the longitudinal turbulent intensity I_x is defined as the standard deviation of the longitudinal wind fluctuations σ_u divided by the mean longitudinal wind speed u. Draxler (1979) gives the wind shear parameter based on Saffman's (1962) derivation as:

$$\sigma_{xs}^2 = \frac{1}{u} \sqrt{\frac{1}{25} \alpha^2 K_z t^3} \tag{10}$$

The turbulent component is approximately equal to σ_y and the shear component is a function of wind shear and the vertical dispersion (Hanna, 1996). Smith (1965) suggests the following relationship for the wind shear contribution:

$$\sigma_{xs}^2 = \left(\frac{t}{\sqrt{12}} \frac{du}{dz} \right) \sigma_z \tag{11}$$

If there is strong wind shear present with very little vertical dispersion (i.e., a very stable boundary layer), the cloud tilts in the along-wind direction but there is little along-wind turbulent dispersion over the full depth of the cloud. In general, σ_z is small when du/dz is large (stable conditions), and σ_z is large when du/dz is small (unstable conditions). Also, Smith's (1965) formula is difficult to interpret near the ground since du/dz is not constant but is inversely proportional to the height.

Several empirical expressions for σ_x have been developed based on short-range measurements. Drivas and Shair (1974) released a quasi-instantaneous line source of SF_6 from the exhaust of an

automobile moving along Interstate 405 in Los Angeles, California. The length of the release was approximately 2.4 km in most of the six trials. This section of highway runs parallel to the Pacific Ocean coastline about 6 km inland. During the afternoon a brisk sea breeze normally blows inland perpendicular across the highway. SF_6 measurements were obtained as a function of time at various locations along Venice Boulevard which runs inland in a straight line perpendicular to the highway for over 6 km. Of the six trials, two were conducted in the summer while four were run in the winter. Using the results of Saffman (1962), Drivas and Shair (1974) found that $\sigma_x \sim t^b$, where b ranged from 1.11 to 1.47. While they do not explicitly show how σ_x varies with stability, Drivas and Shair (1974) indicate that b is inversely proportional to the standard deviation of the horizontal wind direction σ_θ.

Draxler (1979) examined data from three experiments in which aircraft were used to create line sources by releasing fluorescent particles (FP) upwind and parallel to sampling lines. The first experiment consisted of 36 trials, all after 1800 LST, conducted in Ft. Wayne, Indiana. Each trial consisted of two FP releases by separate aircraft several kilometers upwind of the city at altitudes of 91 and 214 m. The sampling array consisted of 5 arcs, each 16 km in length. One arc was upwind of Ft. Wayne, three were located within the city, and the last was downwind in a rural area about 15 km from the release line. The second study was a tracer test in Victoria, Texas consisted of 17 offshore FP releases near Corpus Christi. The tracer was released from an aircraft early in the evening. The 160-km flight path was a few kilometers offshore and parallel to the coast. Most of the releases were at a height of 90 m. A total of six sampling lines were utilized. Four of them were parallel to the coastline about 160 km in length spaced evenly from 40 to 180 km downwind of the release line. Another 16-km sampling line was set up along the beach. The last sampling line was normal to the others through the midpoint of the release line. The third tracer study in Oceanside, California consisted of several types of FP releases and sampling methods designed to characterize diffusion in a shoreline region. Aircraft releases were made several kilometers offshore and most were at a height of 60 m. However, the total number of samplers used in this study was not as extensive as the previous two mentioned experiments.

Through regression analysis, Draxler (1979) determined the following relationship based on data from the Victoria experiment as:

$$\sigma_x = 7.3\, t^{1.3} \tag{12}$$

with σ_x in meters and t in minutes. In a follow-up study, Draxler (1984) determines a relationship for σ_x based on regression fits for the Victoria and Oceanside experiments as:

$$\sigma_x = 0.9\, t^{1.1} \tag{13}$$

where, for this empirical equation, σ_x and the transport time t are both in minutes. Draxler (1979) concluded that the along-wind dispersion is the result of both turbulence and wind shear. Although considerable scatter was apparent in these data, he felt they were representative. Draxler (1979) also

recommended that more attention be focused on the quality of sequential sampler data and that sufficient meteorological measurements are obtained to accurately test along-wind dispersion formulations.

Whitacre et al. (1987) used the following parameterization for σ_x in the D2PC model:

$$\sigma_x = 0.1522\, x^{0.9294} \tag{14}$$

where σ_x and downwind distance x are both in meters.

Several authors have attempted to develop stability-dependent expressions for σ_x. For example, Hansen (1979) defines σ_x as:

$$\sigma_x = \sigma_{xo} + 0.74\, a\, x^{0.9} \tag{15}$$

where σ_{xo} is an initial source dimension and the coefficient a ranges from 0.4 to 0.076 depending on the Pasquill stability category.

Wilson (1981) proposed a generalized analytical formula for σ_x for all stability's assuming a logarithmic wind profile. Wilson (1981) uses theoretical reasoning to derive:

$$\sigma_x = \left[0.09 \left(\frac{x}{z_r \ln (z_c / z_o)} \right)^2 + \left(\frac{\sigma_{xt}}{\sigma_z} \right)^2 \right]^{1/2} \sigma_z \tag{16}$$

where z_o is the surface roughness length, and z_r and z_c are defined as:

$$z_r = h + 0.5\, \sigma_z \tag{17}$$

$$z_c = h + 0.17\, \sigma_z \tag{18}$$

where h is the release height. The first term of (16) accounts for the effects of wind shear while the second term accounts for turbulence effects. Wilson (1981) points out that, except for very close to the source, along-wind diffusion tends to be dominated by vertical diffusion in combination with shear advection. Unfortunately, Wilson (1981) does not compare his parameterization of σ_x against field data.

Dumbauld and Bowers (1983) propose a simple, semi-empirical σ_x formula that also includes

the effects of both atmospheric turbulence and vertical wind shear. Their expression is:

$$\sigma_x = \left[\left(a I_x (x + x_v)^b \right)^2 + \left(E_S \left(\frac{\Delta u}{u} \right) x \right)^2 \right]^{1/2} \tag{19}$$

where a, b, and E_s are empirical coefficients, x_v is the virtual distance used to account for initial source dimensions, and Δu is the change in wind speed between the top and bottom of the puff. Dumbauld and Bowers (1983) adjust the along-wind turbulence intensity for source duration by:

$$I_x(\tau) = I_x(\tau_o) \left(\frac{\tau}{\tau_o} \right)^{0.2} \tag{20}$$

where τ_o is the sampling time for $I_x(\tau_o)$ (typically 10 to 60 min) and τ is the source duration, which is not allowed to be less than 2.5 s for a quasi-instantaneous source. If along-wind turbulence intensity measurements are not available, Dumbauld and Bowers (1983) use the parameterization of $I_x = 1.33 I_y$ suggested by Counihan (1975) in which I_y is the cross-wind turbulence intensity. Dumbauld and Bowers (1983) also suggest that a and b are both approximately equal to unity and conclude that E_s is about 0.06 based on data from Nikola (1971). Given the recommended coefficients, Dumbauld and Bowers (1983) show that values of σ_x obtained from (19) compare to those obtained by Drivas and Shair (1974) to within a factor of about 1.5. Bowers (1992) points out that Dumbauld and Bowers (1983) must use an urban wind speed profile methodology to estimate $\Delta u/u$ because Drivas and Shair (1974) do not report any information on wind profile.

Van Ulden (1992) uses Monin-Obukhov similarity theory to derive an analytical model that accounts turbulence intensity and wind shear as well as for the effects of large horizontal eddies. For neutral conditions near the source, Van Ulden (1992) shows that his σ_x values are nearly the same as that given by Chatwin (1968) but with a leading constant of 0.84 rather than 0.596. Because of the compensating effects of wind shear and vertical dispersion, values of σ_x derived from Van Ulden's (1992) parameterization show little variation with stability.

Bowers et al. (1994) determined σ_x over the ocean for a range of 5 to 105 km based on concentrations of SF_6 downwind from a quasi-instantaneous line source released by aircraft. A regression of σ_x as a function of downwind distance for 13 trials yields the following:

$$\sigma_x = 1.06\, x^{0.63} \tag{21}$$

In summary, a review of the theoretical and empirical expressions presented, show little agreement about how σ_x varies with distance, time, and atmospheric stability. The data currently available (generally restricted to downwind distances less than 3 km) suggest that σ_x varies approximately linearly with distance or time (Bowers, 1992). There are several theoretical, empirical,

or semi-empirical relationships that define σ_x as a function of distance, time, and/or stability. However, there are insufficient σ_x data to define an along wind cloud growth algorithm suitable for use in dispersion models. The need for additional data, particularly for downwind distances in the 2 to 20 km range, served as the motivation for the OLAD Field Experiment.

3 Data

3.1 Site Description

The West Desert Test Center of the Dugway Proving Ground is located near the southeast edge of the Great Salt Lake Desert about 125 km west-southwest of Salt Lake City, Utah. The prehistoric Lake Bonneville, a fresh water lake which existed 25,000 to 10,000 years ago and had an area of 52,000 km^2, once covered this area. The test range lies between two regions of the lake bed known as the Great Salt Lake Desert or Salt flats and the Seiver Basin (Figure 1). OLAD tests were conducted on a plain approximately 24 km (east-west) by 40 km (north-south) which connects these areas. Mountain ranges running approximately north-south border the plane on the east, west, and south. These mountains vary in height from 300 to 1200 m above the floor of the valley and provide a topographic channel for southeast and northwest wind flow. The area to the north is open to the Great Salt Lake Salt Flats. The test range terrain is relatively uniform and flat with a slight southeast to northwest downward slope. Tests were carried out in an area between Target S grid (1333 m MSL) to the south and Horizontal Grid (1311 m MSL) to the north (Figure 2). This shallow sloping channel influenced much of the diurnal wind flow during the September OLAD tests.

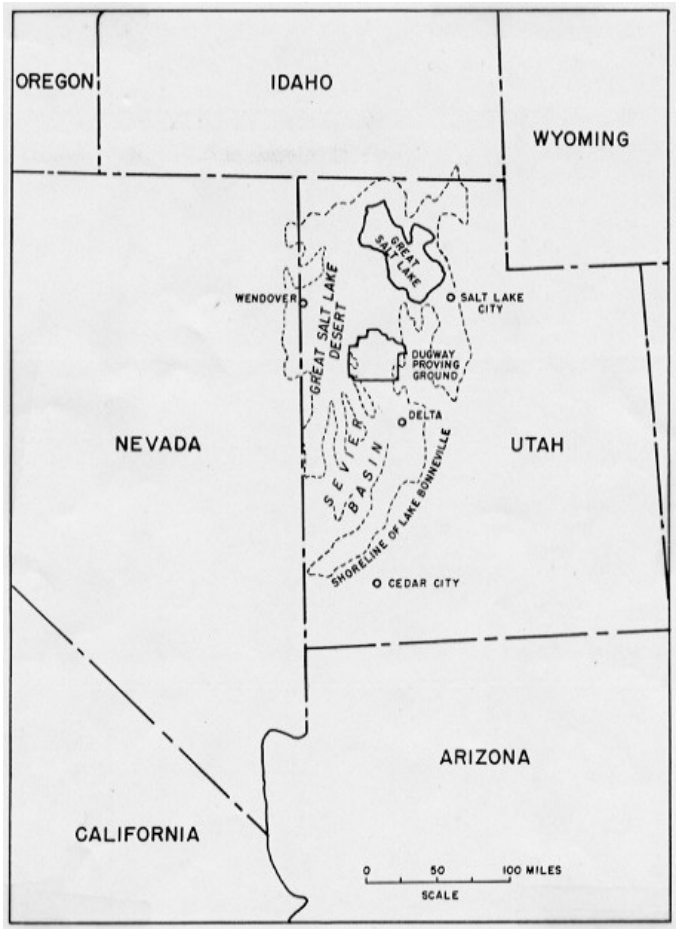

Figure 1. Dugway Proving Ground and surrounding area (Shearer, 1956).

There is little vegetation on the mountains which surround the test area. Vegetation on the plane consists primarily of shadescale and gray molly spaced 20 to 60 cm apart and growing to a height of 5 to 20 cm above ground, and greasewood which grows to over 75 cm tall and 100 cm in diameter. The soil is fine grain alluvial silty clay which can be detached from the ground at wind speeds of 8 to 12 m s^{-1}. The wind speed maximum criteria for OLAD tests was 8 m s^{-1} so that blowing dust would not impede OLAD operations (Biltoft et al., 1997). The Salt Flats are flat and barren with a high albedo.

3.2 Climatology

The winds in the OLAD test area during September are influenced by traveling synoptic disturbances and under stationary high pressure systems by local scale features driven by diurnal heating and cooling. The local wind is driven by temperature differences between the Salt Flats and Seiver basin and channeled by the nearby mountains. During the daytime, in the absence of moderate or strong synoptic forcing, solar heating of the sparsely vegetated mountains and valleys produces vertical air movement. The surface temperature is lower at the Salt Flat because of the higher albedo and the cooler air is drawn across the test area from the north. At night, strong radiational cooling off the barren mountains reverses the situation; cool air descends into the valleys and down the gently sloped test area toward the north. OLAD was designed to take advantage of these nocturnal drainage flows.

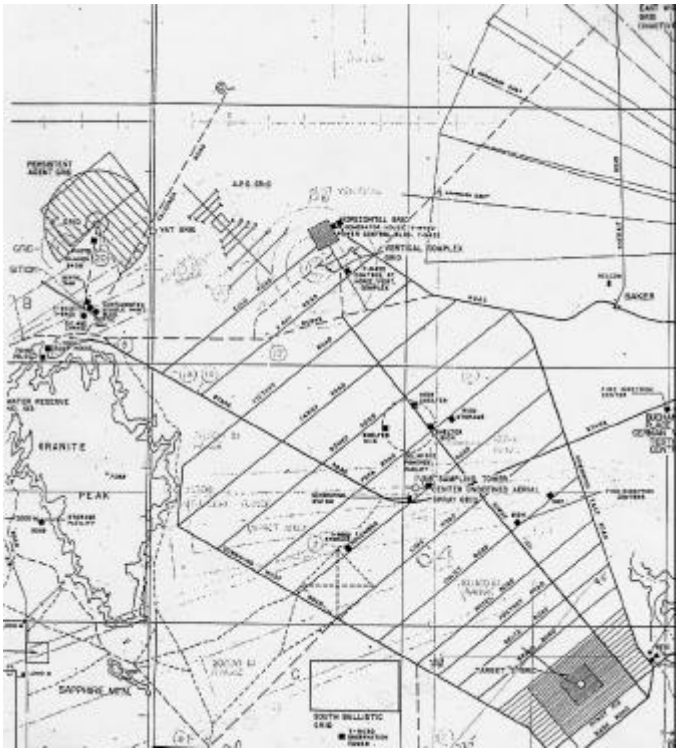

Figure 2. Dugway Proving Ground test area.

Meteorological records are available for the Horizontal Grid beginning in 1951 and the Target S Grid in 1952. The climatology for the month of September indicates a high frequency of nighttime drainage winds from the east-southeast through south at S Grid, and Horizontal Grid (Shearer, 1957) following the diurnal heating/cooling cycle. Wind roses for the Autumn season, nighttime (1800-0500) indicate a preponderance of southeast and south winds in the 0 to 6 m s^{-1} range at Target S Grid, and south and southeast winds at Horizontal Grid.

3.3 Experimental Summary

OLAD tests were held from 8 September through 25 September 1998. There were 14 tracer releases, ten releases from the ground and four from the air. The experiment was performed over distances ranging from 2.5 km to 20 km. SF_6 was released in a 10 km line, at the surface from a truck and, from an aircraft, at an altitude of 100 m. Ground releases consisted of 10 kg of SF_6 while air releases consisted of 100 kg of SF_6. The tests are summarized in Table 1. There were three sampling lines at approximately 2, 5, and 10 km downwind from the release track for the ground releases. During aircraft releases sampling took place at three lines located approximately 10, 15, and 20 km downwind of the release line. Each sampling line consisted of fifteen whole air samplers spaced 100 m apart. Continuous analyzers in vans were positioned at the ends of each sampling line (Figures 3 and 4). There was one continuous analyzer in an aircraft.

Table 1. OLAD test summary.

Test	Date	Trial[1] (JJJ)	Release (MDT)	Sampling line[2]	Sampler start (MDT)	Release type	Comments
1	08 SEP	251	7:05	1	6:30	Ground	
				2	6:30		
				3	7:00		
2	09 SEP	252	6:45	1	6:45	Ground	
				2	6:45		
				3	7:15		
3	10 SEP	253	7:29	1	6:45	Air	only Line 1 analyzed
				2	6:45		
				3	7:15		
4	11 SEP	254	6:56	1	6:45	Air	
				2	6:45		
				3	7:15		
5	12 SEP	255	6:57	1	6:45	Ground	flow controller replaced
				2	6:45		
				3	6:45		
6a	15 SEP	258-1	6:44	1	6:30	Ground	
6b		258-2	7:54	2	6:30		
6c		258-3	8:38	3	6:30		
7	15 SEP	258-4	10:53	no analysis		Ground	SF_6 missed grid
8	16 SEP	259	no release	no analysis		Ground	release canceled
9	17 SEP	260	6:48	1	6:45	Air	
				2	6:45		
				3	7:15		
10	18 SEP	261	7:55	1	6:45	Ground	bad release
				2	6:45		
				3	6:45		
11	24 SEP	267	7:09	1	7:30	Air	only Line 1 analyzed
				2	7:30		
				3	8:00		
12	25 SEP	268-1	4:00	1	4:00	Ground	first release bad
				2	4:00		
				3	4:30		
13	25 SEP	268-2	8:54	no analysis			SF_6 missed grid

1. Julian Day (JJJ). 2. Sampling lines for ground releases are: 1-Foxtrot, 2-Julliet, 3-Papa. Sampling lines for the air releases are: 1-Lima, 2-Tango, 3-Zulu.

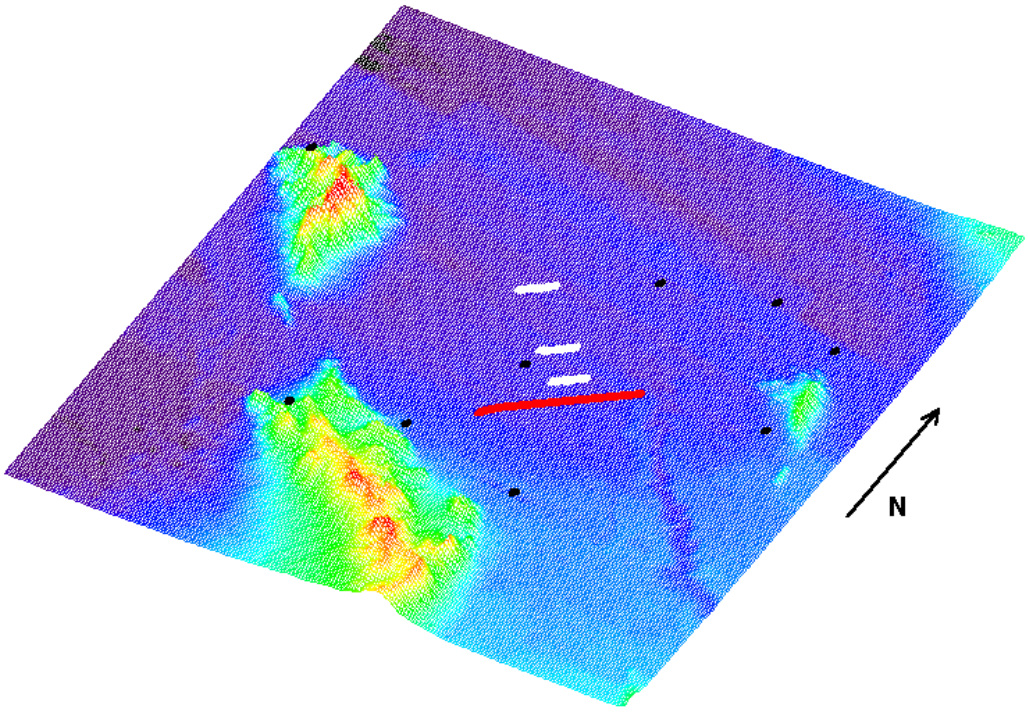

Figure 3. Topography of test site with locations of release (red) and sampling (white) lines for ground release. Black dots represent meteorological towers. The area of the figure is 43 km (north-south) by 35 km (east-west).

During Test 3, the nocturnal inversion broke up before the SF_6 cloud traveled to Sampling Line 2. Only samples from Line 1 were analyzed for this test. The aircraft GPS data was not recorded during this test. Samples from Tests 7 and 13 were not analyzed because the cloud did not travel to the sampling grid. There was no release during Test 8. The sampling aircraft did not fly during Test 12.

There were problems with the release mechanism during Tests 5, 10, and 12. These problems are discussed in detail below.

3.4 Dissemination methods

The boiling point of SF_6 at 1 atm is -64 °C. In a cylinder, at 20 °C, most of the SF_6 is a liquid with a vapor pressure of only about 300 psig. The vaporization of 100 kg of SF_6 requires 659 kJ of energy. When a cylinder is opened and the gas is released to the atmosphere, evaporation occurs, and

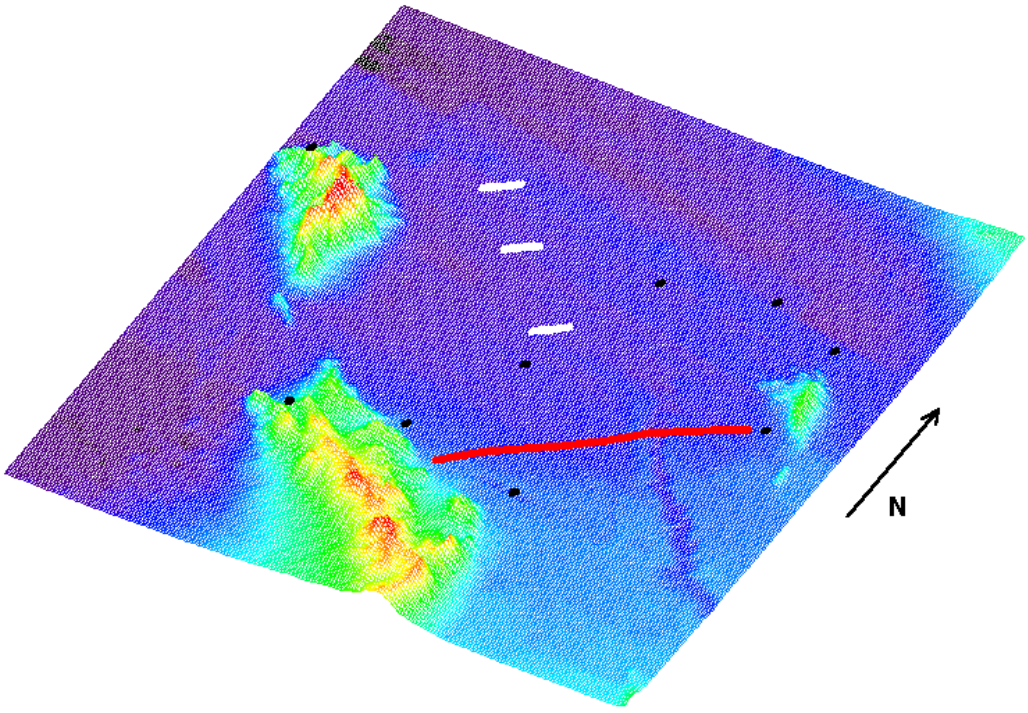

Figure 4. Topography of test site with locations of release (red) and sampling (white) lines for aircraft release. Black dots represent meteorological towers. The area of the figure is 43 km (north-south) by 35 km (east-west).

the temperature of the system drops. This significantly lowers the vapor pressure and can cause changes in the release rate. The tank must be heated to maintain a constant vapor pressure during the dissemination. The cooling also affects the performance of pressure regulators, flow regulators, and flow metering devices. It is not possible to release large quantities of SF_6 using only vapor pressure as the driving force of the release without adding large quantities of energy to the system.

3.4.1 Aircraft Release

The OLAD airborne releases consisted of the dissemination of 100 kg of SF_6 along a 10 km line. At an air speed of 200 km hr^{-1}, this required a release rate of 33.3 kg min^{-1}. This rate must be held within narrow limits and be accurately measured. To accomplish this while maintaining a constant SF_6 vapor pressure would require a 3.7 kW heater. These requirements could not be met in an aircraft installation with the techniques and equipment we have used in previous projects. Therefore, FRD designed and built a new release system for the OLAD field program. This system uses pressurized nitrogen to drive the release of liquid SF_6 and the ambient energy available in the

atmosphere to accomplish the vaporization. In addition to the performance requirements imposed by the scientific goals of the project, the system for mounting the components in the aircraft had to be designed, fabricated, and installed to meet standards set by the Federal Aviation Administration (FAA).

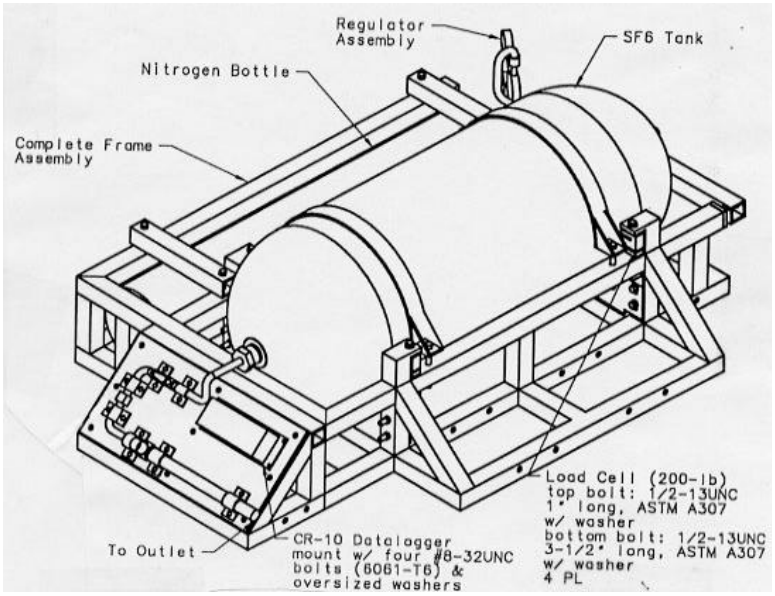

Figure 5. Aircraft dissemination system mounting frame.

Engineers from Lockheed Martin Idaho Technologies Corporation (LMITCO) designed an aluminum frame to mount the SF_6 dissemination system securely in the aircraft (Figure 5). The frame design was approved by GS Engineering of Afton, Wyoming (FAA Designated Engineering Representative NM-2338) and was fabricated by Dal-Fab & Machine Inc. of Idaho Falls, Idaho. The aircraft installation was inspected and approved by the FAA Salt Lake City Flight Standards District Office.

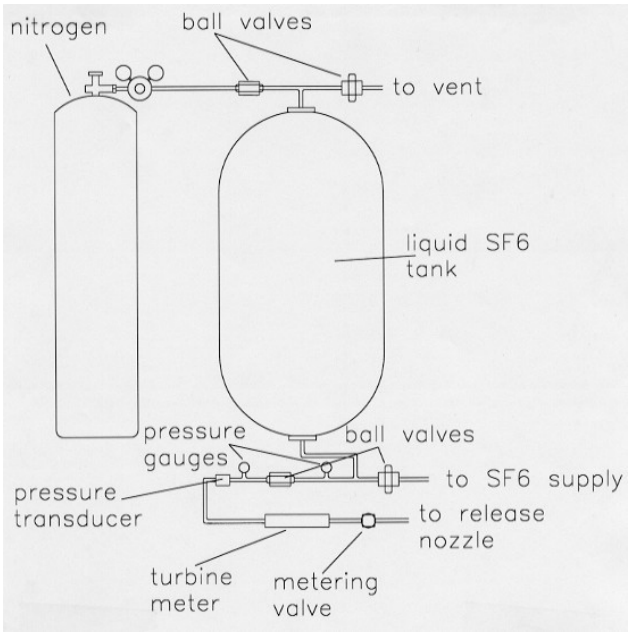

Figure 6. Components of the aircraft dissemination system.

The components of the system (Figure 6) are a nitrogen tank and regulator, a 0.2 m^3 filament wound aluminum cylinder (Structural Composites Industries of Pamona, California) an analogue pressure gauge and a pressure transducer (Dresser Industries of Stratford, Connecticut), a liquid turbine meter (model FTB-106, Omega Engineering of Stamford, Connecticut), four load cells (model RL2000 A-1K, Rice Lake Weighing Systems of Rice Lake, Wisconsin), a differential GPS system (OMNISTAR, Inc. of Houston, Texas), a CR-10 data logger (Campbell Scientific of Logan, Utah), and a laptop computer.

The liquid SF_6 tank has two 0.5 in diameter stainless steel tubes that extend into the interior of the tank at a 45° angle. One ends at the top of the tank and is used to introduce nitrogen into the tank. The other ends near the bottom of the tank and is the exit for liquid SF_6 (Figure 7).

The SF_6 used in tracer experiments is usually commercially supplied and shipped in DOT #AA 2015 cylinders containing 52 kg of material. The tracer is loaded into the release system by pressurizing the shipping cylinders with 1000 psig of nitrogen, inverting the cylinder so the liquid SF_6 flows directly out the valve, and allowing the pressure to drive the SF_6 into the liquid tank. Ball valves are used to open a vent to bleed off gas from the top of the tank as the SF_6 is introduced and to shut off the lines to the nitrogen tank and release nozzle. The storage tank can be filled with up to 300 kg of SF_6. Four load cells are used to measure the mass of SF_6 in the tank before and after the release as a check on the flow meter data.

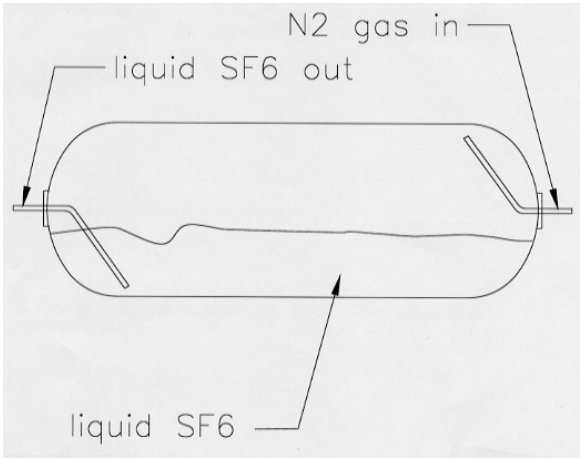

Figure 7. Configuration of the SF_6 tank inlet and outlet plumbing.

Dissemination is accomplished by driving SF_6 in its liquid state from the storage tank with 500 psig of nitrogen. The liquid flow rate is measured with a turbine meter. The flow rate is regulated with a valve that is manually adjusted based on the turbine meter reading. After the rate adjustment valve, the liquid SF_6 is at atmospheric pressure and begins to vaporize. A flexible stainless steel line with a one-inch inside diameter was used to transport the tracer to an outlet nozzle mounted at the tail eight inches from the skin of the aircraft. During the 3-min, condensation of atmospheric water vapor caused by cooling from vaporization of SF_6 resulted in the formation of a layer of ice on the outside of the tubing one to two cm thick. This had no effect on the dissemination rate.

Data from the pressure transducer, the flow meter, and the GPS data were collected by the CR-10 data logger and recorded and displayed on a laptop computer. The data collection rate is 4 Hz. Release data from each of the tests is found in Table 2.

3.4.2 Ground Release

Approximately 10 kg of SF_6 was released from a small pickup truck during the ground releases, again along a 10 km line. This system relied on the SF_6 vapor pressure in the cylinders to drive the release and a gas phase flow controller to regulate the flow rate. The decrease in vapor pressure from cooling during vaporization was small because only 10 kg of SF_6 was being released. Sufficient vapor pressure to maintain a constant flow rate was achieved by using two SF_6 cylinders configured in parallel to supply SF_6 (Figure 8). The release rate was nominally 1.5 kg min^{-1}. The cylinders were weighed before and after the release as a check on the measured flow rates. Continuous time and position information were provided by a differential GPS. Release rate, GPS time and position, and release line pressure are recorded at a rate of 4 Hz using a CR-10 data logger and a laptop computer.

Table 2. OLAD releases.

Test	Trial	Release vehicle	Average rate (kg min^{-1})	Standard deviation (kg min^{-1})	95% confidence (2σ)	Relative 95% confidence (%)
1	251	truck	1.52	3.6×10^{-2}	7.2×10^{-2}	4.7
2	252	truck	1.51	3.7×10^{-2}	7.4×10^{-2}	4.9
3	253	plane	32.88	1.97	6.0×10^{-2}	12.0
4	254	plane	33.00	1.75	5.3×10^{-2}	10.6
5	255	truck	1.50	5.4×10^{-2}	0.109	7.3
6-A	258-1	truck	1.52	3.6×10^{-2}	7.2×10^{-2}	4.7
6-B	258-2	truck	1.37	0.13	0.25	18.6
6-C	258-3	truck	1.49	4.6×10^{-2}	9.2×10^{-2}	6.2
7	258-4	truck	1.51	4.06×10^{-2}	8.0×10^{-2}	5.3
9	260	plane	32.93	1.41	2.8	8.6
10	261	truck	0.79	0.33	0.66	83
11	267	plane	32.84	2.29	4.6	14.0
12	268	truck	1.53[a]	3.1×10^{-2}	6.1×10^{-2}	4.0
			1.35[b]	2.9×10^{-2}	5.8×10^{-2}	42.9

a. After flow meter repair.
b. Complete release.

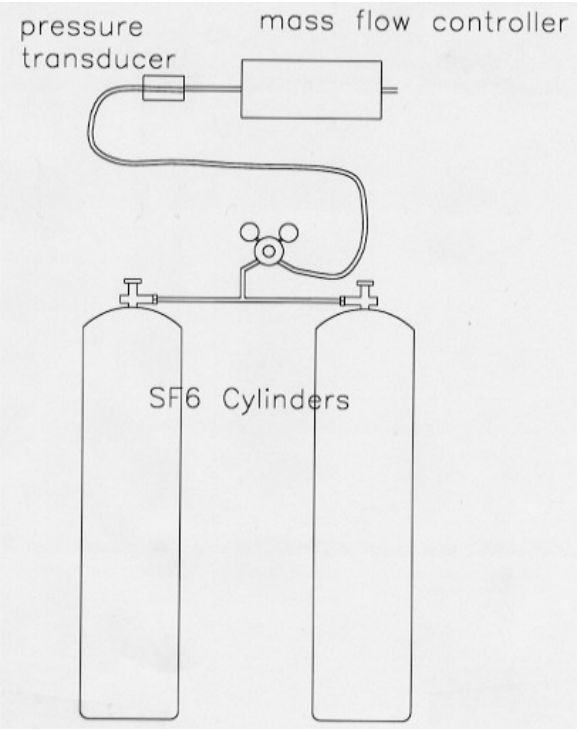

Figure 8. Components of the ground release dissemination system.

Mass flow controller failures occurred during three of the ground releases. The first failure was on 12 September 1997 during Test 5. The flow controller jammed at the start of the release and would not release SF_6. A spare controller was installed. The release was reinitiated after a delay of 12 min and was successfully completed. The second failure occurred on 18 September 1997 during Test 10. The release rate dropped in a stepwise manner two times during the transit of the release line. The third failure occurred on 25 September 1997 during Test 12 (Trial 268-1). The mass flow controller quit in the middle of the release. It was replaced with a spare unit and the release continued after a 5-min delay.

The release data shows that there is good agreement between the total mass release calculated from the flow meter data and the measured change in mass.

3.4.3 Quality Assurance

There were nine ground releases and four airborne releases. The mean release rate, the standard deviation, and the absolute and relative 95% (2σ) confidence limits are given in Table 2. The aircraft releases were all successful with a maximum relative 95% confidence limit of 14% (Test 11). The mass of tracer released calculated from the mass flow rate is in good agreement with the measured change in mass from the data taken from the load cells.

Six of the nine ground releases had 95% (2σ) confidence limits of less than 10%. The two Tests, 11 and 12, during which the flow controller failed have large relative confidence limits of 83% and 42%. In addition, there was one ground release, Test 6-B where the confidence limit is 18.6%. The reasons for these failures are not clear but we believe that they are related to the cooling of the flow controllers caused by the vaporization of the SF_6. The SF_6 used in the tests was 99.8% pure. A contaminant such as water vapor could condense in the cold flow controller and plug the regulator valve causing failure. The fact that the flow controller functioned normally after it was allowed the return to ambient temperature supports this conclusion. In the future, we will use a system with a design similar to the one used in the aircraft which will eliminate this problem.

3.5 SF_6 sampling methods

3.5.1 Continuous Analyzers

Continuous SF_6 concentration measurements were made using the TGA-4000 (Tracer Gas Analyzer) manufactured by Scientech Inc. of Pullman, Washington. This is a fast response instrument designed specifically to measure the concentration of SF_6 in ambient air. Six van-mounted instruments were deployed at the ends of each sampling line. One TGA was installed in an aircraft. The TGA instrument and calibration system is described in detail by Watson et al. (1998). It will be briefly described below.

The TGA-4000 uses an electron capture detector (ECD) to detect SF_6. The ECD is very sensitive to halogenated compounds such as chloro-fluorocarbons and SF_6. Its mass detection limit for these compounds is on the order of one picogram. The TGA-4000 is incorporated into an air sampling and calibration system that allows multi-point calibrations of the analyzer with a single calibration standard by changing the amount of calibration gas mixed into the ambient air flow. Zero air can also be substituted for the calibration gas and the incoming ambient sample diluted. In this way high sample concentrations can be brought into the calibrated range of the instrument when it over-ranges. Over-ranging occurs at approximately 7000 pptv.

The TGA signal along with real time differential GPS position, data from the flow controllers or flow meters, instrument temperatures, ambient pressure, and valve positions are collected by a CR-10 data logger at a rate of 4 Hz. The data are transferred to a laptop computer where they are stored and the TGA signal is graphically displayed.

Two quantities that are useful for evaluating instrument performance are the limit of detection (LOD) and the limit of quantitation (LOQ). The LOD is the lowest concentration at which there is 99% certainty that the analyte is detected. The LOQ is the minimum concentration, which can be measured with a relative error of ±30% at the 95% confidence level. The LOD is defined as three times the standard deviation obtained as the concentration goes to zero (σ_o) (Taylor, 1987). The quantity σ_o can be estimated by extrapolation to zero concentration of the standard deviations calculated for repeated measurements of a series of calibration concentrations or from a measurement of the signal noise. The LOQ is defined as ten times σ_o. The LOD and LOQ, as determined from instrument performance during OLAD, are given in Table 3. The value of σ_o was determined from analysis of signal noise. The confidence limits determined from laboratory measurements of calibration standards treated as unknowns are given in Table 4.

Table 3. Performance statistics for TGA-4000 continuous analyzers during OLAD.

Unit	σ_o (pptv)	LOD (pptv)	LOQ (pptv)
Aircraft	8.2	25	82
2	3.1	9.3	31
3	24	71	240
3[1]	14	42	138
4	3.3	10	33
5	5.7	17	57
6	10.1	31	101
7	14	42	140
mean	10	29	98
mean[1]	8	25	83

1. Excluding 9/24 & 9/25.

Table 4. Performance statistics for TGA-4000 continuous analyzers from laboratory measurements.

Standard concentration (pptv)	Mean measured concentration (pptv)	Standard deviation (pptv)	95% confidence ($2s$) Limit (pptv)	Relative 95% confidence limit
40	32.3	3.56	7	0.18
200	180	10.8	22	0.11
813	745	26.5	43	0.05
1560	1470	34.4	69	0.04
5000	5231	167	334	0.07

There is a fairly wide range in the performance of the seven instruments. LOQs range from 31 to 240 pptv. Unit 3 had the most noise: the average σ_o was 24 resulting in an average LOQ of 240. This instrument exhibited significant signal deterioration on 24 September and 25 September, the last two days tests were held. If these days are excluded, then the average LOQ for Unit 3 is 140.

This is in line with results from the other instruments. Therefore, when using data from Unit 3, caution should be used in interpreting the data from those days.

The response time for the TGA-4000 has been measured as 0.86 s (Benner and Lamb, 1985). We have confirmed this in our laboratory. No data files are generated if no SF_6 is detected by the TGA. Consequently, there are no data files for Test 3 (Vans 5, 6, 7), Test 5 (Vans 4, 5), Test 7 (Vans 4, 5, 6, 7), and Test 11 (Vans 4, 5, 6, 7).

A computer crash occurred in Van 6 during Test 1. Consequently there is no data from this Unit for Test 1. There is a large noise spike caused by a radio transmission in the plume detected during Test 4 by Van 7. The plume seen by Van 2 during Test 5 has a step caused by the initiation of sample dilution in response to instrument over-ranging in the high concentration plume. During Test 12, the aircraft unit did not fly.

3.5.2 Whole Air Samplers

The FRD whole air sampling method has been described in detail elsewhere (Watson, 1995; Watson et al., 1998). A brief description will be given here. The method is built around programmable air samplers, which fill twelve, one-liter Tedlar® bags housed in a removable cartridge, and an automated analytical system. The sampler can be programmed to fill bags during time periods ranging from ten minutes to several days. The bags are filled sequentially so that a single sampler can collect twelve consecutive, integrated samples before the cartridge must be changed. The unit is powered by a single "D" cell battery, which has sufficient capacity to fill 60 sample bags. Analysis is accomplished using gas chromatography with electron capture detection. A personal computer (PC) controls the system operation and records the raw detector signal as well as other important system parameters. The PC also processes the signal. The data is stored on disk in both raw and processed forms.

Calibration of the analytical system was performed using SF_6 in ultra zero air (Scott-Marin of Riverside, California) at the beginning of each analytical shift and after every 120 (ten sample cartridges) analyses. Control charts (Taylor, 1987) were also constructed for the entire experiment and for each test within the experiment. Four analytical systems were used to analyze the OLAD tests. They were run continuously throughout the program. A single test took approximately 8 hours to analyze; all tests were analyzed within 36 hours of sample collection.

The precision of the analytical method was determined using a linear fit of the standard deviation of the instrument response to each calibration standard versus concentration. The intercept of this fit is an estimation of the standard deviation at zero concentration or the baseline noise, σ_o. The LOD ($3\,\sigma_o$) and LOQ (σ_o) determined in this manner for each GC system are found in Table 5. GCs 1-3 were operated at a detector attenuation of 256. On this range, the background concentration of SF_6 could be resolved, but peaks over 300 pptv were clipped. When clipped peaks were encountered, the samples were run on GC 4. This GC was run on an attenuation of 2^{14}. The baseline noise level of this instrument is therefore treated separately from the other GCs in the table.

Table 5. Performance statistics for gas chromatographs estimated from calibration standards.

Unit*	σ_o (pptv)	LOD (pptv)	LOQ (pptv)
1	0.92	2.8	9.2
2	1.22	3.7	12.2
3	0.63	1.9	6.3
Means	0.92	2.8	9.2
4	10	30	100

*Units 1-3 attenuation 256, unit 4 attenuation 2^{14}

The precision of the analysis method can also be estimated from the reanalysis of samples. During OLAD, 205 samples were analyzed twice. The results were highly correlated. A linear fit between the two analyses resulted in a line with a slope of 0.93 ± 0.01, an intercept of 9 ± 10 pptv, and a correlation coefficient (r^2) of 0.98 (Figure 9). Since both the absolute and relative differences in the measurements are a function of the concentration of SF_6 in the sample, the absolute and relative differences between duplicate samples over a series of concentration ranges give the most meaningful estimate of analytical precision. The mean absolute difference is defined as the absolute value of the difference between the first analysis and the second analysis. The mean absolute relative difference is defined as the mean absolute difference divided by the average of first and second analyses. These quantities, over seven concentration ranges, are given in Table 6. If the standard deviation of the quantity is greater than the mean, then it, rather than the mean is used to determine the confidence interval. This replicate analysis data places a somewhat higher value on the analytical LOQ of 50 pptv.

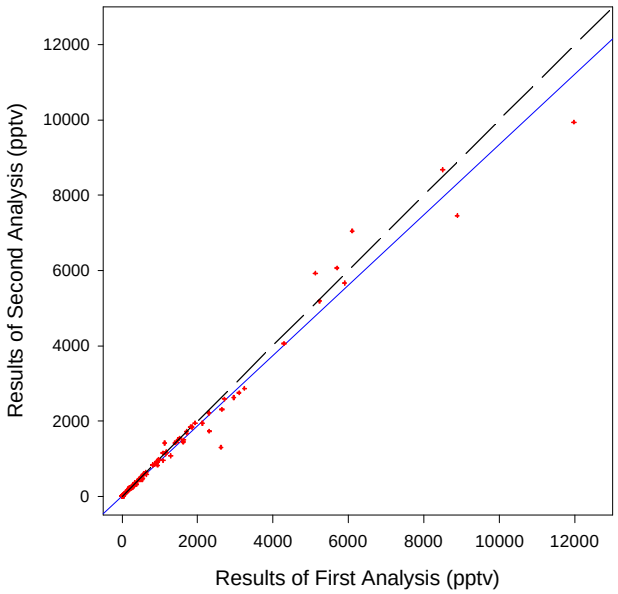

Figure 9. Comparison of reanalysis of samples. The solid line is a linear fit to the data: y = (0.93 ±0.01) x + (9 ±10), r^2 = 0.98, N = 205. The dashed line is y = x.

Table 6. Performance statistics for gas chromatographs estimated from replicate analyses.

SF_6 range (pptv)	Mean absolute difference (pptv)	Standard deviation (pptv)	Mean absolute relative difference	Standard deviation	Relative 95% confidence level (2σ)	Number of points
< LOD = 3	2.2	1.4	0.51	0.30	1.0	10
< LOQ = 10	0.64	0.85	0.14	0.20	0.40	145
LOQ - 50	3	6	0.14	0.31	0.62	49
50 - 100	1.4	1.4	0.02	0.03	0.06	7
100 - 500	13	14	0.05	0.06	0.12	44
500 - 1000	33	35	0.05	0.06	0.12	18
> 1000	308	452	0.10	0.12	0.24	36

The samplers were programmed to execute 200 pumping cycles during each 15-min sampling period. The samplers on the first and second lines were usually programmed to start at the same time. The samplers on the third line were usually programmed to start 30-min later than Lines 1 and 2.

During OLAD, 4236 ambient air samples were collected. Sampler failures, incorrectly handled cartridges, or analytical errors made 607 of these samples unusable. There were 173 or 4% of the samples which were suspect. The resulting data recovery rate was 82%. The sample recovery rate and suspect samples are discussed in detail below. The SF_6 plume missed the sampler grid during Tests 7, 8, and 13. Samples from these tests were not analyzed.

The precision and accuracy of the laboratory analytical method does not necessarily reflect the precision and accuracy of the SF_6 measurements made by collecting field samples and analyzing them in the laboratory. The processes of sampling and sample handling introduce additional uncertainties into the measured quantities. The accuracy and precision of the sampling method were determined using dynamic blanks, dynamic spikes, and duplicate samples. The details of collecting these samples are described by Watson et al. (1998).

One blank sampler and one spike sampler were located at Position 8 on each sampling line. Duplicate samplers were located at positions 1 and 15 of each line (see Appendix A for sampler locations). The blanks provide a measurement that is equivalent to a baseline noise measurement of an analytical instrument as well as a means of detecting contamination. Analysis of the results from 159 blank samples showed that the mean level of SF_6 measured in these samples was 4 pptv with a standard deviation of 3 pptv, indicating that there was no contamination (Figure 10). From this result we determined that the noise level of the sampling method was 4 pptv resulting in an LOD of 12 pptv and an LOQ of 40 pptv. These values are higher than the equivalent values determined for the analytical method and are the limiting values for the coupled sampling and analysis system.

The spike samples provide a calibration of the sampling method that is equivalent to the calibration of an analytical instrument. Comparison of the concentration values resulting from the analysis of 127 spiked samples to the concentration of the standards as reported by the supplier (Figure 11) resulted in a linear fit with a slope of 0.970 ± 0.004, an intercept of -13 ± 7 pptv, and a correlation coefficient (r^2) of 0.997. The standard deviation of the results for these spikes versus reported concentration was also plotted and fit with a straight line (Figure 12). The resulting equation, y = (0.02 ± 0.008) x + (24 ± 15) (r^2 = 0.36) can be used to estimate the relative standard deviation of measurements over 100 pptv as 2%. This value is in good agreement with the measured standard deviations for the spike samples presented in Table 7.

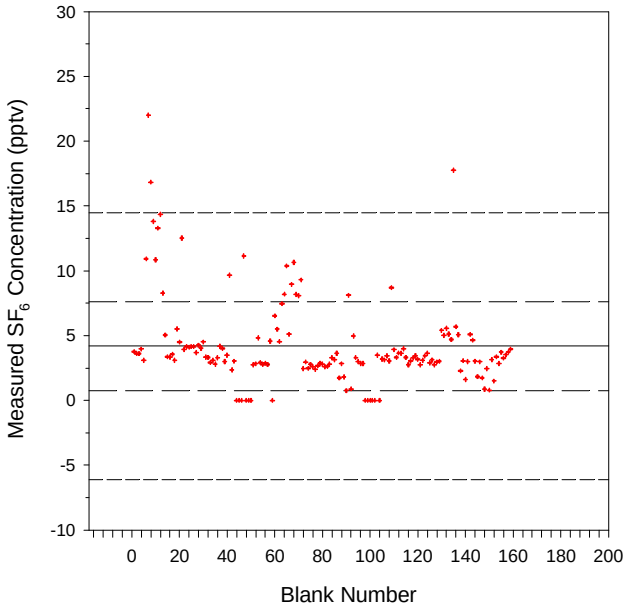

Figure 10. Results of analysis of blank samples. The solid line is the mean. The dashed lines are one and two standard deviations about the mean. Mean = 4 ± 3.4 pptv, N = 159.

Table 7. Results of analysis of spike samples.

Standard #	Standard conc. (pptv)	Mean measured conc. (pptv)	Standard deviation	Mean absolute difference	Mean relative difference	Number of points
1	2.0	4.0	3.7	2.1	0.52	9
2	3.5	5.1	3.3	2.0	0.38	11
3	8.3	8.0	1.5	1.0	0.18	10
4	20	19.9	1.5	1.1	0.06	10
5	40.6	39.9	2.0	1.2	0.04	10
6	83.5	80.2	5.4	4.0	0.06	10
7	200	182	21	19	0.11	11
8	410	379	54	35	0.16	10
9	844	834	29	21	0.03	10
10	1560	1483	66	82	0.4	9
11	2065	1868	173	197	0.08	6
11a	2512	2290	123	221	0.05	5
12	5240	5161	60	84	0.01	9

The precision of the sampling method can also be estimated by comparing the results of 205 duplicate samples. Concentrations measured in the duplicate samples were highly correlated (Figure 13). A linear fit between concentrations obtained from these samples, weighted with the standard deviation given by the equation from Figure 12, resulted in a slope of 0.940 ± 0.006, an intercept of 5 ± 8, and a correlation coefficient (r^2) of 0.99. The relative difference between duplicate samples can be examined by grouping the data into concentration ranges. This was done for three ranges: less than 100, 100 to 500, and greater than 500 pptv. The ranges were chosen to include a sufficient number of points in each group to enable a meaningful statistical analysis and still provide enough groups to establish the concentration dependence. A relative difference for each range was then established by taking the absolute value of the difference between the two measurements, and dividing by their average as shown in Table 8. The precision of the SF_6 whole air sampler data can be estimated from this analysis at the 95% (2σ) confidence level as ±56% for the 0 to 100, ±24% 100 to 500 pptv range and ±20% for values over 500 pptv.

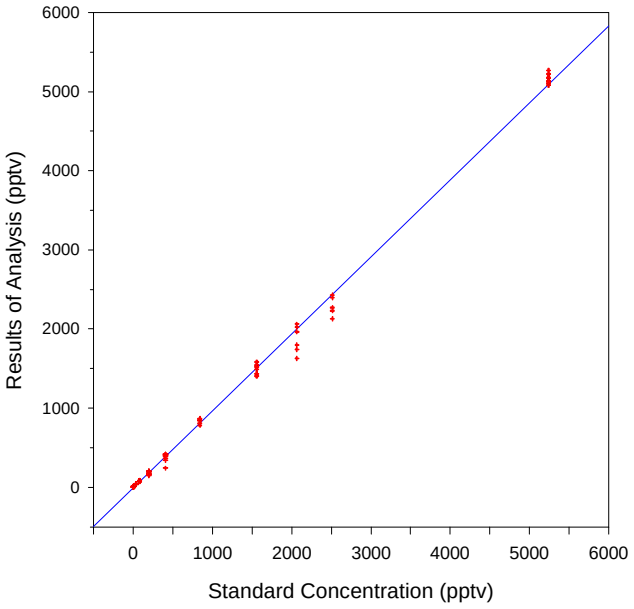

Figure 11. Results of the analysis of 127 spiked samples versus the concentration of the standards. The solid line is a linear fit to the data: y = (0.97 ± 0.004) x + (13 ± 7), r^2 = 0.997, N = 127.

Table 8. Performance statistics for the whole air sampling method over three concentration ranges estimated from duplicate samples.

SF_6 range (pptv)	Mean absolute difference (pptv)	Standard deviation (pptv)	Mean absolute relative difference	Standard deviation	Relative 95% confidence level (2σ)	Number of points
<100	2.9	5.63	0.25	0.28	0.56	139
100 - 500	19	24	0.09	0.12	0.24	33
> 500	220	228	0.10	0.09	0.20	33

The poor sample recovery rate of 82% was caused by a large number of sampler failures. We have determined that this resulted from a problem with the sampler program that caused an incorrect

memory address to be loaded into the sampler microprocessor under certain conditions. See Appendix K for a description of the sampler program downloading system.

During the first two field experiments using the TimeWand II as downloaders, an unexpectedly large number of intermittent failures were observed on the air samplers. Efforts to locate the cause of the problem during these studies were unsuccessful. During the early spring of 1998, an exhaustive test program was undertaken to identify and correct this problem. The testing was successful in duplicating the error conditions, but several months of effort were required before the cause could be identified.

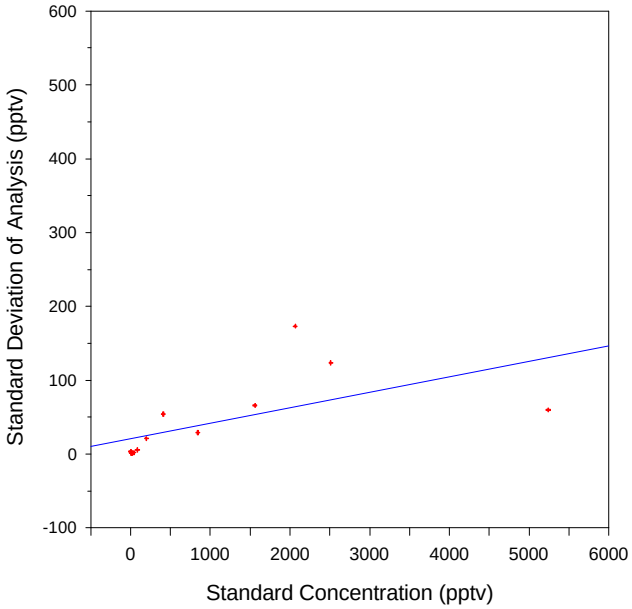

Figure 12. The standard deviation of measurements of spiked samples versus the concentration of the standards. The solid line is a linear fit to the data: $y = (0.02 \pm 0.008)\ x + (24 \pm 15)$, $r^2 = 0.36$, N = 205.

The downloader programs the sampler by sending it a string of 26 data bytes over an RS-232 serial connection. This string contains the control parameters for the sampler including start time, time per bag, number of strokes per bag, etc. One of the parameters in this string was the address of the RS-232 receive buffer in sampler memory. This was erroneously being sent as 0 instead of 26.

When the sampler was first powered up, the receive buffer address was correctly initialized to 26. The first download was always successful, but the receive buffer address was reset to 0 which points to active memory. Subsequent downloads would then write their data into active memory locations. If the timing of the download was such that data was written into locations the microcontroller was currently updating, corrupted data values would be left in memory and the sampler would behave in very unusual ways. Consequently, the problem would never show up on first downloads and only sometimes on subsequent downloads. When it did show up there were a variety of seemingly unrelated symptoms.

This intermittent nature of the receive buffer address problem made it extremely difficult to diagnose. The TimeWand II download program underwent extensive testing before being used in any field projects. However, all the testing was done with the samplers being reset just before the test and the problem did not show up.

During OLAD, the problem was dealt with by keeping spare samplers on each line. The operators checked each deployed sampler as the test started to see if it was operating properly. If a problem was detected, one of the spares was programmed and substituted for the malfunctioning sampler. After OLAD, the cause of the problem was identified, and a simple software modification on the TimeWand II implemented to correct it.

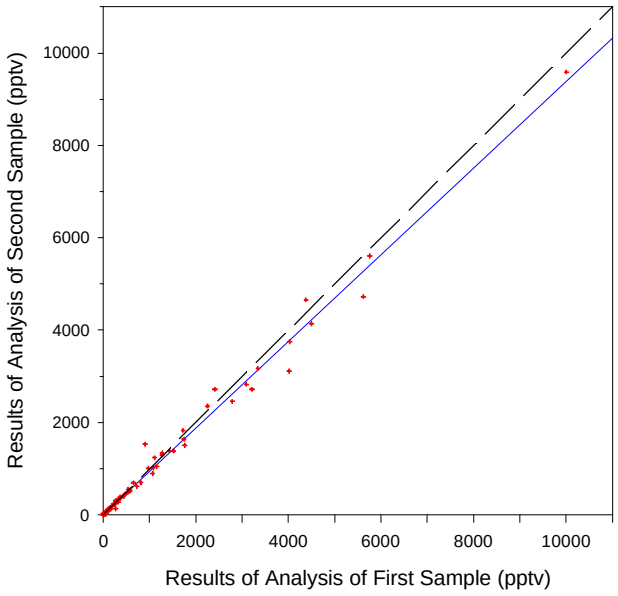

Figure 13. Results of analysis of duplicate samples. The solid line is a linear fit to the data: $y = (0.94 \pm 0.006)\ x + (5 \pm 8)$, $r^2 = 0.99$, N = 205. The dashed line is y = x.

There were 173 samples where the measured concentration was obviously the result of contamination or a source of SF_6 other than that of the release. During Test 1, there were 138 of these suspect samples. Most were in samples taken from Line 3. Higher concentrations were seen on Line 3 than Line 1 and at times before the tracer was detected on Line 1. Two co-located TGA-4000s did not measure any SF_6 during these times. This points to a contamination problem. All sample cartridges were cleaned and analyzed for contamination before use in OLAD. One possible explanation for the contamination is the use of the analytical technician as a driver of the release truck during the first several releases. The release operator was also in the analytical lab during the early tests and could have contaminated samples. The operator's breath was analyzed and found to contain several parts per million of SF_6. These facts could explain the extreme levels, as high as 33000 pptv, observed in Test 1. The suspect concentrations are reported in the data and are flagged with a "7". They are not used in the data analysis.

4 Methodology

4.1 Meteorological Data

The 2-m wind speed and direction were recorded every ten seconds from eight towers located on the test grid. Vector averages of wind direction and vector and scalar averages of wind speed were calculated over time periods of interest. Error limits for wind speed are conventional standard deviation calculations. The error in the wind direction, σ_θ, was calculated using the following algorithm (Yamartino, 1984):

$$\theta = \tan^{-1}\left(\frac{U_x}{U_y}\right) \tag{22}$$

where:

$$U_x = \frac{1}{N}\sum_{i=1}^{N} \sin\theta_i \tag{23a}$$

$$U_y = \frac{1}{N}\sum_{i=1}^{N} \cos\theta_i \tag{23b}$$

The standard deviation of the mean wind direction is given by:

$$\sigma_\theta = \sin^{-1}(\varepsilon)\,(1 + 0.1547\,\varepsilon^3) \tag{24}$$

where:

$$\varepsilon = \left[1 - (U_x^2 + U_y^2)\right]^{1/2} \tag{25}$$

4.2 Whole Air Sampler Data

The variability of the SF_6 concentrations on each sampling line was quantified by calculating a relative standard deviation (*rsd*) for each contemporaneous sample. The *rsd* is a value representing a snapshot of the SF_6 concentration along the sampling line during a sampling period. This value is calculated by determining a mean concentration and standard deviation of the SF_6 concentration of contemporaneous samples from each line and calculating the ratio of the standard deviation to the

mean. Mathematically this is expressed as:

$$C_{ik} = \frac{1}{N_1} \sum_{j=1}^{N_1} C_{ijk} \tag{26}$$

where C_{ijk} is the measured concentration in an individual sample, i is the sampling line number and ranges from 1 to 3, j is the location number and ranges from 1 to 15, k is the sample bag number and ranges from 1 to 12, and N_1 is the number of sample locations averaged (up to 15 depending on sample recovery). Note that this is a different system then used for the location numbering.

Standard deviations for these means, σ_{ik}, are calculated in the usually manner. The relative standard deviation (*rsd*) of C_{ik} is given by:

$$rsd_{ik} = \frac{\sigma_{ik}}{C_{ik}} \tag{27}$$

The mean relative standard deviation (*mrsd*) is calculated by classifying the *rsd* in various groups to make comparisons. For example, all samples in a line for an entire test can be compared. A mean relative standard deviation (*mrsd*) for all samples in each line for a test is given by:

$$mrsd_i = \frac{1}{N} \sum_{k=1}^{N} rsd_{ik} \tag{28}$$

where N equals 12. This comparison is somewhat misleading because samples of background levels of SF_6 are near the instrument detection limit and are likely to have large *rsd* values. A more meaningful comparison is to group the *rsd* by mean SF_6 concentration and calculate *mrsd* over various concentration ranges. The standard deviation of this quantity is also computed in the usual manner. Values of *mrsd* computed for all lines in the experiment are reported in Tables 9 and 10. The values computed for individual tests are reported in Appendix B through J.

4.3 Continuous Analyzer Data

Four methods were used to calculate Gaussian fits to the continuous analyzer data. These methods are explained in detail by Bowers et al. (1994). The along-wind concentration distribution is assumed to be of the form:

$$\chi(t) = \chi_o \exp\left[\frac{1}{2}\left(\frac{t - t_o}{\sigma_t}\right)^2\right] \tag{29}$$

where $\chi(t)$ is the SF_6 concentration at time t after the release, χ_o is the peak SF_6 concentration, and t_o is the time after the release that the center of mass passed the analyzer. The passage time of the center of mass is given by:

$$t_o = \frac{\Sigma \chi_i t_i}{\Sigma \chi_i} \tag{30}$$

4.3.1 Method 1: Center of Mass

The peak arrival time, t_o, peak width, σ_t, and maximum concentration, χ_o are calculated directly using equation 30 and the following expressions:

$$\sigma_t^2 = \frac{\Sigma \chi_i t_i^2}{\Sigma \chi_i} - t_o^2 \tag{31}$$

$$\chi_o = \frac{A}{(2\pi)^{1/2} \sigma_t} \tag{32}$$

A is the numerically integrated area of the measured peak.

4.3.2 Method 2: Peak / Area Match

In this method, along-wind diffusion is determined by the following expression

$$\sigma_t = \frac{A}{(2\pi)^{1/2} \chi_o} \tag{33}$$

The position of t_o, the time of the peak maximum, is adjusted to minimize rms error between the actual profile and the fitted Gaussian profiles.

4.3.3 Method 3: Width at 10%

A Gaussian profile has the property that at the two points where the dependent variable is 10% of the profile maximum, the difference in the independent variables is 4.3σ. The difference between the two times when the concentration of the leading and trailing edges of the profile was 10% of the peak value were determined and σ_t calculated using:

$$\sigma_t = \frac{t_{10\%} - t_{10\%}}{4.3} \tag{34}$$

Again, the position of t_o, the time of the peak maximum, is adjusted to minimize rms error between the actual profile and the fitted Gaussian profile.

4.3.4 Method 4: Width at 2/3 Area

Another property of a Gaussian profile is 2/3 of the area is within $t_{o-\sigma}$ and $t_{o+\sigma}$. This property can be used to determine σ_t in the same manner as the width at 10% method.

$$\sigma_t = \frac{t_{A=67\%} - t_{A=67\%}}{2} \tag{35}$$

The position of t_o, is adjusted to minimize rms error.

4.4 Coordinate Transformation

The speed at which the SF_6 was transported, the width of the SF_6 cloud as it passed the sampling locations, and the maximum concentration seen at each sampling location are three transport parameters of particular interest. Analysis of these quantities requires the conversion of spatial information recorded as latitude and longitude into a coordinate system based on linear measurement. This was accomplished in three steps. First, the latitude and longitude data of the release path and sampler locations were converted into a distance from an arbitrary origin selected at 40° N, 113° W. A length of a degree of latitude of 85.398 km and of a length of one degree of longitude of 111.0475 km was used for this conversion (List, 1951) as follows:

$$x = 85.398 \left[longitude - (-113) \right] \tag{36}$$

$$y = 111.0475 \left[latitude - 40 \right] \tag{37}$$

Second, the coordinate system was translated to make the west end of the release line the origin. Third, the coordinate system was rotated 42° to make the release line the y axis. The result is a Cartesian coordinate system where the sampling lines are in the first quadrant and parallel to the y axis (Figures 14 and 15).

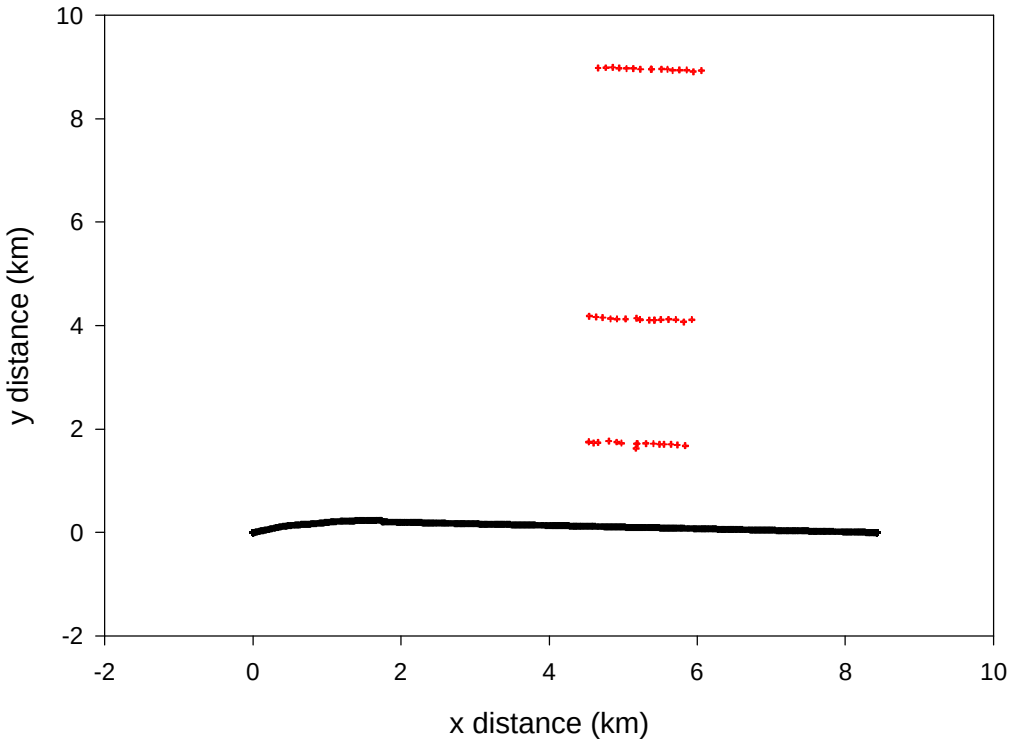

Figure 14. Analysis coordinate system for ground releases. The black line represents the ground release line and the red crosses represent the individual samplers that comprise each sampling line.

4.5 Transport Properties

An average perpendicular distance from the release line to each sampling line was calculated. A trajectory distance was estimated using the mean wind direction and this perpendicular distance. The mean wind was calculated, over the entire test range, from the period beginning with the start of the release until the cloud had passed over the sampling line.

$$d_t = \frac{d_\perp}{\sin \phi} \tag{38}$$

where d_t is the distance along the trajectory, $d_\perp$ is the perpendicular distance from the sampling line to the release line, and ϕ is the average wind direction adjusted for the new coordinate system.

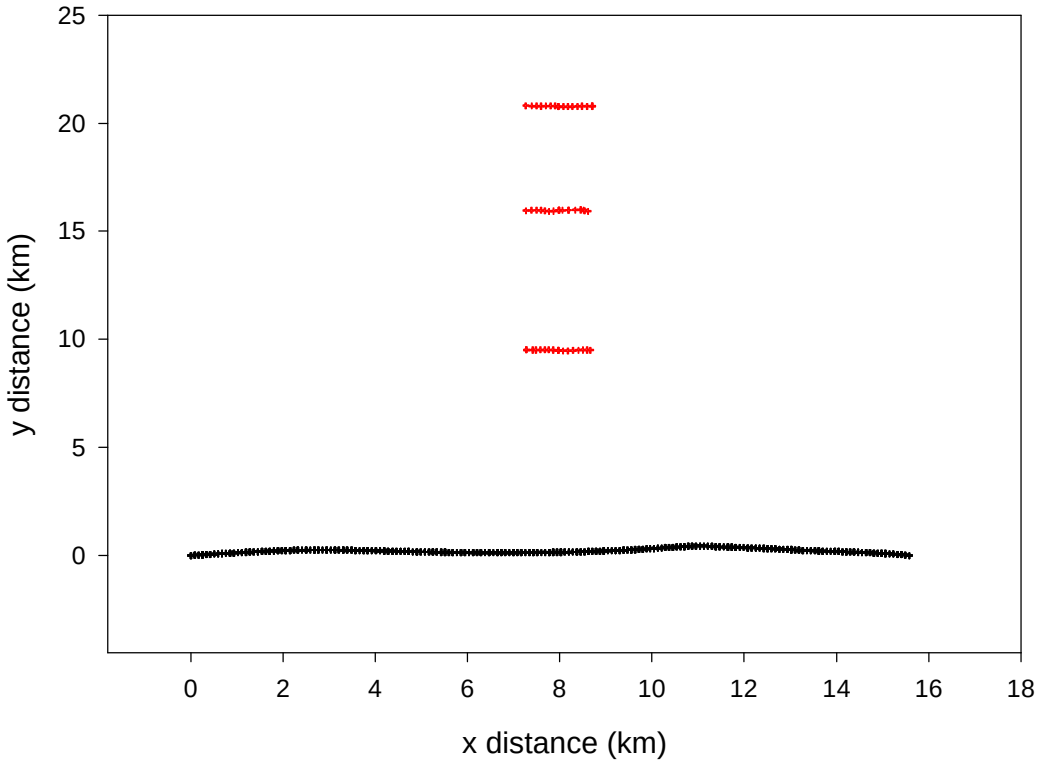

Figure 15. Analysis coordinate system for aircraft releases. The black line represents the aircraft release line and the red crosses represent the individual samplers that comprise each sampling line.

The peak arrival time was calculated from the average of the four values of t_o determined from the Gaussian fits. This value was used along with the average release time to calculate an SF_6 transit time (Δt). The transit time and the mean trajectory distance were used to calculate the SF_6 velocity. The peak width parameter, σ_t, averaged from the fits and the SF_6 velocity were used to calculate the spatial peak width, σ_x. All stated error limits on calculated values were determined by the addition in quadrature of the products of partial derivatives of the dependent variable, with respect to each independent variable and the uncertainty in the independent variable. The coordinate transformation and trajectory calculations were performed using a Fortran computer program. The SF_6 velocity and peak width calculations were performed using routines in the Sigma Plot spreadsheet transform language. The results of these calculations for each test are presented in Appendix B through J.

5 Results and Discussion

One of the primary purposes OLAD was to test the uniformity of the crosswind concentration measurements obtained following a dissemination of SF_6 tracer, at a constant rate, in a crosswind line. The line was 10 km long, sufficiently long that edge effects should be eliminated from the middle of the resulting cloud at least 10 km down wind. We measured the variability across the center region of the cloud with an array of samplers. Our quality control procedures allow us to discriminate between the concentration variations resulting from experimental uncertainty and the variations caused by atmospheric mechanisms. The duplicate samples provide the criterion; if the variability in tracer concentration across the line is greater than the variability of the duplicate samples, then the variations are the result of atmospheric effects. To the best of our knowledge, OLAD is the first experiment to directly test this assumption.

5.1 Individual Test Results

5.1.1 Test 1

During Test 1, the mean wind speed was 1 ± 0.5 m s^{-1} with a mean direction of $175° \pm 45°$. In the grid coordinate system this corresponds to a wind direction of 220°. The SF_6 concentrations measured in the whole air samples taken on Line 1 were highly variable (Table B1, Figure B1). The *rsd* for all bags on this line was 1.1 with a standard deviation of 1.0. The mean peak concentration (Table B2) was 9960 pptv with a standard deviation of 2000 pptv and a *rsd* of 0.2. This variability is the same as the results of the duplicate samplers for this concentration range. The Line 1 *rsd* for all samples in the concentration range < 100 pptv was 1.2 ± 0.9 and for the concentration range > 500 pptv was 1.0 ± 1.1. These values are both greater than the duplicate results. Because of the wind direction, the SF_6 line missed the first six samplers on Line 2 (Figure B2) and missed Line 3 entirely, therefore, data from this test cannot be used for evaluation of the line source assumption or along-wind dispersion.

The SF_6 velocities calculated from data recorded by the continuous analyzers located on Line 1 were 0.8 ± 0.1 and 0.5 ± 0.1 m s^{-1} and were not in agreement (Table B3). The velocities calculated from the Line 2 analyzer data were in agreement and had a mean of 1.2 ± 0.6 m s^{-1}. All calculated SF_6 velocities were in agreement with the mean 2-m wind speed. The along-wind dispersion parameter, σ_x, calculated from the two sets of Line 1 data were in agreement with a mean of 570 ± 317 m. The Line 2 σ_x values were also in agreement with a mean value of 710 ± 590 m. The arrival times calculated from the Line 1 data were not in agreement with values of 2200 ± 270 s and 3700 ± 640 s. The Line 2 arrival times were not in agreement as well with values of $6{,}100 \pm 180$ s and 3600 ± 1800 s. The peak SF_6 concentrations seen by the two analyzers on Line 1 were in agreement, principally because of the large error limits. The mean peak concentration was 9300 ± 6800 pptv. The peak concentrations detected by the analyzers on Line 2 were not in agreement reflecting passage of the edge of the tracer cloud passing over the western end of the sampling line. The peak SF_6 concentration values calculated using data from the analyzer on the western end of the line was 340 ± 160 pptv and the value from the eastern end was 6800 ± 1050 pptv.

Eight aircraft cloud passes were recorded for Test 1 at altitudes between 20 and 50 m above ground-level (agl) (Table B4). The first SF_6 detected by the aircraft analyzer was recorded at 69 minutes after the release at a concentration of 70 ± 40 pptv, an altitude of 50 m above ground-level (agl) and a distance of 1500 m downwind of the release line. This was well after the SF_6 had been detected on the first sampling line 36 minutes after the release at a concentration of 9300 ± 6800 pptv, and a distance of 1616 m. This delay at detecting the SF_6 at 50 m agl indicates that the tracer remained close to the ground during the first hour of the test. There was no discernable correlation between σ_x and downwind distance or time.

5.1.2 Test 2

The mean wind speed ranged from 2.9 to 3.2 m s^{-1} during Test 2 with a direction of 141 ± 5° (Table C1). This wind direction is 183° in grid coordinates, which is nearly perpendicular to the sampling lines. The mean maximum concentration seen on the first line was 1800 pptv with a standard deviation of 900 pptv. This results in a *rsd* of 0.5, well above the significant level for that concentration range. The peak concentrations for Lines 2 and 3 showed *rsd* of 0.1, well below the significant level. Overall, *mrsd* for all concentration ranges were well above significant levels (Table C2).

The SF_6 velocities calculated from the data recorded by the continuous analyzers located on Line 1 were in agreement at 4.6 ± 1.2 m s^{-1} (Table C3). The velocities calculated from the Line 2 analyzer data were in agreement and had a mean of 5.0 ± 0.6 m s^{-1}. The velocities calculated from the Line 3 analyzer data were also in agreement and had a mean of 5.5 ± 0.2 m s^{-1}. All calculated SF_6 velocities were significantly greater than the mean 2-m wind speed. The along-wind dispersion parameter, σ_x, calculated from the two sets of Line 1 data were in agreement with a mean of 305 ± 140 m. The Line 2 σ_x values were in agreement with a value of 820 ± 60 m. The Line 3 σ_x values were also in agreement with a value of 1135 ± 90 m. The peak arrival times were in agreement for all lines. The Line 1 arrival time had a mean of 350 ± 155 s; Line 2, 795 ± 100 s; and Line 3, 1600 ± 65 s. The peak SF_6 concentrations calculated from the data taken by the pairs of analyzers on Line 1, 2, and 3 were not in agreement. Calculations using the Line 1 data resulted in values of 10700 ± 530 pptv and 16800 ± 1400 pptv; the results from Line 2 were 2100 ± 730 pptv and 3100 ± 210 pptv; and the peak Line 3 results were 1000 ± 70 pptv and 700 ± 50 pptv.

Twelve aircraft cloud passes were recorded for Test 2 at altitudes between 9 and 40 m agl (Table C4). The aircraft analyzer first detected the SF_6 23 minutes after release at a concentration of 870 ± 200 pptv, an altitude of 40 m agl and a distance of 8000 m downwind of the release line. This was well after the SF_6 had been detected on the ground at the first sampling line. The tracer was first observed on the ground 14 minutes after the release, on Line 1 at a distance of 1616 m, and with a concentration of 16800 ± 1400 pptv. This indicates that the tracer remained close to the ground during the first twenty minutes of the test. The last pass through the cloud occurred one hour and 44 minutes after the release, at a position 26,000 m from the release line, and at an altitude of 30 m agl. Figure C3 shows that all the aircraft encounters with the tracer cloud occurred downrange of the first two sampling lines. There was a significant correlation between σ_x and downwind distance

(Figure C5). A linear fit of σ_x versus distance data resulted in a slope of 0.81 and intercept of 127, and a correlation coefficient (r^2) of 0.81. The transport velocity of SF_6 calculated from the aircraft data had a mean of 5.0 with a standard deviation of 0.6 m s^{-1}. This is in agreement with the SF_6 velocity observed on the ground of 5.0 ± 0.4 m s^{-1}.

5.1.3 Test 3

Test 3 was an aircraft release. During this test, the SF_6 cloud moved very slowly. Apparently, the nocturnal inversion broke up before the SF_6 cloud had traveled to sampling Line 2. The continuous analyzers on sampling Line 2 did not detect any SF_6 until 3 hours after the release, after the samplers had stopped. Only samples from Line 1 were analyzed and aircraft GPS data was not recorded during this test. No further analysis was performed on this data.

5.1.4 Test 4

The tracer was released from the aircraft during Test 4. The mean wind speed ranged from 4.1 to 4.4 m s^{-1} with a standard deviation of 1 m s^{-1} (Table D1). Wind direction was 147 ± 7° resulting in a wind direction in grid coordinates of 189°. The peak concentrations in samples collected during this test exhibit a much different pattern than the samples collected in the ground release trials. This reflects the differences in atmospheric structure between ground-level and 100 m agl in a stable boundary layer and the greater distances from the release line of the sampling grid. Peak values are lower overall and the second and third sampling lines had peak values greater than the first line. The Line 1 mean peak concentration was 508 ± 140 pptv giving a *rsd* of 0.27. The Line 2 mean peak concentration was 690 ± 201 pptv for a *rsd* of 0.29. The Line 3 mean peak concentration was 580 ± 105 pptv for a *rsd* of 0.18 (Table D2). The *mrsd* values were all in agreement or nearly in agreement with the duplicate sampler values.

The SF_6 transport speeds, calculated from the data recorded by the two continuous analyzers located on Line 1, were in agreement at 10 ± 1 m s^{-1}. The velocity calculated from the single analyzer providing data on Line 2 was 7.7 ± 0.3 m s^{-1}. The velocities calculated from the Line 3 analyzer data were not in agreement and had values of 7.3 ± 0.3 m s^{-1} and 6.7 ± 0.2 m s^{-1}. All calculated SF_6 velocities were significantly greater than the mean 2-m wind speed. The along-wind dispersion parameter calculated from the two sets of Line 1 data were not in agreement and had values of 1100 ± 120 m and 915 ± 100 m. The Line 2 σ_x value was 2250 ± 150 m. The Line 3 σ_x values were in agreement with a mean value of 3275 ± 700 m. The arrival times calculated for Lines 1 were in agreement with a mean value of 975 ± 160 s. The single value calculated for Line 2 was 2060 ± 90 s. The arrival times calculated for Line 3 were not in agreement with values of 2850 ± 140 s and 3100 ± 100 s. The peak SF_6 concentrations seen by the two analyzers on Line 1 were in agreement, with a mean value of 2400 ± 180 pptv. The single peak SF_6 concentration calculated from data taken on Line 2 was 1300 ± 70. The peak SF_6 concentrations calculated from data taken by the two analyzers on Line 3 were not in agreement, with values of 700 ± 180 and 930 ± 35.

Fourteen aircraft cloud passes were recorded for Test 4, at altitudes ranging from 17 to 260 m agl (Table D4). The aircraft analyzer first detected the SF_6 16 minutes after release at a concentration of 370 ± 260 pptv, an altitude of 155 m agl, and a distance of 13800 m downwind from the release line. This was at about the same time the cloud was detected on the ground at a distance of 9562 m. The last pass through the cloud 124 minutes after the release, at a position 39000 m from the release line, and at an altitude of 40 m agl. There was no significant correlation between σ_x and downwind distance. The transport velocity of SF_6 calculated from the aircraft data had a mean of 8.6 with a standard deviation of 2.8 m s^{-1}. This is in agreement with the mean SF_6 velocity observed on the ground of 8.3 ± 1.6 m s^{-1}.

5.1.5 Test 5

During Test 5, the 2-m mean wind speed was 0.9 to 1.1 m s^{-1} with a standard deviation ranging from 0.3 to 0.4 m s^{-1}. The mean direction was 128° with a standard deviation of 17° (Table E1). This corresponds to a direction of 160° in the grid coordinate system. Mean peak concentration measured in samples collected on Line 1 was 7500 with a standard deviation of 4900 resulting in a *rsd* of 0.64. Mean peak concentration on Line 2 was 4,800 with a standard deviation of 1400 resulting in a *rsd* of 0.29 pptv. Mean peak concentration on Line 3 was 330 with a standard deviation of 70 resulting in a *rsd* of 0.22 pptv. Again, the variability of Line 1 was greater than expected from measurement error while the variability in Lines 2 and 3 were close to and in agreement with those determined from the duplicate samples. Overall, the *mrsd* for concentration ranges 0 - 100 pptv was 0.7, 100 - 500 pptv was 0.4, and > 500 pptv 1.0 (Table E1). These values were all greater than the values expected from measurement error alone.

The SF_6 transport speeds calculated from the continuous analyzer data collected on Line 1 were in agreement with a mean of 1.1 ± 0.2 m s^{-1} (Table E3). The velocities calculated from the Line 2 data were in agreement and had a mean of 1.4 ± 0.1 m s^{-1}. There was no data from the Line 3 analyzers. All calculated SF_6 velocities were in agreement with the mean 2-m wind speed. The along-wind dispersion parameter calculated from the two sets of Line 1 data were in agreement and had a mean value of 420 ± 70 m. The Line 2 σ_x values were in agreement with a mean value of 880 ± 300 m. The transport times calculated for Line 1 were not in agreement with values of 1400 ± 95 s and 1630 ± 95 s. The Line 2 transport times were also not in agreement with values of 3200 ± 60 s and 2900 ± 95 s. The peak SF_6 concentrations calculated from the Line 1 data were in agreement, with a mean value of 1500 ± 155 pptv. The peak SF_6 concentrations from Line 2 data were not in agreement with values of 3200 ± 60 m and 2900 ± 95 m.

Twenty-nine aircraft cloud passes were recorded for Test 5 at altitudes ranging from 16 to 260 m agl (Table E4). The aircraft analyzer first detected the SF_6 17 minutes after release at a concentration of 1500 ± 840 pptv, an altitude of 24 m agl and a distance of 2170 m downwind of the release line. This was before the cloud was detected on the ground 23 minutes after release, at a distance of 1616 m, and with a peak concentration of 17300 ± 1140 pptv. The last pass through the cloud occurred three hours after the release, at a distance 3410 m from the release line, and at an altitude of 150 m agl. The greatest distance at which the aircraft detected SF_6 was 7680 m

downwind; this was well before sampling Line 3 at 8860 m. The SF_6 cloud stalled between the first and third sampling lines (Figure E3). There was no significant correlation between σ_x and downwind distance. The transport speed of SF_6 calculated from the aircraft data had a mean of 1.1 with a standard deviation of 0.5 m s^{-1}. This is in agreement with the mean SF_6 velocity observed on the ground of 1.2 ± 1.7 m s^{-1}.

5.1.6 Test 6

Test 6 was a unique case among the OLAD trials. The winds were strong and steady with a mean 2-m speed of 6 ± 1 m s^{-1}, a mean direction of 133° and a standard deviation of only 6° (Table F1). This direction corresponds to 175° in grid coordinates. The first cloud cleared the third sampling line about 25 minutes after the release. Two more releases were made during the three hours the samplers were running. The peak concentration on Line 1 for the three clouds was 520 ± 264 pptv, 431 ± 173 pptv, and 428 ± 182 pptv. These peak values are surprisingly consistent from release to release (Table F2). The *rsd* values for the three Line 1 peaks was 0.51, 0.4, 0.4. Again consistent from release to release, yet greater than the variability that would be expected from sampling and analytical uncertainty alone. The mean peak SF_6 concentration and *rsd* behave similarly for all three peaks on Lines 2 and 3. Variability on these lines is near or below the level expected from measurement variability. The *mrsd* values for all Test 6 samples and for concentration ranges 0 - 100 and 100 - 500 pptv were a remarkably consistent 0.3 (Table F1). This is slightly larger than would be expected from the duplicate samplers.

The release 1 SF_6 velocities calculated from the ground continuous analyzer data were significantly different between the east and west analyzers on Lines 1 (Table F3); the east speed was 7.8 ± 0.2 m s^{-1} and the west end speed was 10 ± 1 m s^{-1}. The same situation occurred on Line 2. The east speed was 8.8 ± 0.1 m s^{-1} while the west speed was 13.8 ± 0.3 m s^{-1}. These speeds were also faster than the mean wind speed which was constant at 5.7 ± 1.0 m s^{-1} until cloud 1 cleared the test grid. The SF_6 transport speeds calculated from the data collected by the two continuous analyzers on Line 3 were in agreement with a mean value of 11.5 ± 1.1 m s^{-1} and were the highest speeds observed for this plume. Calculated values of sx were in agreement for the data from the two continuous analyzers on Lines 1 and 3 but not for those on Line 2. Arrival times were significantly different for all but Line 3. Maximum SF_6 values were also different for Lines 1 and 2 but not for Line 3.

Seven aircraft cloud passes were recorded for Test 6, release 1, at altitudes ranging from 30 to 150 m agl (Table F6). The aircraft analyzer first detected the SF_6 8 minutes after release at a concentration of 104 ± 90 pptv, an altitude of 160 m agl and a distance of 6500 m downwind of the release line. This was after the cloud was detected on the ground at 4 minutes after release, a distance of 1616 m, and a peak concentration of 4600 ± 500 pptv. The last pass through the cloud occurred 45 minutes after the release, at a distance 26500 m from the release line, at an altitude of 50 m agl, and had a peak concentration of 100 ± 25 pptv. The transport speed of SF_6 calculated from the aircraft data had a mean of 11.5 with a standard deviation of 1.2 m s^{-1} which is in agreement with the mean SF_6 velocity observed on the ground of 10.6 ± 2.2 m s^{-1}.

During Test 6, release 2, the mean 2-m wind speed had increased to 5.9 ± 1.6 m s^{-1}. The SF_6 velocities calculated from the two Line 1 TGA data sets were not in agreement at 8.2 ± 0.2 m s^{-1} and 7.7 ± 0.2 m s^{-1} (Table F4). There was similar disagreement for both Lines 2 and 3. All calculated SF_6 speeds are from 2 to 5 m s^{-1} faster than the mean wind speed. The σ_x values were in agreement for all three lines, although the error limits are large. Arrival times were nearly in agreement for Lines 1 and 2 and significantly different for Line 3. Maximum SF_6 concentrations were significantly different for Line 1 and in agreement for Lines 2 and 3.

Seven aircraft cloud passes were recorded for Test 6, release 2, at altitudes ranging from 17 to 30 m agl (Table F7). The aircraft analyzer first detected the SF_6 2 minutes after release at a concentration of 5400 ± 3700 pptv, an altitude of 30 m agl and a distance of 950 m downwind of the release line. This was before the cloud was detected on the ground at 3.3 minutes after release, a distance of 1616 m, and a peak concentration of 11000 ± 1100 pptv. The last pass through the cloud occurred 32 minutes after the release, at a distance of 19800 m from the release line, an altitude of 26 m agl, and with a peak concentration of 171 ± 50 pptv. The transport speed of SF_6 calculated from the aircraft data had a mean of 9.9 with a standard deviation of 1.2 m s^{-1} which is in agreement with the mean SF_6 velocity observed on the ground of 9.5 ± 1.4 m s^{-1}.

The mean 2-m wind speed had increased to 6.8 ± 1 m s^{-1} for the third release of the test (Table F5). The SF_6 velocities calculated from the ground continuous analyzer data were in agreement for Line 1 with a mean of 8.4 ± 0.4 m s^{-1} and significantly different for Lines 2 and 3. These velocities are from 1 to 4 m s^{-1} faster than the mean wind speed. The σ_x values were in agreement for all three lines; again, the error limits were large. Arrival times were nearly in agreement for Line 1 and significantly different for Lines 2 and 3. Maximum SF_6 concentrations were significantly different for all lines.

Seven aircraft cloud passes were recorded for Test 6, release 3 at altitudes ranging from 20 to 35 m agl (Table F8). The aircraft analyzer first detected the SF_6 2.7 minutes after release at a concentration of 5700 ± 3500 pptv, an altitude of 25 m agl and a distance of 966 m downwind of the release line. This was before the cloud was detected on the ground at 3.2 minutes after release, a distance of 1616 m, and a peak concentration of 7000 ± 730 pptv. The last pass through the cloud occurred 33 minutes after the release, at a distance 20350 m from the release line, an altitude of 25 m agl, and had a peak concentration of 270 ± 60 pptv. The transport speed of SF_6 calculated from the aircraft data had a mean of 9.2 with a standard deviation of 1.2 m s^{-1} which is in agreement with the mean SF_6 velocity observed on the ground of 9.6 ± 1.5 m s^{-1}.

There was a weak correlation between σ_x and distance downwind. A linear fit of σ_x versus x data from all three releases resulted in a line with the equation $\sigma_x = 0.08\ x + 150$ and a correlation coefficient (r^2) of 0.69 (Figure F4).

5.1.7 Test 9

Test 9 was an aircraft release. During Test 9, the mean 2-m wind was 1.5 ± 1 m s^{-1} and had

a mean direction of 150° ± 40° (Table G1). This corresponds to a direction of 190° in the grid coordinate system. Mean peak concentration on Line 1 was 545 pptv with a standard deviation of 160 pptv resulting in a *rsd* of 0.29 (Table G2). Mean peak concentration measured in the samples collected on Line 2 was 190 with a standard deviation of 70 resulting in a *rsd* of 0.35 pptv. Mean peak concentration on Line 3 was 46 with a standard deviation of 16 pptv resulting in a *rsd* of 0.35. The variability of all three lines was greater than expected from measurement error. Overall, the *mrsd* for the concentration ranges 0 - 100 and 100 - 500 pptv were 0.5 (Table G1). This is greater than that expected from measurement error alone.

The SF_6 speed calculated from the data recorded from analyzers positioned at the ends of sampling Line 1 were not in agreement with values of 0.94 ± 0.4 m s^{-1} and 1.1 ± 0.2 m s^{-1} (Table G2). The transport speeds calculated from Line 2 data were not in agreement with values of 1.8 ± 0.04 m $s^{-1}$and 1.7 ± 0.2 m s^{-1}. Transport speeds calculated from Line 3 data were in agreement with a mean value of 1.9 ± 0.3 m s^{-1}. The along-wind dispersion parameter values were in agreement for all three lines. Arrival times were significantly different for all three lines and peak values different for Line 1 and in agreement for Lines 2 and 3.

Twenty-nine aircraft cloud passes were recorded for Test 9 at altitudes ranging from 10 to 200 m agl (Table G4). The aircraft analyzer first detected the SF_6 27 minutes after release at a concentration of 800 ± 300 pptv, an altitude of 138 m agl, and a distance of 785 m downwind of the release line. The cloud was detected on the ground 2 hours and 35 minutes after release, at distance of 9560 m, and with a peak concentration of 1000 ± 100 pptv. The last aircraft transit of the cloud occurred at 3 hours and 40 minutes after the release at a distance 15500 m from the release line, an altitude of 155 m agl, and with a peak concentration of 90 ± 11 pptv. The SF_6 cloud aloft did not move much past sampling Line 2 (Figure G3). The transport speed of SF_6 calculated from the aircraft data had a mean of 1.1 m s^{-1} with a standard deviation of 0.5 m s^{-1} which is in agreement with the mean SF_6 velocity observed on the ground of 1.5 ± 0.4 m s^{-1}.

5.1.8 Test 10

During Test 10 the mean 2-m wind speed was 2.2 to 2.3 m s^{-1} with a standard deviation of 0.6 to 0.8 m s^{-1} (Table H1). The mean direction was ranged from 150° to 161° with standard deviation of from 22° to 30°. In the grid coordinate system this was an angle between 192° and 204°. The mean peak SF_6 concentrations seen were: Line 1, 2050 with a standard deviation of 1600 resulting in an *rsd* of 0.77 (Table H2); Line 2, 1000 with a standard deviation of 120 for an *rsd* of 0.12; and Line 3, 490 with a standard deviation of 100 for an *rsd* of 0.21. Overall *mrsd* for each line and for the three concentration ranges were all greater than would be expected it the variation was caused by measurement error alone.

The SF_6 velocities calculated from the ground continuous analyzer data were significantly different for Line 1 (Table H3) with values of 2.2 ± 0.3 m s^{-1} and 3.6 ± 7 m s^{-1}. The same situation occurred on Line 2 with values of 3.5 ± 0.2 m s^{-1} and 4.3 ± 0.3 m s^{-1}. The SF_6 velocities calculated from the Line 3 data were in agreement with a mean value of 4.8 ± 1.5 m s^{-1}. These transport speeds

were faster than the mean wind speed. The values of σ_x calculated from the continuous analyzer data from Line 1 were not in agreement with values of 180 ± 24 m and 370 ± 160 m. The values of σ_x calculated from the Line 2 data were in agreement with a mean value of 665 ± 185 m. The values of σ_x calculated from the Line 3 data were also in agreement with a mean value of 2200 ± 1850 m. Arrival times were significantly different for all but Line 3. Maximum SF_6 values were in agreement for all lines.

Twelve aircraft cloud passes were recorded during Test 10 at altitudes ranging from 10 to 150 m agl (Table H4). The aircraft analyzer first detected the SF_6 3 minutes after release at a concentration of 6300 ± 3500 pptv, an altitude of 16 m agl, and a distance of 933 m downwind of the release line. The cloud was detected on the ground 13 minutes after release at a distance of 1616 m and a peak concentration of 6900 ± 2000 pptv. The last aircraft transit of the cloud occurred at 68 minutes after the release at a distance 16950 m from the release line, an altitude of 50 m agl, and a peak concentration of 100 ± 23 pptv. The transport speed of SF_6 calculated from the aircraft data had a mean of 4.7 ± 1.0 m s^{-1} which is in agreement with the mean SF_6 velocity observed on the ground of 3.7 ± 0.9 m s^{-1}.

There was a weak correlation between σ_x calculated from aircraft data and the distance the peak concentration was encountered downwind of the release. A linear fit of all the σ_x versus x data from Test 10 resulted in a line with the equation $\sigma_x = 0.07\ x + 187$ and a correlation coefficient (r^2) of 0.7 (Figure H5). When only data from passes with altitudes less than 50 m agl were considered, the fit was considerably better with the equation $\sigma_x = 0.12\ x + 302$ and a correlation coefficient (r^2) of 0.9 (Figure H6).

5.1.9 Test 11

During Test 11 the winds were very light and variable with a mean wind speed of 0.70 ± 0.05 m s^{-1} and a direction of 158 ± 57°. The SF_6 cloud just cleared the first sample line by 10:30 when the whole air sampling was completed. Only samples from Line 1 were analyzed for this test. The sampler and ground based continuous analyzer data was not processed further.

Thirty-two aircraft cloud passes were recorded during Test 10 at altitudes ranging from 10 to 200 m agl (Table I1). The aircraft analyzer first detected the SF_6 21 minutes after release at a concentration of 6600 ± 2300 pptv, an altitude of 70 m agl, and a distance of 3690 m downwind of the release line. The last aircraft transit of the cloud occurred at 3 hours and 18 minutes after the release, at a distance 7930 m from the release line, an altitude of 170 m agl, and a peak concentration of 430 ± 300 pptv. Figure I1 shows the position and altitude on the test grid where the aircraft encountered the SF_6. The cloud appears to stall over the front part of the sampling grid to disperse over an area centered on sampling Line 1, never moving past sampling Line 2. The transport speed of SF_6 calculated from the aircraft data had a mean of 1.5 m s^{-1} with a standard deviation of 0.7 m s^{-1}. The transport speed actually decreased from a value of 2.9 m s^{-1} during the first pass to 0.7 m s^{-1} during the last encounter.

5.1.10 Test 12

During Test 12 the mean 2-m wind speed was 0.9 ± 0.4 m s^{-1} (Table J1). The mean direction ranged from 138° to 142° with standard deviation of from 41° to 47°. In the grid coordinate system this was an angle between 181° and 184°. The mean peak SF_6 concentrations measured in whole air samples were: Line 1, 8400 with a standard deviation of 2700 resulting in an *rsd* of 0.3 (Table J2); Line 2, 5300 with a standard deviation of 900 for an *rsd* of 0.2; Line 3, 2400 with a standard deviation of 660 for an *rsd* of 0.3. Overall *mrsd* for each line and for the three concentration ranges were all greater than would be expected it the variation was caused by measurement error alone (Table J1).

The SF_6 velocities calculated from the ground continuous analyzer data were in agreement for Line 1 (Table J3) with a mean value of 0.7 ± 0.3 m s^{-1}. The same situation occurred on Line 2 with a mean value of 0.7 ± 0.2 m s^{-1}. The SF_6 velocities calculated from the Line 3 data were in agreement with a mean value of 1.0 ± 0.2 m s^{-1}. These transport speeds were in agreement with the mean wind speed. The values of σ_x calculated from the continuous analyzer data from Line 1 were not in agreement with values of 215 ± 35 m and 422 ± 146 m. The values of σ_x calculated from the Line 2 data were in agreement with a mean value of 1060 ± 180 m. The values of σ_x calculated from the Line 3 data were significantly different with a values of 8521 ± 146 m and 9244 ± 48 m. Arrival times were in agreement for Lines 1 and 2 and significantly different for Line 3. Maximum SF_6 values were significantly different for Lines 1 and 2 and in agreement for Line 3.

5.2 Summary Results: Whole Air Samples

Summaries of the whole air sampling results for all tests are given in Table 8. Values of the variation in the duplicate samples taken from Table 9 are given in the far right column for comparison. Note that the variation in the duplicate samples is reported at the 95% confidence (2σ) level.

Table 9. Variation in cross-line SF_6 concentrations for all tests.

Sampling line	Concentration range	mrsd	Standard deviation mrsd	Number of points	mrsd from duplicate samplers (2σ)
All cross line RSD	all	0.7	0.7	307	
	< 100	0.8	0.8	208	0.56
	100 - 500	0.6	0.6	43	0.24
	> 500	0.5	0.7	56	0.20

Table 9 presents the variation in cross-line SF_6 concentration for all samples in the test program broken down into concentration ranges. It is clear that in most every case, the variation across the sample lines is significantly greater than the variation in the duplicate samples. This can be seen in the three dimensional plots of sample concentration versus position and bag number given in the figures of Appendix B through J. Elimination of the data from Tests 10 and 12, the tests with

release problems, does not significantly change the results.

5.2.1 Ground Releases

Table 10 presents the variation in cross-line SF_6 concentration for all samples collected during ground releases broken down into concentration ranges. For Line 1, the variation across the sample lines is significantly greater than the variation in the duplicate samples. This is also the case for Line 2. Line 3, however, has variation on the order of or less than that found in the duplicate samples. As in the aggregate results presented above, elimination of the data from the tests with release problems does not significantly change the results.

Table 10. Variation in cross-line SF_6 concentrations for all ground release tests.

Sampling line	Concentration range	mrsd	Standard deviation mrsd	Number of points	mrsd from duplicate samplers (2σ)
100	all	0.9	0.8	91	
	< 100	0.9	0.8	60	0.56
	100 - 500	0.65	0.34	9	0.24
	> 500	0.8	0.9	22	0.20
200	all	0.7	0.8	84	
	< 100	0.8	0.9	46	0.56
	100 - 500	0.9	0.9	46	0.24
	> 500	0.4	0.4	23	0.20
300	all	0.5	0.5	60	
	< 100	0.6	0.6	42	0.56
	100 - 500	0.3	0.1	11	0.24
	> 500	0.1	0.1	7	0.20

Line 100 is the closest line to the release track at a mean distance of 1616 m (Table 11). The *mrsd* of this line is greater than those of the duplicate samples over all concentration ranges. Line 200, the middle line, at a mean distance of 4024 m, also has variability greater than the duplicates in all cases. The degree of the difference for the middle line, however, is much less for the > 500 pptv concentration range than for the first line: Line 200 has a *mrsd* of 0.4 versus 0.8 for Line 100. The sampling line farthest from the release line, Line 300, with a mean distance of 8859 m, shows the smallest variability of the three lines. All three concentration ranges on the third line show less variability than the first and second lines and the *mrsd* are substantially in agreement with the 95% confidence limits established for the duplicate samples. For the > 500 pptv range, the variability is actually less than that determined for the same concentration range for the duplicate samples. This contradicts the reasoning behind the line source assumption which holds that at distances from the release line nearly equal to the length of the line, the edge effects should become significant and cross line variability should increase relative to the variability of the cloud closer to the initial release. The number of points, 7, in the 500 pptv concentration range is relative small so these results are not unequivocal, but overall they are significant. The trend toward more uniformity at longer distances

indicates that the line source is fragmented close to the release causing a high degree of spatial variability in the concentration of the tracer. Over longer distances the scattered pieces of the cloud are mixed together and the concentration becomes more uniform.

Table 11. Mean distance of sampling lines from release line.

Sampling line	$d_\perp$ (m)	Standard deviation (m)
Ground releases		
100	1,616	0.5
200	4,024	0.5
300	8.859	1.0
Aircraft releases		
1100	9,562	20
1200	15,980	20
1300	20,800	20

5.2.2 Aircraft releases

The aircraft release sampler results show much less variability than the ground release results (Table 12). This supports the result from the ground release that the cross-wind variability in tracer concentration is less at greater distance from the release line. Sampling Line 1100 was located at a mean distance of 9560 m from the release line. The *mrsd* from this line was substantially in agreement with the duplicate sampler results. Sampling Line 1200, at a mean distance of 15980 m, exhibited greater variability than the closest line. The < 100 pptv concentration range *mrsd* of 0.7 was substantially larger than the duplicate result of 0.56. The > 100 pptv concentration range value of 0.4 was not in agreement with the duplicate result of 0.24. This value was based on the mean of only four points and may not be significant. The farthest line, 1300 at 20800 m from the release line showed substantial agreement with the variability measured in the duplicate samples. Again, however, a limited number of points were used to calculate these values, and they may not be representative.

5.3 Summary Results: Continuous Analyzers

The data from the continuous analyzers was fit to Gaussian profiles using four different methods. The Gaussian approximation had mixed success in reproducing the data. The results of the four methods were averaged to produce the mean SF_6 transport parameters and the standard deviations. These results are presented on a test by test basis in Appendices B through J. Using the average of the four different methods to determine σ_t, peak center time, and downwind distance provides the best estimate of these parameters from the data. The standard deviations of these means provide a measure of the goodness of the fits and are used as the confidence limits. When the Gaussian is a good approximation to the concentration profile, the four methods are in good agreement. When the Gaussian is a bad approximation, one method may provide a better profile or estimate of peak concentration while another method provides a better estimate of the arrival time

of the concentration peak. The standard deviation of the mean is an estimate of how good the fits approximate reality and is used as a measure of uncertainty in comparisons of the parameters.

Table 12. Variation in cross line SF_6 concentrations for all aircraft releases.

Sampling line	Concentration range	mrsd	Standard deviation mrsd	Number of points	mrsd from duplicate samplers (2σ)
1100	All	0.5	0.5	24	
	< 100	0.6	0.6	18	0.56
	100 - 500	0.3	0.05	6	0.24
1200	All	0.7	0.7	28	
	< 100	0.7	0.7	24	0.56
	100 - 700	0.4	0.1	4	0.24
1300	All	0.7	0.7	24	
	< 100	0.6	0.6	21	0.56
	> 100	0.17	0.4	3	0.24

There is no discernable pattern in the relationship between transport parameters calculated from data taken by two continuous analyzers positioned at the ends of a sampler line. Table 13 gives a summary of the agreement between the parameters calculated from the data collected by the two analyzers on each line.

The two SF_6 transport speeds may be in agreement but σ_x, peak arrival times, and peak concentration may not. Agreement is independent of mean 2-m wind speed or SF_6 transport speed and may occur on one line and not on the next for a given parameter. The most consistent agreement between parameters occurred during Test 2. Only the peak SF_6 concentration values were significantly different in this case. Test 2 was also one of the few tests where σ_x versus x has a significant correlation.

5.3.1 σ_x versus *x*

A linear fit of the σ_x versus x using values calculated from ground based continuous analyzer data was relatively good and resulted in $\sigma_x = (0.105 \pm 0.01)\ x + (165 \pm 85)$ and a correlation coefficient of $r^2 = 0.7$ (Figure 16). Segregating this data according to wind speed, SF_6 transport speed, or by aircraft or ground release, did not improve the relationship. Elimination of the data from Tests 10 and 12, where there were problems with the release, resulted in a better correlation coefficient of $r^2 = 0.8$ and an equation of $\sigma_x = (0.11 \pm 0.01)\ x + (114 \pm 83)$. There is no significant change in the values of the slope or intercept.

Table 13. Agreement between parameters calculated from data collected by two TGA-4000 continuous analyzers positioned on the ends of the sampling lines. O indicates agreement. X indicates not in agreement.

Test line	V_{SF6}	σx	Δt	Peak SF_6 conc.	Mean WS ($m\ s^{-1}$)	σ_θ (deg)
Test 1						
100	X	O	X	O	1.0	45
200	O	O	X	X		
300	NA	NA	NA	NA		
Test 2						
100	O	O	O	X	2.9 to 3.2	5
200	O	O	O	X		
300	O	O	O	X		
Test 4						
1100	O	X	O	O	4.1 to 4.4	7
1200	NA	NA	NA	NA		
1300	X	O	X	X		
Test 5						
100	O	O	X	O	0.9 to 1.1	17
200	O	O	X	X		
300	NA	NA	NA	NA		
Test 6						
100a	X	O	X	X	6.0	6
200a	X	X	X	X		
300a	O	O	O	O		
100b	X	O	X	X	5.9	6
200b	X	O	X	O		
300b	X	O	X	O		
100c	O	O	X	X	6.8	6
200c	X	O	X	X		
300c	X	O	X	X		
Test 9						
100	X	X	X	O	1.5	40
200	X	O	X	O		
300	O	O	O	O		
Test 10						
100	X	X	X	O	2.2 to 2.3	22
200	X	O	X	O		
300	O	O	O	O		

The linear fit to the aircraft data was very poor. A fit using all data resulted in $\sigma_x = (0.05 \pm 0.006)$ x + (670 ± 85) and a correlation coefficient of $r^2 = 0.3$ (Figure 17). A fit using only the data from tests where the tracer was released by the aircraft was worse resulting in $\sigma_x = (0.04 \pm 0.009)$ x + (800 ± 150) and a correlation coefficient of $r^2 = 0.2$. A fit using only the data from ground tracer releases was better resulting in $\sigma_x = (0.09 \pm 0.008)$ x + (430 ± 90) and a correlation coefficient of $r^2 = 0.6$ (Figure 18). This equation is very close to that obtained from the ground continuous analyzer data. Segregating the σ_x values by altitude or SF_6 transport speed did not improve the relationship. Elimination of the data from Tests 10 and 12 did not result in any improvement in the correlation.

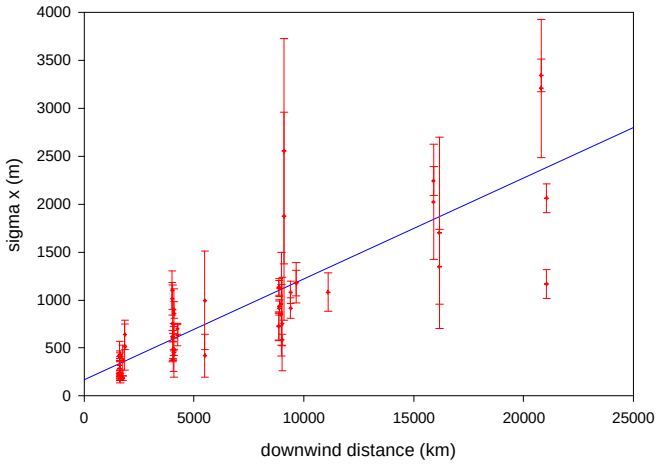

Figure 16. σ_x versus *x*. The data plotted are from ground-based continuous analyzers. The solid line is a linear fit to the data with the equation $\sigma_x = (0.105 \pm 0.01)\ x + (165 \pm 85)$ and a correlation coefficient of $r^2 = 0.7$, N = 57.

Examination of σ_x versus x on a test by test basis reveals three tests with correlation coefficients greater than 0.5: Test 2 resulting in $\sigma_x = (0.13 \pm 0.02)$ x + (130 ± 40) and a correlation coefficient of $r^2 = 0.8$ (Figure C5); Test 6 resulting in $\sigma_x = (0.08 \pm 0.01)$ x + (150 ± 20) and a correlation coefficient of $r^2 = 0.7$ (Figure F6); and Test 10 $\sigma_x = (0.11 \pm 0.02)$ x + (200 ± 200) and a correlation coefficient of $r^2 = 0.7$ (Figure H5). The Test 10 relationship improved dramatically when only data from passes with altitudes less than 50 m agl were considered; the fit was considerably better with the equation $\sigma_x = (0.12 \pm 0.02)$ x + (302 ± 140) and a correlation coefficient $r^2 = 0.9$ (Figure H6). These tests are all

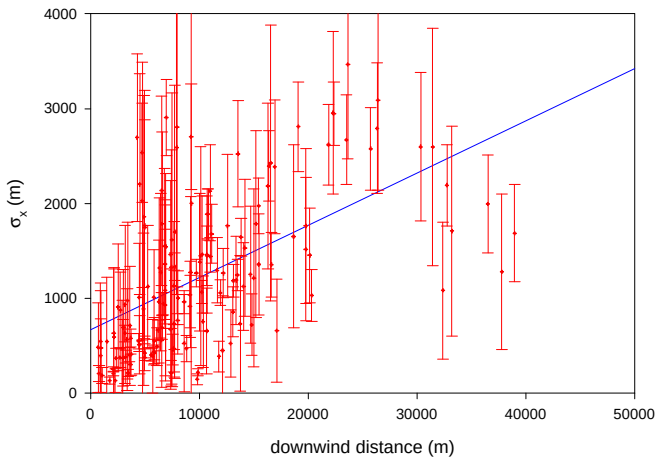

Figure 17. σ_x versus *x*. The data plotted are from the aircraft-based continuous analyzer. The solid line is a linear fit to the data with the equation $\sigma_x = (0.05 \pm 0.006)\ x + (670 \pm 85)$ and a correlation coefficient of $r^2 = 0.3$, N = 157.

ground release tests with mean 2-m winds greater than 2 m s^{-1}.

The relationship between the mean SF_6 transport speed determined from the ground data and the same parameter calculated from the aircraft data was clear; they were in agreement for every test (Table 14).

The SF_6 transport speed determined from the ground data versus the mean 2-m wind speed exhibited a significant correlation (Figure 19). A fit of the data resulted in a line with a slope of 1.7 ± 0.1, an intercept of 0.3 ± 0.3, and a correlation coefficient $r^2 = 0.9$.

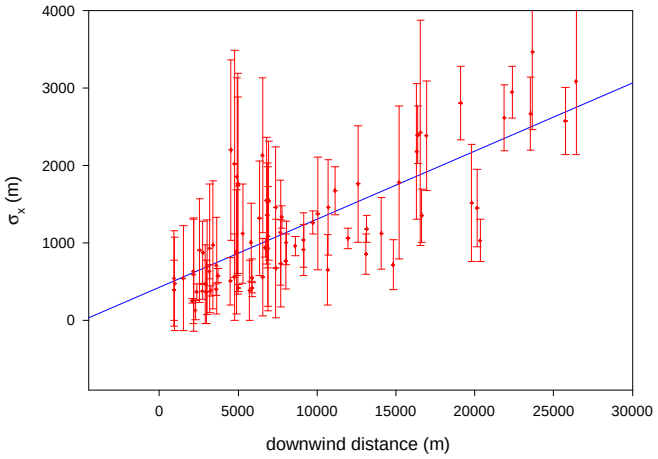

Figure 18. σ_x versus x. The data plotted are from the aircraft-based continuous analyzer recorded during ground releases. The solid line is a linear fit to the data with the equation $\sigma_x = (0.09 \pm 0.008)\, x + (430 \pm 90)$ and a correlation coefficient of $r^2 = 0.6$, N = 82.

Table 14. Mean SF_6 velocity calculated from ground-based and aircraft continuous analyzer data.

Test	Mean V_{SF6} ground (m s^{-1})	Standard Deviation (m s^{-1})	Mean V_{SF6} aircraft (m s^{-1})	Standard Deviation (m s^{-1})
1	0.9	0.4	0.5	0.05
2	5.0	0.4	5.0	0.6
4	8.3	1.6	8.6	2.8
5	1.2	1.7	1.1	0.5
6a	10.6	2.2	11.5	1.2
6b	9.5	1.4	9.9	1.2
6c	9.6	1.5	9.2	1.2
9	1.5	0.4	1.1	0.5
10	3.7	0.9	4.7	1.0

5.3.2 Whole-Air Samplers versus Continuous Analyzers

A comparison of the concentration measured by the TGA-4000 continuous analyzers with the results of the whole air samplers in the same location was made. The whole air samplers integrate

the SF_6 concentration over the sampling period. The TGA-4000 has a response time of less than 1 s and can accurately resolve concentration changes occurring over the course of 10 s. Therefore, the TGA data must be integrated over the sampling period used in collecting the whole air samples before the results can be compared. A correlation plot of the integrated TGA concentration versus the sampler results is given in Figure 20. A linear fit to the data has a slope of 0.99 ± 0.05, an intercept of 112 ± 135 pptv, and r^2 = 0.64. The poor correlation coefficient reflects the scatter in the data while the slope indicates that the scatter is both above and below the y = x line. Data in Tables 15, 16, and 17 also indicate that the variability between the TGA measurements and those of the samplers are the result of atmospheric processes. This result was a surprise. The sampling mast of the TGA-4000 instruments is mounted on the roof of conventional cargo vans, about 1.5 m higher than the height of the samplers. The sampling mast could also have been shifted laterally several meters from the location of the sampler because of the way the vans were parked. These results again point to large variability in the concentration of SF_6 over small scales.

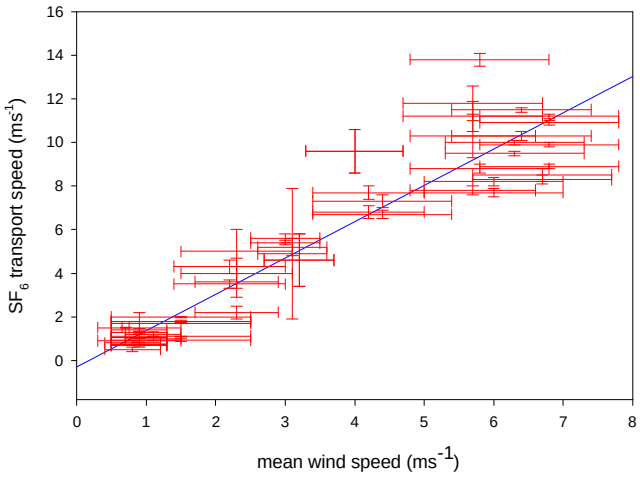

Figure 19. SF_6 transport speed versus 2-m mean wind speed from ground continuous analyzer data. The line is a fit to the data with an equation of y = (1.7 ± 0.1) *x* + (0.3 ± 0.3), N = 57.

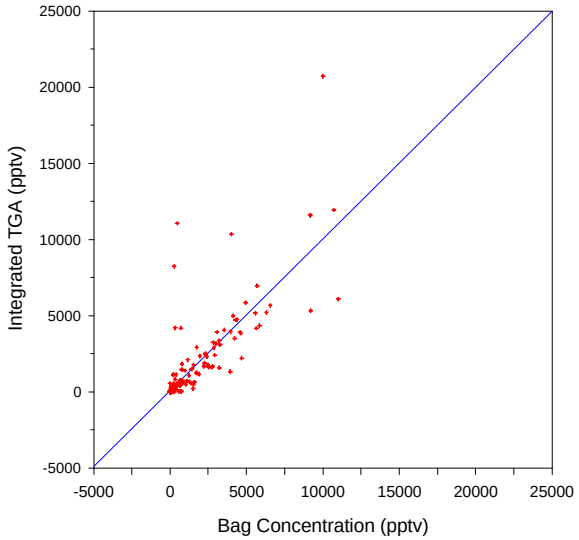

Figure 20. Integrated SF_6 concentration from continuous analyzers versus sample concentration from whole air samplers for all tests. The line is a fit to the data with an equation of y = (0.99 ± 0.05) *x* + (112 ± 135), r^2 = 0.64, N = 189.

Table 15. Comparison of the whole air samplers against TGA-4000 continuous analyzers.

Concentration range (pptv)	Mean relative difference	Number of points
< 100	1.01	60
100 - 500	0.53	45
> 500	0.42	81

Table 16. Variation of TGA-4000 integrated SF_6 concentrations and sampler results for all ground releases.

Sampling line	Concentration range	mrsd	Standard Deviation mrsd	Number of points	mrsd from duplicate samplers (2σ)
100	all	0.6	0.7	41	
	< 100	1.3	0.8	6	0.56
	100 - 500	0.7	0.7	6	0.24
	> 500	0.5	0.5	29	0.20
200	all	0.6	0.7	48	
	< 100	1.3	1.0	11	0.56
	100 - 500	0.5	0.6	12	0.24
	> 500	0.5	0.5	29	0.20
300	all	0.6	0.8	37	
	< 100	0.8	1.1	16	0.56
	100 - 500	0.6	0.7	5	0.24
	> 500	0.5	0.4	14	0.20

Table 17. Variation of TGA-4000 integrated SF_6 concentrations and sampler results for all aircraft releases.

Sampling line	Concentration range	mrsd	Standard Deviation mrsd	Number of points	mrsd from duplicate samplers (2σ)
1100	all	0.6	0.7	29	
	< 100	1.3	0.8	5	0.56
	100 - 500	0.7	0.7	13	0.24
	> 500	0.3	0.3	11	0.20
1200	all	0.4	0.3	14	
	< 100	0.3	0.2	8	0.56
	> 100	0.4	0.4	6	0.24
1300	all	1.0	1.0	19	
	< 100	1.3	1	14	0.56
	> 100	0.2	0.2	5	0.24

6 Conclusions and Recommendations

Samplers were positioned 100 m apart on three sampling lines for both ground and air releases at nominally 2, 5, and 10 and 10, 15, and 20 km, respectively, downwind of the release lines. Continuous analyzers were positioned at the ends of each line, 1.5 km apart, and within several meters both vertically and horizontally of whole air samplers. The observed concentration variability in whole air samples, between continuous analyzers positioned at opposite ends of the sampling lines, and between integrated continuous analyzer results and samplers in same locations is real and is caused by atmospheric processes. The line source does not eliminate cross-wind variability from the concentration measurements, particularly over distances less than 10 km.

The fact that the SF_6 transport speeds are generally greater than the mean 2-m wind speed by a factor of 1.7, suggests that wind shear coupled with vertical turbulence is important in transporting the cloud and that along-wind dispersion is influenced by this coupling. It also appears that the tracer transport speed at the ground is not significantly different from the speed up to 250 m above the surface. The transport speeds calculated from the ground based analyzer data and those calculated from the aircraft analyzer were in agreement for all tests.

When tracer is released at the surface and 2-m wind speed is greater than 2 m s^{-1}, there is a correlation between σ_x and down wind distance x. Correlation is not evident for elevated releases. This effect cannot be quantified because of a lack of upper air and turbulence data.

The wind profiles, boundary layer structure, and nature of the turbulence at the release line and above the test grid during the OLAD tests are largely unknown. This lack of data has significantly hindered the quantification of a relationship for along-wind dispersion. The conditions which are common among Tests 2, 6, and 10 and which result in the relatively good correlation coefficients in plots of σ_x versus x discussed above, cannot be identified. In any future program of this type it will be essential to obtain better upper air and turbulence data. This can be accomplished with mini-sodar to measure wind shear, sonic anemometers to measure turbulence, radar profilers to measure mixing layer depth and upper air winds, and instrumentation on the SF_6 sampling aircraft to measure standard meteorological parameters. The use of tethersondes should also be employed when they can be operated safely along with aircraft operations.

The sample variability also needs to be more exactly quantified. The quality control procedures we instituted for OLAD allowed us to determine the variability associated with the sampling and analysis methods. The differences observed in duplicate samples for various concentration ranges were the criteria we used to establish the inherent measurement variability. This difference was determined to be approximately 20% for levels of SF_6 above the quantitation limit. Two factors lead us to believe that this is a significant overestimate of the precision of the method. First, the duplicate samplers were not precisely co-located. One of the samplers was placed on the ground at the base of the stake supporting the other sampler; the two samplers were separated by about 1.1 m. Second, the variability of the spike samples was less than 10% for all samples except the lowest concentration levels. If the two samplers were collecting air from the same air mass, the

variability should approach that of the spike samples.

The sampling and measurement variability can be precisely determined in a field experiment in which a large number of duplicate samples are collected. These samplers should be exactly co-located (at the same height and with inlets as close as possible to each other). Some pairs of samplers should be connected to manifolds which are actively ventilated to insure both samplers collect from the same air mass. Continuous analyzers should also be co-located with samplers at several sites.

The horizontal and vertical scale of atmospheric variability can also be determined in such an experiment. A small-scale array, with sampler locations from 2 to 5 m apart, can be established in the center of the most likely tracer trajectory. Two samplers would be placed at each location. The difference between variability caused by the method and the variability caused by the placement of samplers can then be readily established. An equivalent experiment can be done to measure vertically variability. A 10 to 20-m tower with sampler locations every 2 m can be erected at the same location as the small scale array. All locations would have at least two samplers. The vertically variability could then be readily determined.

Acknowledgments

The authors wish to thank William Peterson and Carmen Nappo for providing a critical review of this document. The authors wish to thank Dianne Hoover, Joyce Silvester, and Paula Fee for their assistance. OLAD was conducted at the West Desert Test Center (WDTC) of the U. S. Army Dugway Proving Ground under sponsorship of the Joint Chemical/Biological Contact Point and Test (Project DO49) program and the Naval Surface Warfare Center, Dahlgren Division, Dahlgren, Virginia.

References

Benner, R. L., and B. Lamb, 1985: A fast response continuous analyzer for halogenated atmospheric tracers. *J. Atmos. Oceanic Technol.*, **2**, 582-589.

Biltoft, C., B. Grim, and S. Turley, 1997: Customer test plan over-land atmospheric dispersion trials. Internal Report, U. S. Army Dugway Proving Ground, Dugway, UT.

Bowers, J. F., 1992: Literature review of long-range overwater transport and diffusion. DPG/JOD-92/036, U. S. Army Dugway Proving Ground, Dugway, UT, 64 p.

Bowers, J. F., G. E. Start, R. G. Carter, T. B. Watson, K. L. Clawson, and T. L. Crawford, 1994: Experimental design and results for the Long-Range Overwater Diffusion (LROD) Experiment. DPG/JCP-94/012, U. S. Army Dugway Proving Ground, Dugway, UT.

Calder, K. L., 1965: On the equation of atmospheric diffusion. *Quart. J. Roy. Meteor. Soc.*, **91**, 514-517.

Chatwin, P. C., 1968: The dispersion of a puff of passive contaminant in the constant stress region. *Quart. J. Roy. Meteor. Soc.*, **94**, 350-360.

Corrsin, S., 1959: Outline of some topics in homogeneous turbulence flow. *J. Geophys. Res.*, **64**, 2134-2150.

Csanady, G. T., 1969: Diffusion in an Ekman layer. *J. Atmos. Sci.*, **26**, 414-426.

Counihan, J., 1975: Review paper: adiabatic atmospheric boundary layers: a review and analysis of data from the period 1880-1972. *Atmos. Environ.*, **9**, 871-905.

Draxler, R. R., 1979: Some observations of the along-wind dispersion parameter. Preprint, *Fourth Symposium on Turbulence, Diffusion, and Air Pollution*, Reno, NV, Amer. Meteor. Soc., 5-8.

Draxler, R. R., 1984: Diffusion and transport experiments. *Atmospheric Science and Power Production*, D. Randerson (Ed.), U. S. Department of Energy, Washington, D.C., 367-422.

Dumbauld, R. K., and J. F. Bowers, 1983: Functional methodologies for characterizing wind-speed and turbulence profiles and turbulent diffusion coefficients within and above vegetative canopies and urban domains. H. E. Cramer Co., Inc., Rep. No. TR-83-341-01, prepared for U.S. Army Atmospheric Sciences Laboratory, White Sands Missile Range, NM.

Drivas, P. J., and F. H. Shair, 1974: Dispersion of an instantaneous cross-wind line source of tracer released from an urban highway. *Atmos. Environ.*, **8**, 475-485.

Hanna, S. R., 1996: Along-wind dispersion of short-duration accidental releases of hazardous gases. Preprint, *Ninth Joint Conference on Applications of Air Pollution Meteorology with AWMA*, Atlanta, GA, Amer. Meteor. Soc., 55-58.

Hanna, S. R., R. J. Paine, and L. L. Schulman, 1984: User's guide to the Offshore and Coastal Dispersion (OCD) Model. Doc. No. 84-0069, Minerals Management Service, Reston, VA.

Hansen, F. V., 1979: Engineering estimates for the calculation of atmospheric dispersion coefficients. ASL Internal Report, U.S. Army Atmospheric Sciences Laboratory, White Sands Missile Range, NM.

List, R. L., 1951: *Smithsonian Meteorological Tables*, Smithsonian Institution, Washington D. C.

Monin, A. S., and A. M. Yaglom, 1971: *Statistical Fluid Mechanics*, MIT Press, Cambridge, MA, 769 p.

Nikola, P. W., 1971: Measurement of the movement, concentration and dimension of clouds resulting from instantaneous point sources. *J. Appl. Meteor.*, **10**, 962-973.

Pasquill, F., 1974: *Atmospheric Diffusion (2nd Ed.)*, Halsted Press, New York, 429 p.

Petersen, W. B., and L. G. Lavdas, 1986: INPUFF 2.0-a multiple source Gaussian puff dispersion algorithm user's guide. EPA-600/8-86-024, Office of Research and Development, Research Triangle Park, NC.

Priestly, C. H. B., 1959: *Turbulent Transfer in the Lower Atmosphere*, University of Chicago Press, Chicago.

Saffman, P. G., 1962: The effect of wind shear on horizontal spread from an instantaneous ground source. *Quart. J. Roy. Meteor. Soc.*, **88**, 382-393.

Shearer, D. L., 1957: Climatology Report Number 2, U. S. Army Dugway Proving Ground, Dugway, UT.

Slade, D. H. (Ed.), 1968: *Meteorology and Atomic Energy 1968*, U. S. Atomic Energy Commission, TID-24190, 445 p.

Smith, F. B., 1965: The role of wind shear in horizontal diffusion of ambient particles. *Quart. J. Roy. Meteor. Soc.*, **91**, 318-329.

Smith, F. B., and J. S. Hay, 1961: The expansion of cluster particles in the atmosphere. *Quart. J. Roy. Meteor. Soc.*, **87**, 82-101.

Taylor, J. K., 1987: *Quality Assurance of Chemical Measurements*, Lewis Publishers, Chelsea, MI.

Van Ulden, A. P., 1992: A surface-layer similarity model for the dispersion of a skewed passive puff near the ground. *Atmos. Environ.*, **26A**, 681-692.

Whitacre, C. G., J. H. Griner, M. M. Myirski, and D. W. Sloop, 1987: Personal computer program for chemical hazard predication (D2PC). CRDEC-TR-87021, U. S. Army Chemical Research, Development and Engineering Center, Aberdeen Proving Ground, MD.

Wilson, D. J., 1981: Along-wind diffusion of source transients. *Atmos. Environ.*, **15**, 489-495.

Watson, T. B., 1995: Evaluation of an intensive sampling and analysis method for carbon monoxide. *J. Air Waste Manage. Assoc.*, **45**, 29-35.

Watson, T. B., R. E. Keislar, B. Reese, R. G. Carter, S. Turley, B. Grim, and C. A. Biltoft, 1998: The Defense Special Weapons Agency Dipole Pride 26 Field Experiment, NOAA Tech. Memo. ERL ARL-225, Silver Spring, MD, 90 p.

Yamartino, R. J., 1984: Comparison of several single-pass estimators of the standard deviation of wind direction. *J. Climate Appl. Meteor.*, **23**, 1362-1366.

Appendix A: Sampling Locations and Coordinates

Table A1. Ground release sampling locations and coordinates.

ID	Latitude	Longitude	Line	ID	Latitude	Longitude	Line
LC0101	40.080452	-113.093757	Foxtrot	LC0210	40.101493	-113.104638	Juliet
LC0102	40.080732	-113.093100	Foxtrot	LC0211	40.102090	-113.103932	Juliet
LC0103	40.081105	-113.092578	Foxtrot	LC0212	40.102778	-113.103085	Juliet
LC0104	40.082197	-113.091527	Foxtrot	LC0213	40.103307	-113.102175	Juliet
LC0105	40.082717	-113.090480	Foxtrot	LC0214	40.103683	-113.100932	Juliet
LC0106	40.082980	-113.089762	Foxtrot	LC0215	40.104613	-113.100300	Juliet
LC0107	40.083450	-113.087265	Foxtrot	LC0250	40.101493	-113.104638	Juliet
LC0108	40.084172	-113.087875	Foxtrot	LC0260	40.100382	-113.106388	Juliet
LC0109	40.084917	-113.086850	Foxtrot	LC0270	40.100382	-113.106388	Juliet
LC0110	40.085508	-113.085912	Foxtrot	LC0301	40.129377	-113.149592	Papa
LC0111	40.085950	-113.085153	Foxtrot	LC0302	40.130067	-113.148747	Papa
LC0112	40.086267	-113.084632	Foxtrot	LC0303	40.130640	-113.147958	Papa
LC0113	40.086848	-113.083775	Foxtrot	LC0304	40.131073	-113.147098	Papa
LC0114	40.087308	-113.082963	Foxtrot	LC0305	40.131650	-113.146178	Papa
LC0115	40.087837	-113.081907	Foxtrot	LC0306	40.132203	-113.145363	Papa
LC0150	40.080452	-113.093757	Foxtrot	LC0307	40.132680	-113.144460	Papa
LC0160	40.084172	-113.087875	Foxtrot	LC0308	40.133572	-113.143155	Papa
LC0170	40.084172	-113.087875	Foxtrot	LC0309	40.134430	-113.141997	Papa
LC0201	40.096687	-113.112853	Juliet	LC0310	40.134890	-113.141267	Papa
LC0202	40.097138	-113.111942	Juliet	LC0311	40.135182	-113.140525	Papa
LC0203	40.097605	-113.111077	Juliet	LC0312	40.135757	-113.139738	Papa
LC0204	40.098093	-113.109993	Juliet	LC0313	40.136358	-113.138873	Papa
LC0205	40.098595	-113.109187	Juliet	LC0314	40.136688	-113.137867	Papa
LC0206	40.099302	-113.108188	Juliet	LC0315	40.137490	-113.137112	Papa
LC0207	40.100262	-113.107003	Juliet	LC0350	40.137490	-113.137112	Papa
LC0208	40.100382	-113.106388	Juliet	LC0360	40.133568	-113.143158	Papa
LC0209	40.101103	-113.105198	Juliet	LC0370	40.133567	-113.143162	Papa

Table A2. Air release sampling locations and coordinates.

ID	Latitude	Longitude	Line	ID	Latitude	Longitude	Line
LC1101	40.107462	-113.124958	Lima	LC1210	40.156858	-113.166217	Tango
LC1102	40.108205	-113.123794	Lima	LC1211	40.157837	-113.165017	Tango
LC1103	40.108613	-113.123143	Lima	LC1212	40.158595	-113.164015	Tango
LC1104	40.109245	-113.122258	Lima	LC1213	40.158887	-113.163380	Tango
LC1105	40.109822	-113.121427	Lima	LC1214	40.158748	-113.162945	Tango
LC1106	40.110293	-113.120673	Lima	LC1215	40.159007	-113.162043	Tango
LC1107	40.110822	-113.119765	Lima	LC1250	40.156858	-113.166217	Tango
LC1108	40.111292	-113.118625	Lima	LC1260	40.155667	-113.168097	Tango
LC1109	40.111838	-113.117625	Lima	LC1270	40.155662	-113.168097	Tango
LC1110	40.112428	-113.116705	Lima	LC1301	40.184435	-113.211407	Zulu
LC1111	40.113162	-113.115766	Lima	LC1302	40.185127	-113.210162	Zulu
LC1112	40.113965	-113.114832	Lima	LC1303	40.185688	-113.209257	Zulu
LC1113	40.114592	-113.114047	Lima	LC1304	40.186247	-113.208323	Zulu
LC1114	40.115172	-113.113280	Lima	LC1305	40.186897	-113.207423	Zulu
LC1115	40.115530	-113.112572	Lima	LC1306	40.187593	-113.206560	Zulu
LC1150	40.107462	-113.124958	Lima	LC1307	40.188042	-113.205652	Zulu
LC1160	40.111292	-113.118625	Lima	LC1308	40.188228	-113.204773	Zulu
LC1170	40.111292	-113.118625	Lima	LC1309	40.188868	-113.203798	Zulu
LC1201	40.151343	-113.174272	Tango	LC1310	40.189500	-113.202928	Zulu
LC1202	40.152060	-113.173310	Tango	LC1311	40.190025	-113.202043	Zulu
LC1203	40.152822	-113.172340	Tango	LC1312	40.190855	-113.201212	Zulu
LC1204	40.153368	-113.171445	Tango	LC1313	40.191475	-113.200368	Zulu
LC1205	40.153673	-113.170560	Tango	LC1314	40.192065	-113.199385	Zulu
LC1206	40.154050	-113.169630	Tango	LC1315	40.192758	-113.198393	Zulu
LC1207	40.154675	-113.168777	Tango	LC1350	40.192758	-113.198393	Zulu
LC1208	40.155662	-113.168097	Tango	LC1360	40.188228	-113.204773	Zulu
LC1209	40.156087	-113.167333	Tango	LC1370	40.188225	-113.204773	Zulu

Table A3. Perpendicular and trajectory distances from the ground release line to the sampling lines.

Test	Line 100 Mean Distance (m)	Line 100 Trajectory Distance (m)	Line 200 Mean Distance (m)	Line 200 Trajectory Distance (m)	Line 300 Mean Distance (m)	Line 300 Trajectory Distance (m)
1	1616	1864	4024	5498		
2	1617	1622	4025	4031	8861	8870
5	1616	1639	4024	4080		
6	1617	1623	4025	4038	8859	8882
10	1617	1760	4025	4246	8859	9076
12	1616	1616	4024	4024	8859	8862

Table A4. Perpendicular and trajectory distances from the aircraft release line to the sampling lines.

Test	Line 100 Mean Distance (m)	Line 100 Trajectory Distance (m)	Line 200 Mean Distance (m)	Line 200 Trajectory Distance (m)	Line 300 Mean Distance (m)	Line 300 Trajectory Distance (m)
4	9343	9414	15803	15965	20620	20806
9	9635	9646	16156	16175	21010	21036
11	9707	11108				

Appendix B: Analysis of SF_6 Concentration Data for Test 1

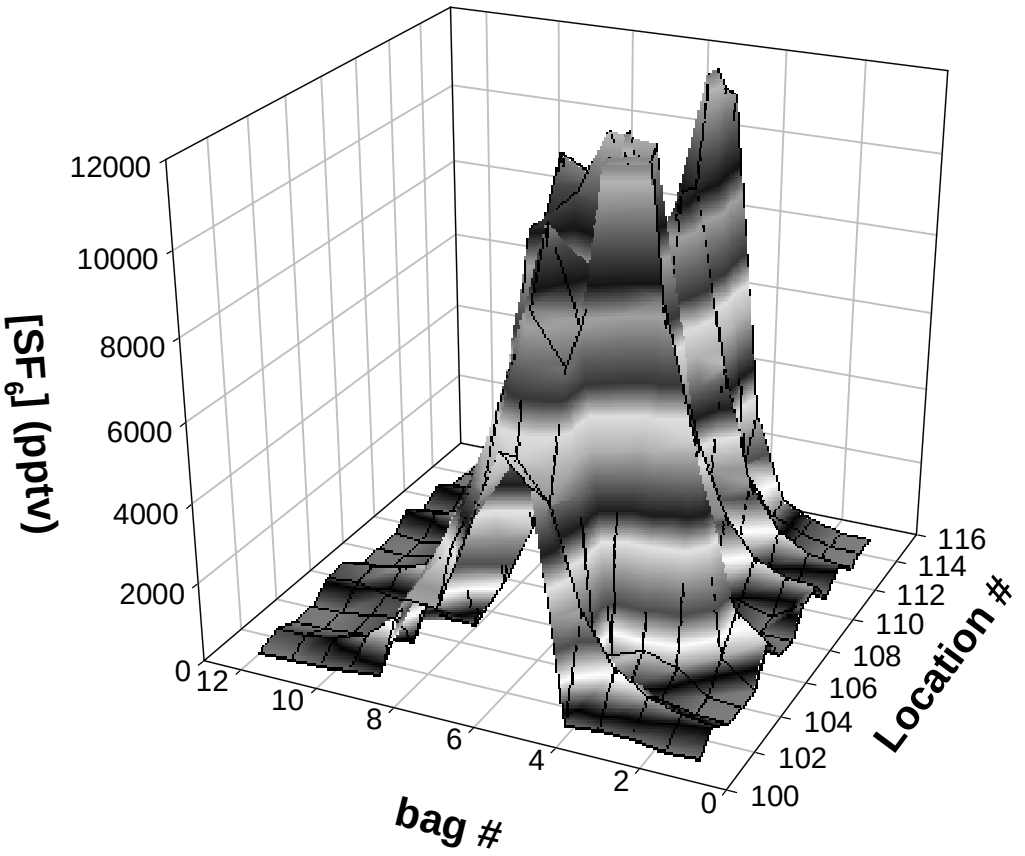

Figure B1. Whole air sampler data for Test 1, Line 1.

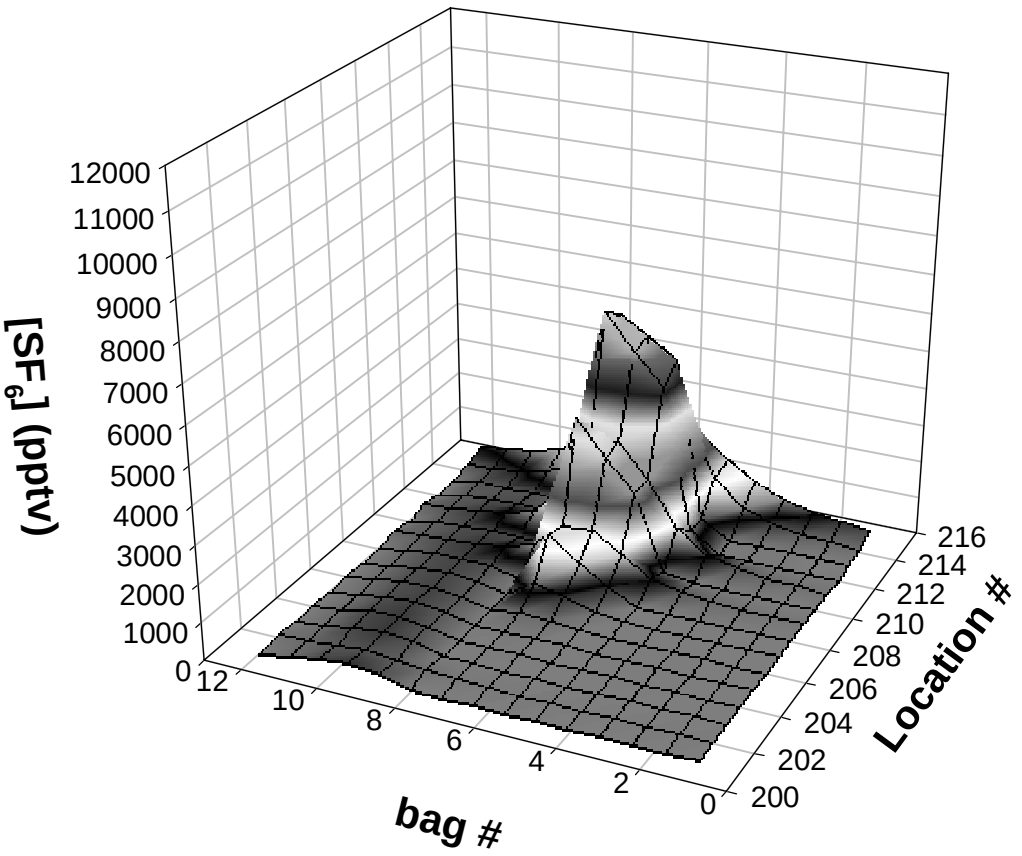

Figure B2. Whole air sampler data for Test 1, Line 2.

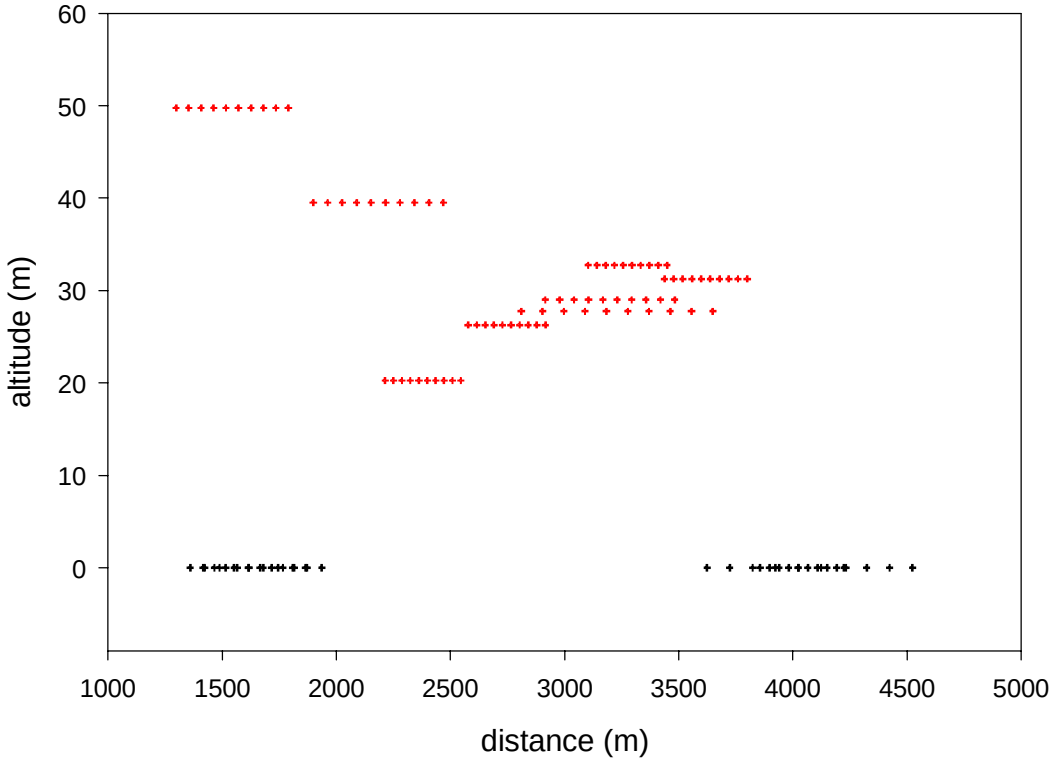

Figure B3. Test 1 continuous analyzer data. Altitude versus downwind distance. The red crosses are aircraft measurements. The black crosses are ground measurements at sampling Lines 1 and 2. The width is ± 1σ from the position of peak concentration.

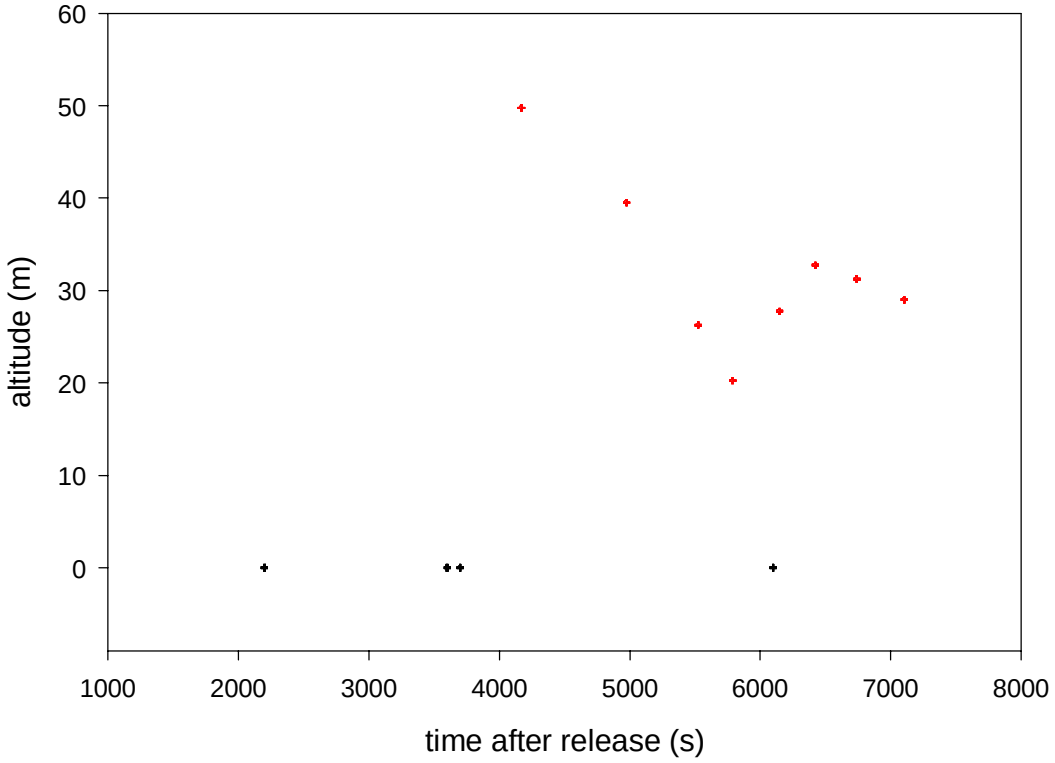

Figure B4. Test 1 continuous analyzer data. Altitude versus time after release. The red crosses are aircraft measurements. The black crosses are ground measurements at sampling Lines 1 and 2.

Table B1. Test 1 sampling line SF_6 concentration variability.

ID	WS ($m\ s^{-1}$)	σ_{ws} ($m\ s^{-1}$)	θ (deg)	σ_{θ} (deg)	mrsd	σ_{mrsd}	N
Line 100	0.8	0.4	168	44	1.1	1.0	12
Line 200	0.9	0.6	181	47	0.8	0.7	12
Line 300							
All					0.9	0.8	24
0 - 100 pptv					0.8	0.8	10
100 - 500 pptv					0.8	0.9	5
> 500 pptv					1.1	0.9	9

Table B2. Test 1 sampling line SF_6 concentration variability by line for each sampling bag.

Line 100				Line 200				Line 300			
Bag	Mean SF_6 (pptv)	σ_{SF6} (pptv)	rsd	Bag	Mean SF_6 (pptv)	σ_{SF6} (pptv)	rsd	Bag	Mean SF_6 (pptv)	σ_{SF6} (pptv)	rsd
1	14	24	1.7	1	5	4	0.8	1			
2	78	195	2.5	2	3	0	0.1	2			
3	846	2740	3.2	3	4	2	0.5	3			
4	2887	4570	1.6	4	4	0	0.1	4			
5	9960	1980	0.2	5	120	210	1.8	5			
6	6980	3700	0.5	6	1250	2050	1.6	6			
7	6255	3370	0.5	7	1920	2680	1.4	7			
8	3888	1830	0.5	8	228	413	1.8	8			
9	696	445	0.6	9	194	31	0.2	9			
10	65	44	0.7	10	283	55	0.2	10			
11	27	9	0.3	11	132	40	0.3	11			
12	48	28	0.6	12	8	4	0.4	12			

Table B3. Test 1 SF_6 transport parameters from ground-based continuous analyzers.

	Location					
	101	115	201	215	301	315
WS ($m\ s^{-1}$)	0.8		0.9			
σ_{ws} ($m\ s^{-1}$)	0.4		0.6			
θ (deg)	168		181			
σ_{θ} (deg)	44		47			
V_{SF6} ($m\ s^{-1}$)	0.8	0.5	0.9	1.5		
Error Limit V_{SF6} ($m\ s^{-1}$)	0.1	0.1	0.03	0.7		
σ_x (m)	500	640	420	1000		
Error Limit σ_x (m)	240	150	220	500		
SF_6 Transport Time (s)	2200	3700	6100	3600		
Error Limit SF_6 Transport Time (s)	270	640	180	1800		
SF_6 Peak (pptv)	12000	6700	340	6800		
Error Limit SF_6 Peak (pptv)	7100	1200	160	1050		

Table B4. Test 1 SF_6 transport parameters from aircraft continuous analyzer.

	Pass							
	1	2	3	4	5	6	7	8
SF_6 Speed ($m\ s^{-1}$)	0.3	0.4	0.4	0.4	0.5	0.5	0.5	0.4
Error SF_6 Speed ($m\ s^{-1}$)	0.10	0.06	0.02	0.01	0.02	0.01	0.02	0.00
σ_x (m)	550	630	380	370	930	380	400	630
Error σ_x (m)	680	670	100	110	830	70	70	90
Peak Detection Time (s)	4170	4980	5530	5790	6150	6420	6740	7100
Error Peak Detection Time (s)	19	19	18	18	18	18	18	18
Peak Concentration (pptv)	70	1680	1940	2530	1160	1820	1020	150
Error Peak Concentration (pptv)	40	1820	420	710	560	270	170	15
Altitude (m)	50	40	30	20	30	30	30	30
Downwind Distance (m)	1500	2200	2700	2400	3200	3300	3600	3200
Error Downwind Distance (m)	500	300	100	100	200	100	200	200

Appendix C: Analysis of SF_6 Concentration Data for Test 2

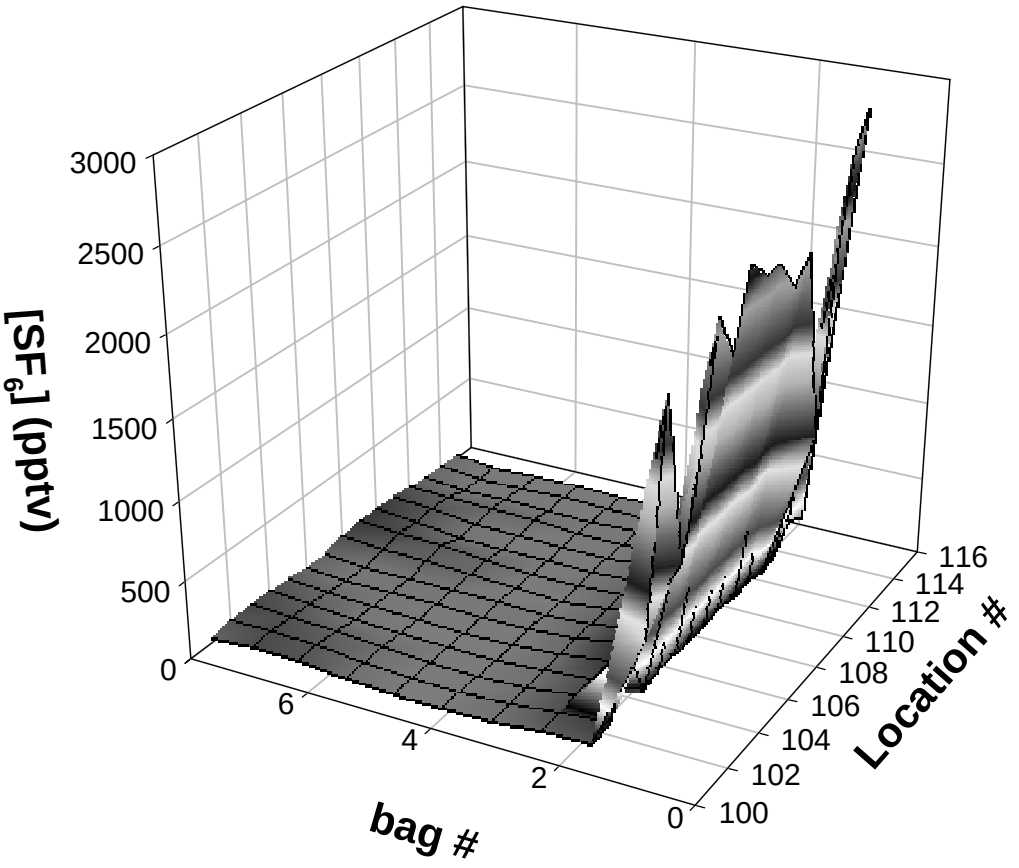

Figure C1. Whole air sampler data for Test 2, Line 1.

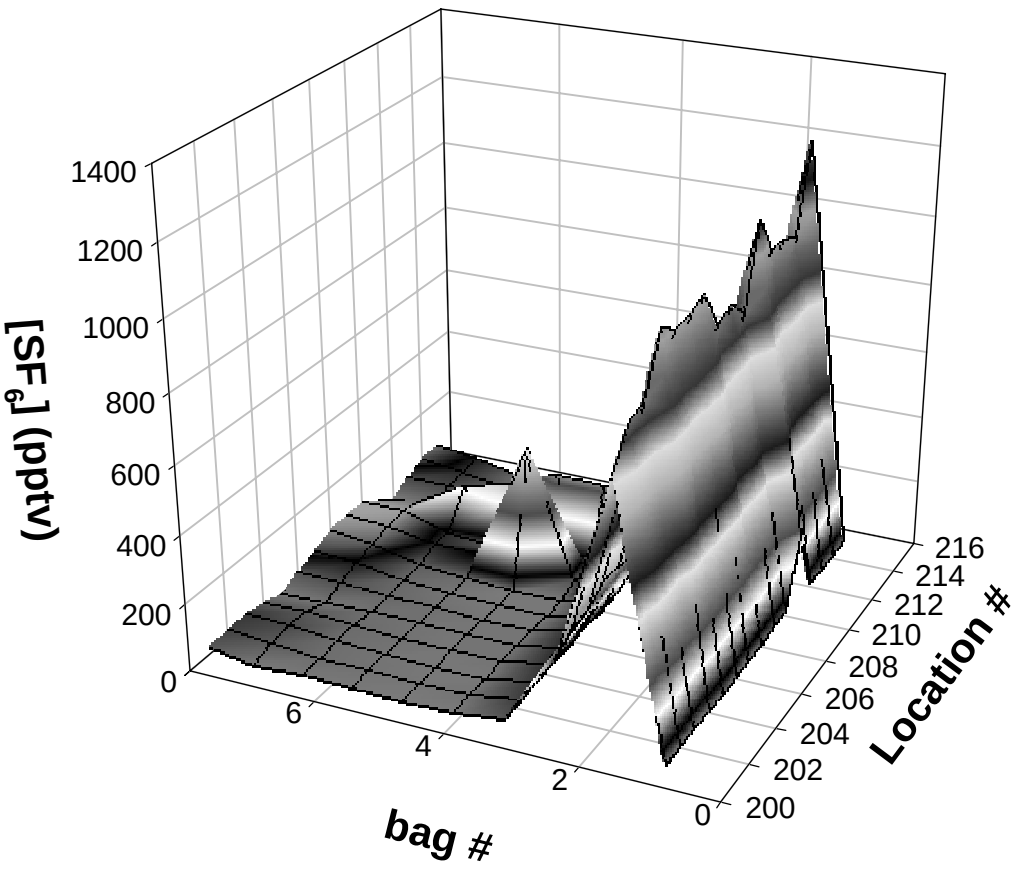

Figure C2. Whole air sampler data for Test 2, Line 2.

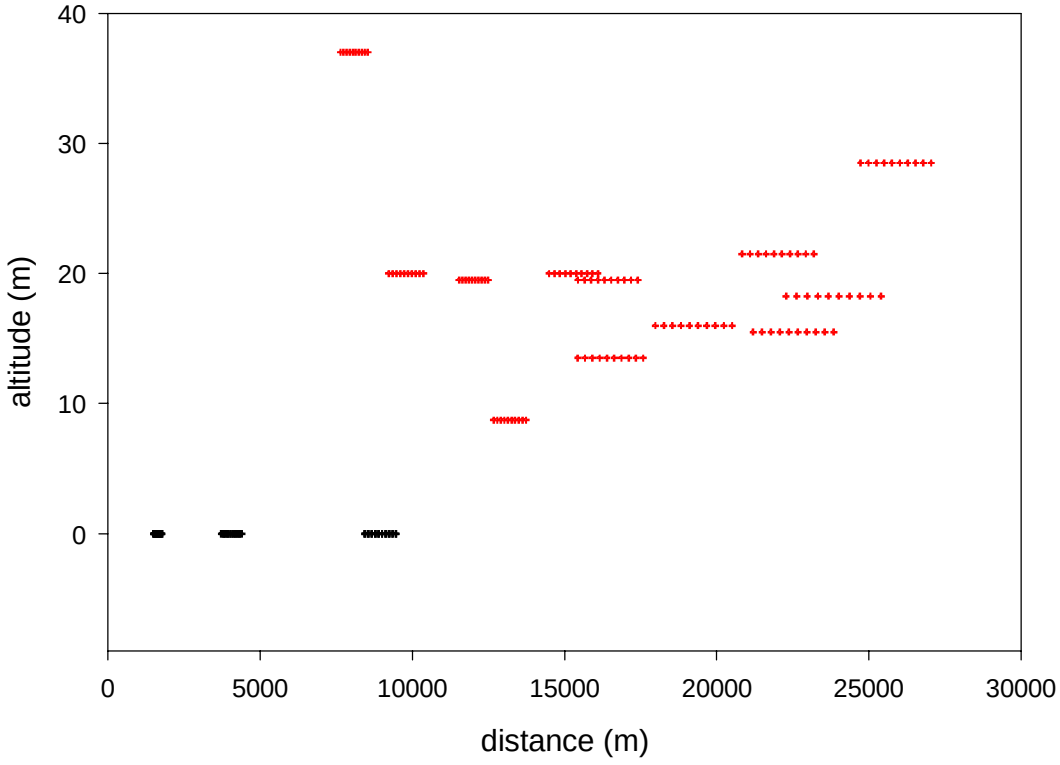

Figure C3. Test 2 continuous analyzer data. Altitude versus downwind distance. The red crosses are aircraft measurements. The black crosses are ground measurements at sampling Lines 1, 2 and 3. The width is ± 1σ from the position of peak concentration.

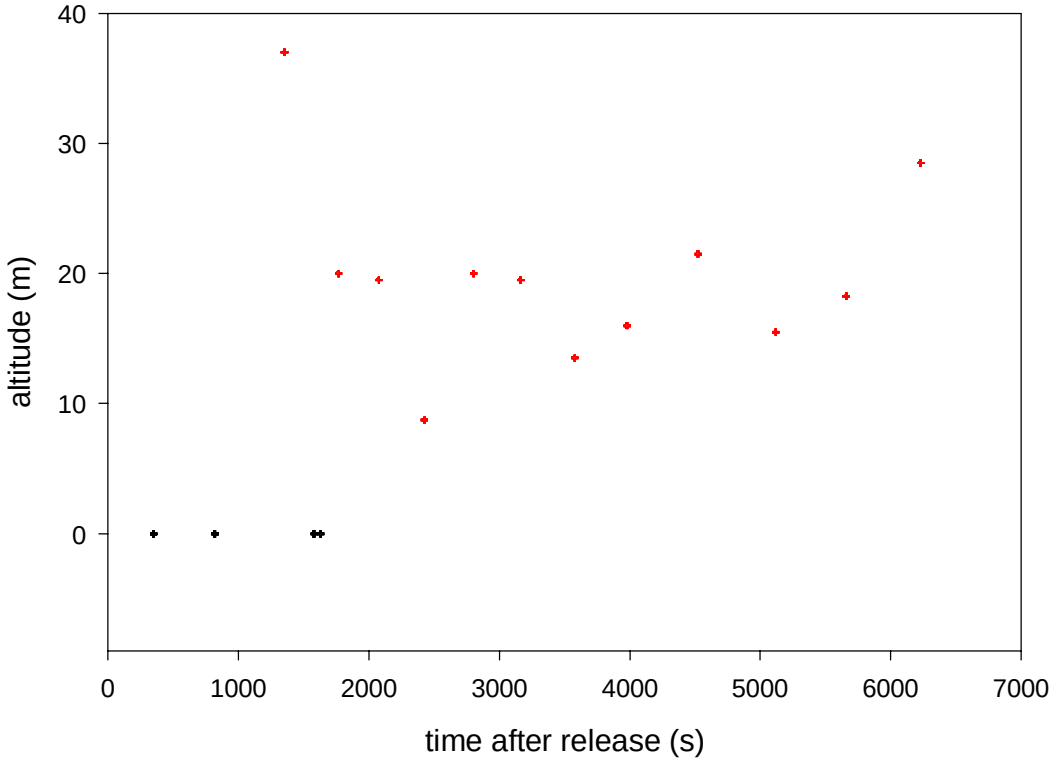

Figure C4. Test 2 continuous analyzer data. Altitude versus time after release. The red crosses are aircraft measurements. The black crosses are ground measurements at sampling Lines 1, 2 and 3.

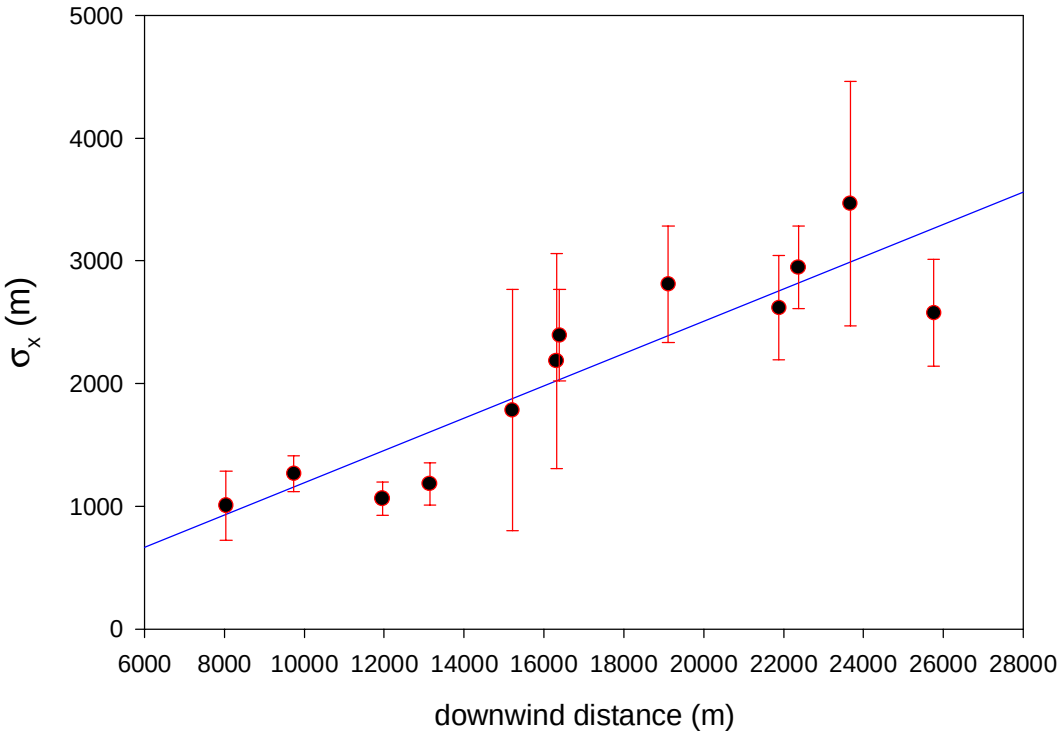

Figure C5. Test 2 σ_x versus downwind distance from aircraft continuous analyzer measurements. The blue line is a linear fit to the data with the equation $\sigma_x = (0.13 \pm 0.02)\ x + (130 \pm 40)$, $r^2 = 0.8$.

Table C1. Test 2 sampling line SF_6 concentration variability.

ID	WS ($m\ s^{-1}$)	σ_{ws} ($m\ s^{-1}$)	θ (deg)	σ_θ (deg)	mrsd	σ_{mrsd}	N
Line 100	3.2	0.5	142	4	0.9	0.5	6
Line 200	3.1	0.5	141	5	2.2	0.9	12
Line 300	2.9	0.5	140	6	0.8	0.6	12
All					1.3	0.9	36
0 - 100 pptv					1.4	0.8	32
100 - 500 pptv							
> 500 pptv					0.9	1.4	4

Table C2. Test 2 sampling line SF_6 concentration variability by line for each sampling bag.

Line 100				Line 200				Line 300			
Bag	Mean SF_6 (pptv)	σ_{SF6} (pptv)	rsd	Bag	Mean SF_6 (pptv)	σ_{SF6} (pptv)	rsd	Bag	Mean SF_6 (pptv)	σ_{SF6} (pptv)	rsd
1	1838	879	0.5	1	21	51	2.4	1	401	40	0.1
2	39	39	1.0	2	1011	114	0.1	2	5	2	0.4
3	7	3	0.5	3	28	70	2.5	3	5	2	0.4
4	6	3	0.5	4	21	59	2.8	4	4	2	0.5
5	5	2	0.4	5	47	117	2.5	5	5	2	0.4
6	8	12	1.5	6	18	47	2.6	6	5	2	0.4
7	15	21	1.3	7	6	5	0.9	7	4	2	0.5
8				8	22	61	2.8	8	3	3	1.0
9				9	21	59	2.7	9	4	6	1.0
10				10	23	53	2.3	10	7	12	1.0
11				11	69	153	2.2	11	2	4	1.0
12				12	443	1310	3.0	12	9	17	2.0

Table C3. Test 2 SF_6 transport parameters from ground-based continuous analyzers.

	Location					
	101	115	201	215	301	315
WS ($m\ s^{-1}$)	3.2		3.1		2.9	
σ_{ws} ($m\ s^{-1}$)	0.5		0.5		0.5	
θ (deg)	142		141		140	
σ_θ (deg)	4		5		6	
V_{SF6} ($m\ s^{-1}$)	4.6	4.6	5.2	4.9	5.4	5.6
Error Limit V_{SF6} ($m\ s^{-1}$)	1.2	1.2	0.4	0.3	0.1	0.1
σ_x (m)	290	320	750	620	1150	1120
Error Limit σ_x (m)	80	90	400	60	90	90
SF_6 Transport Time (s)	350	350	770	820	1630	1580
Error Limit SF_6 Transport Time (s)	95	95	60	60	40	40
SF_6 Peak (pptv)	10700	16800	2100	3100	1000	700
Error Limit SF_6 Peak (pptv)	530	1400	730	210	70	50

Table C4. Test 2 SF_6 transport parameters from aircraft continuous analyzer.

	Pass							
	1	2	3	4	5	6	7	8
SF_6 Speed ($m\ s^{-1}$)	5.9	5.5	5.7	5.4	5.4	5.1	4.5	4.8
Error SF_6 Speed ($m\ s^{-1}$)	0.20	0.04	0.01	0.01	0.10	0.08	0.04	0.03
σ_x (m)	1000	1270	1060	1180	1780	2180	2400	2800
Error σ_x (m)	280	150	130	170	980	880	370	480
Peak Detection Time (s)	1350	1770	2080	2430	2800	3170	3580	3980
Error Peak Detection Time (s)	15	14	14	14	16	15	31	15
Peak Concentration (pptv)	870	760	560	400	280	250	240	260
Error Peak Concentration (pptv)	200	40	40	40	110	70	30	40
Altitude (m)	40	20	20	10	20	20	10	20
Downwind Distance (m)	8000	9700	12000	13100	15200	16300	16400	19100
Error Downwind Distance (m)	300	100	30	40	500	300	1700	100

Table C4. Test 2 SF_6 transport parameters from aircraft continuous analyzer (continued).

	Pass							
	9	10	11	12	13	14	15	16
SF_6 Speed ($m\ s^{-1}$)	4.8	4.3	4.1	4.1				
Error SF_6 Speed ($m\ s^{-1}$)	0.04	0.01	0.04	0.20				
σ_x (m)	2620	2950	3470	2580				
Error σ_x (m)	430	340	1000	440				
Peak Detection Time (s)	4520	5120	5660	6230				
Error Peak Detection Time (s)	15	14	15	26				
Peak Concentration (pptv)	170	240	170	100				
Error Peak Concentration (pptv)	20	10	40	10				
Altitude (m)	20	20	20	30				
Downwind Distance (m)	21900	22400	23700	25800				
Error Downwind Distance (m)	200	70	200	1600				

Appendix D: Analysis of SF_6 Concentration Data for Test 4

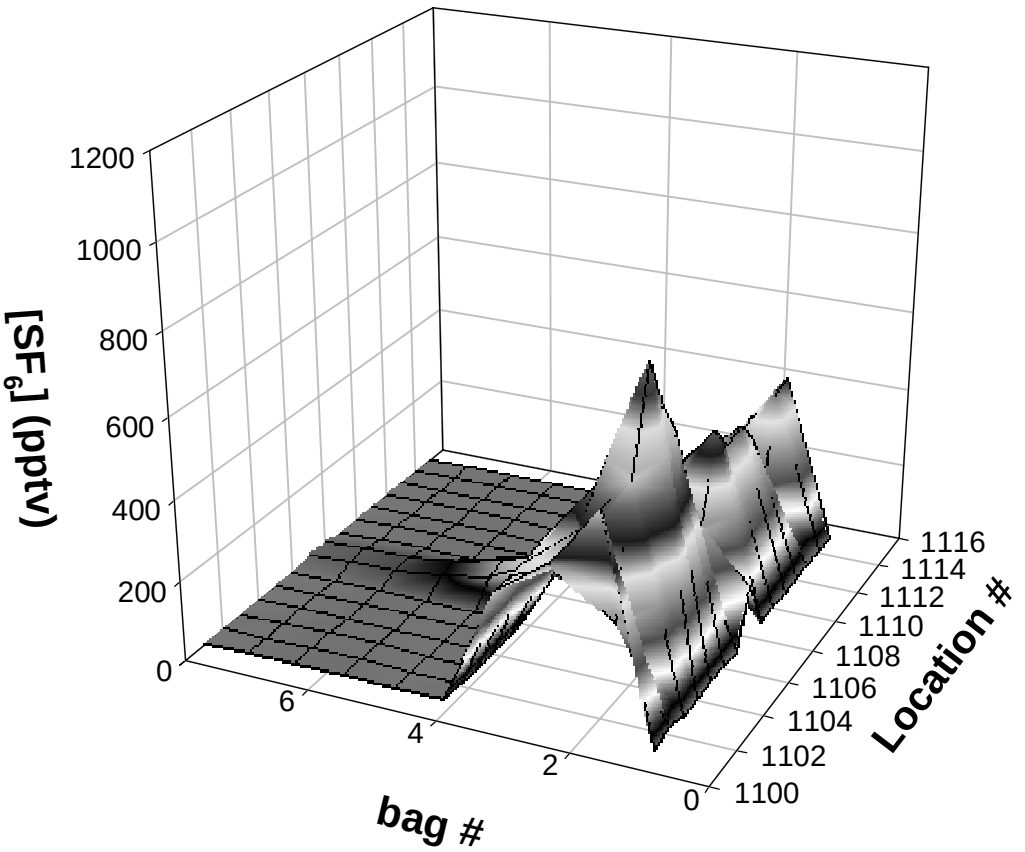

Figure D1. Whole air sampler data for Test 4, Line 1.

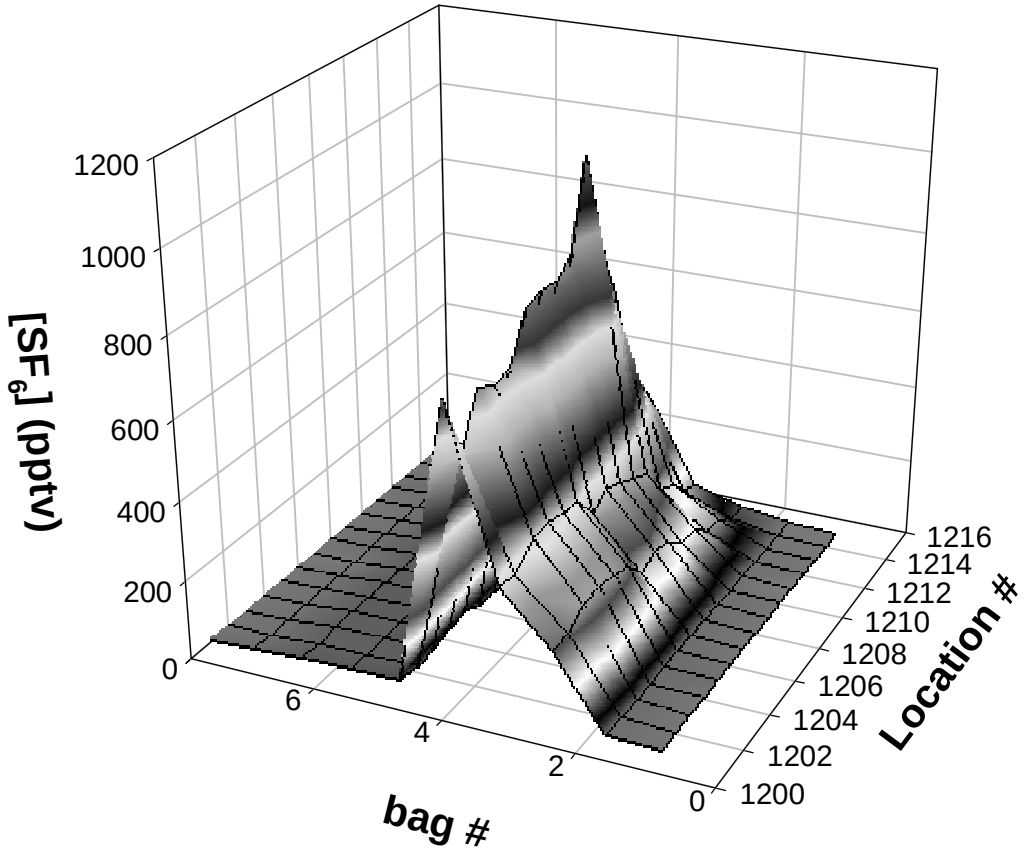

Figure D2. Whole air sampler data for Test 4, Line 2.

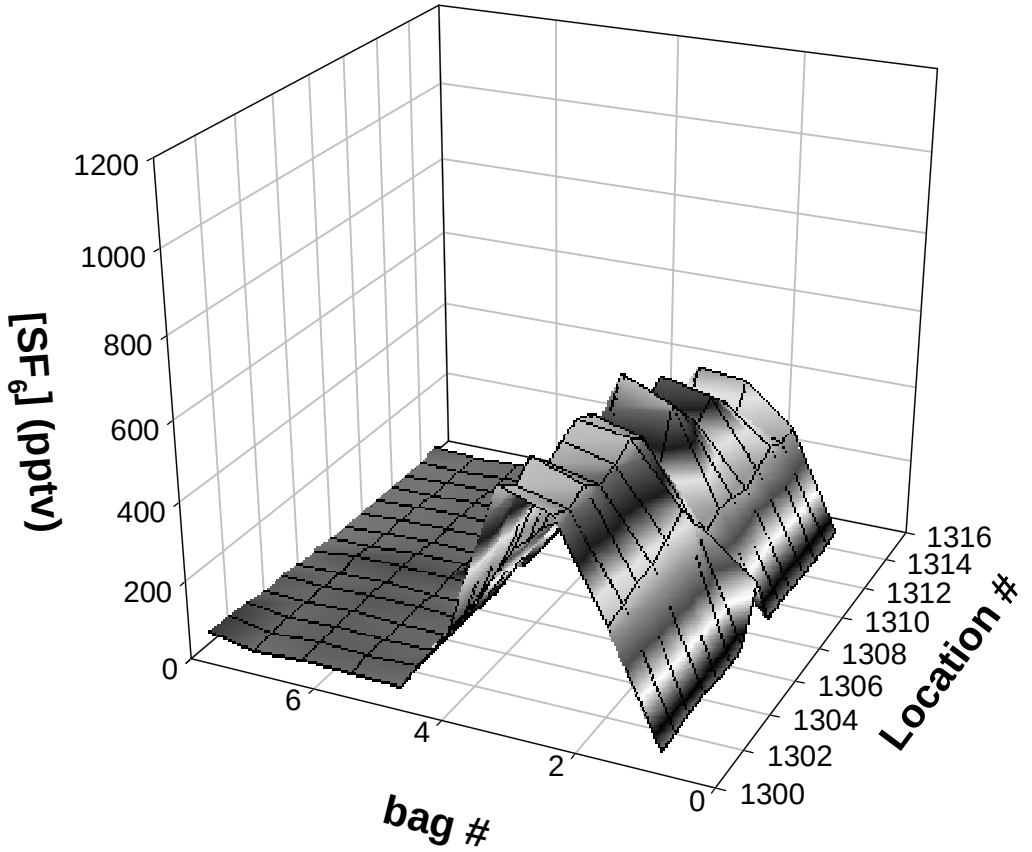

Figure D3. Whole air sampler data for Test 4, Line 3.

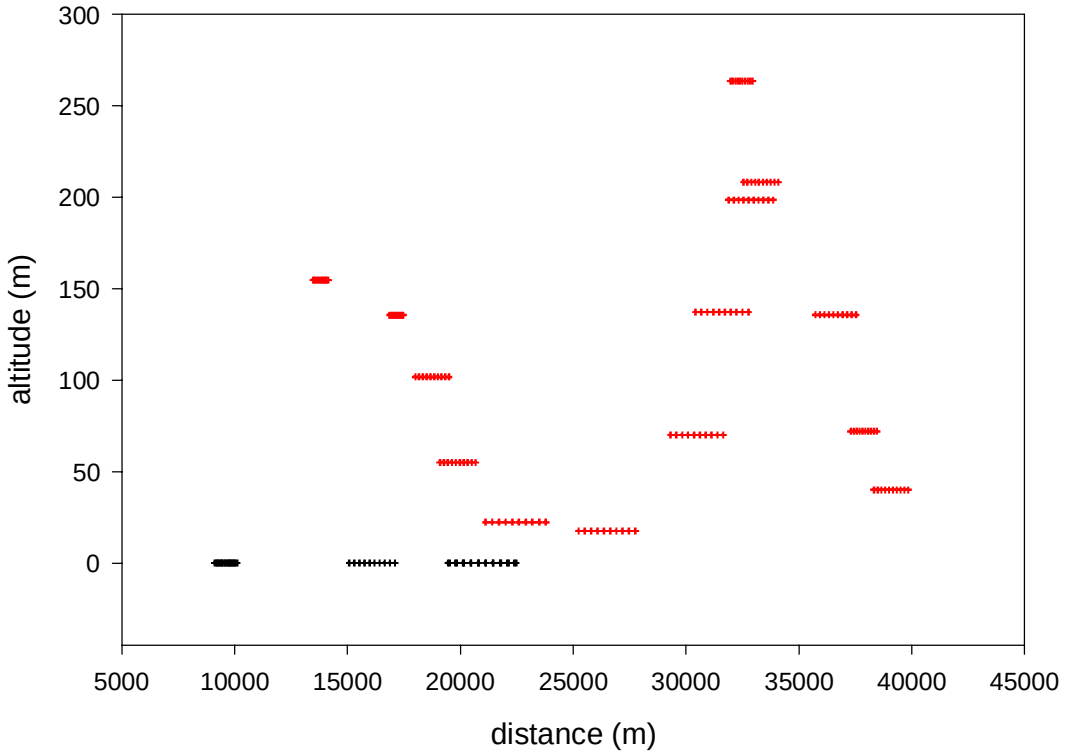

Figure D4. Test 4 continuous analyzer data. Altitude versus downwind distance. The red crosses are aircraft measurements. The black crosses are ground measurements at sampling Lines 1, 2, and 3. The width is ± 1σ from the position of peak concentration.

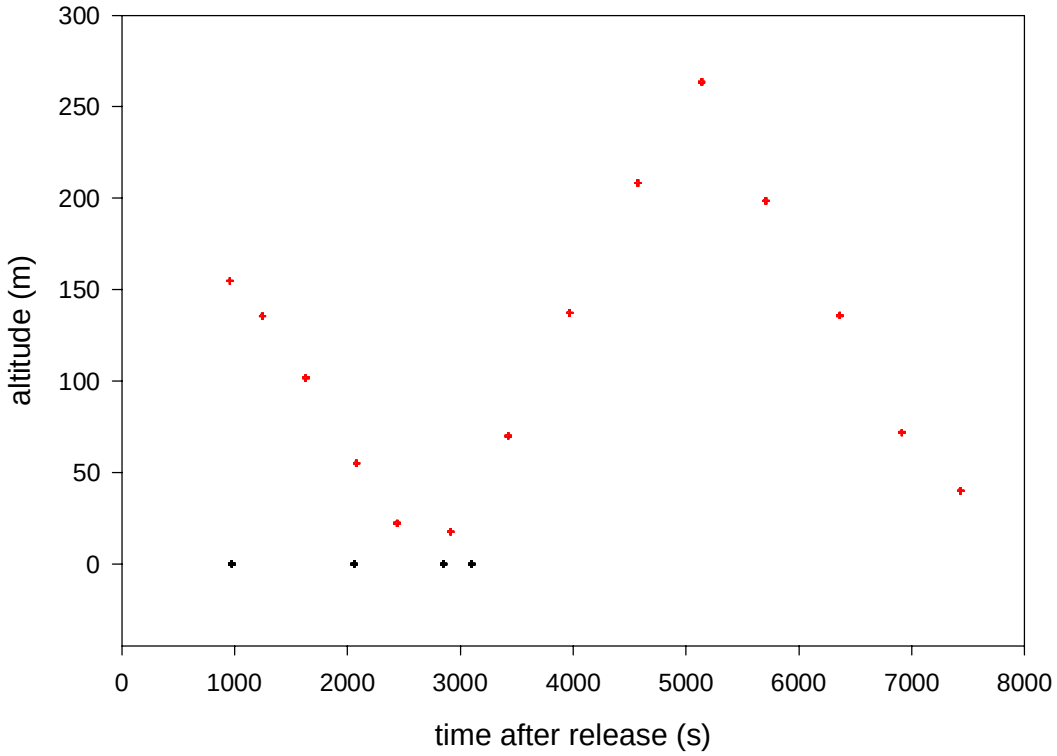

Figure D5. Test 4 continuous analyzer data. Altitude versus time after release. The red crosses are aircraft measurements. The black crosses are ground measurements at sampling Lines 1, 2 and 3.

Table D1. Test 4 sampling line SF_6 concentration variability.

ID	WS ($m\ s^{-1}$)	σ_{ws} ($m\ s^{-1}$)	θ (deg)	σ_θ (deg)	mrsd	σ_{mrsd}	N
Line 100	4.0	0.7	146	4	0.6	0.7	12
Line 200	4.2	0.8	147	7	0.6	0.5	12
Line 300	4.4	0.9	147	7	1.0	0.9	12
All					0.7	0.7	36
0 - 100 pptv					0.8	1.2	5
100 - 500 pptv							
> 500 pptv					0.3	0.1	3

Table D2. Test 4 sampling line SF_6 concentration variability by line for each sampling bag.

Line 1100				Line 1200				Line 1300			
Bag	Mean SF_6 (pptv)	σ_{SF6} (pptv)	rsd	Bag	Mean SF_6 (pptv)	σ_{SF6} (pptv)	rsd	Bag	Mean SF_6 (pptv)	σ_{SF6} (pptv)	rsd
1	6	5	0.8	1	5	1	0.3	1	7	3	0.5
2	508	140	0.3	2	4	1	0.1	2	295	37	0.1
3	281	70	0.2	3	183	112	0.6	3	581	105	0.2
4	6	2	0.3	4	691	201	0.3	4	173	36	0.2
5	5	1	0.1	5	19	11	0.6	5	9	3	0.4
6	5	1	0.1	6	5	2	0.4	6	7	4	0.5
7	5	1	0.1	7	5	2	0.4	7	8	4	0.5
8	4	1	0.1	8	5	1	0.3	8	16	33	2.0
9	4	2	0.4	9	9	14	1.6	9	19	27	1.4
10	3	3	1.1	10	6	2	0.4	10	25	38	1.5
11	7	11	1.5	11	7	6	0.8	11	54	158	3.0
12	13	30	2.0	12	24	44	1.8	12	23	34	1.5

Table D3. Test 4 SF_6 transport parameters from ground-based continuous analyzers.

	Location					
	1101	1115	1201	1215	1301	1315
WS ($m\ s^{-1}$)	4.1		4.2		4.4	
σ_{ws} ($m\ s^{-1}$)	0.7		0.8		0.9	
θ (deg)	146		147		147	
σ_{θ} (deg)	4		7		6.5	
V_{SF6} ($m\ s^{-1}$)	10.0	10.0	7.7		7.3	6.7
Error Limit V_{SF6} ($m\ s^{-1}$)	1.0	1.0	0.3		0.3	0.2
σ_x (m)	1100	915	2250		3200	3350
Error Limit σ_x (m)	120	100	150		700	170
SF_6 Transport Time (s)	975	975	2060		2850	3100
Error Limit SF_6 Transport Time (s)	100	100	90		140	107
SF_6 Peak (pptv)	2400	2418	1300		702	930
Error Limit SF_6 Peak (pptv)	90	130	70		177	35

Table D4. Test 4 SF_6 transport parameters from aircraft continuous analyzer.

	Pass							
	1	2	3	4	5	6	7	8
SF_6 Speed ($m\ s^{-1}$)	14.3	13.7	11.4	9.5	9.1	9.0	8.8	7.9
Error SF_6 Speed ($m\ s^{-1}$)	0.10	0.07	0.04	0.20	0.03	0.10	0.10	0.40
σ_x (m)	730	660	1650	1760	2950	2790	2600	2590
Error σ_x (m)	710	540	970	810	860	690	780	1250
Peak Detection Time (s)	960	1250	1630	2080	2440	2910	3420	3960
Error Peak Detection Time (s)	1	2	1	8	1	7	8	23
Peak Concentration (pptv)	370	1220	1600	1480	1170	750	580	330
Error Peak Concentration (pptv)	260	620	600	470	250	160	170	160
Altitude (m)	150	140	100	60	20	20	70	140
Downwind Distance (m)	13800	17100	18700	19800	22300	26400	30400	31500
Error Downwind Distance (m)	100	90	80	500	80	400	600	1600

Table D4. Test 4 SF_6 transport parameters from aircraft continuous analyzer (continued).

	Pass							
	9	10	11	12	13	14	15	16
SF_6 Speed ($m\ s^{-1}$)	7.2	6.3	5.7	5.7	5.4	5.2		
Error SF_6 Speed ($m\ s^{-1}$)	0.09	0.10	0.10	0.09	0.10	0.06		
σ_x (m)	1700	1080	2190	1990	1280	1680		
Error σ_x (m)	1100	720	420	520	820	510		
Peak Detection Time (s)	4570	5140	5710	6360	6910	7430		
Error Peak Detection Time (s)	6	13	8	10	12	8		
Peak Concentration (pptv)	200	130	110	210	340	240		
Error Peak Concentration (pptv)	110	140	20	50	270	70		
Altitude (m)	210	260	200	140	70	40		
Downwind Distance (m)	33200	32400	32800	36500	37800	39000		
Error Downwind Distance (m)	400	900	600	600	900	500		

Appendix E: Analysis of SF_6 Concentration Data for Test 5

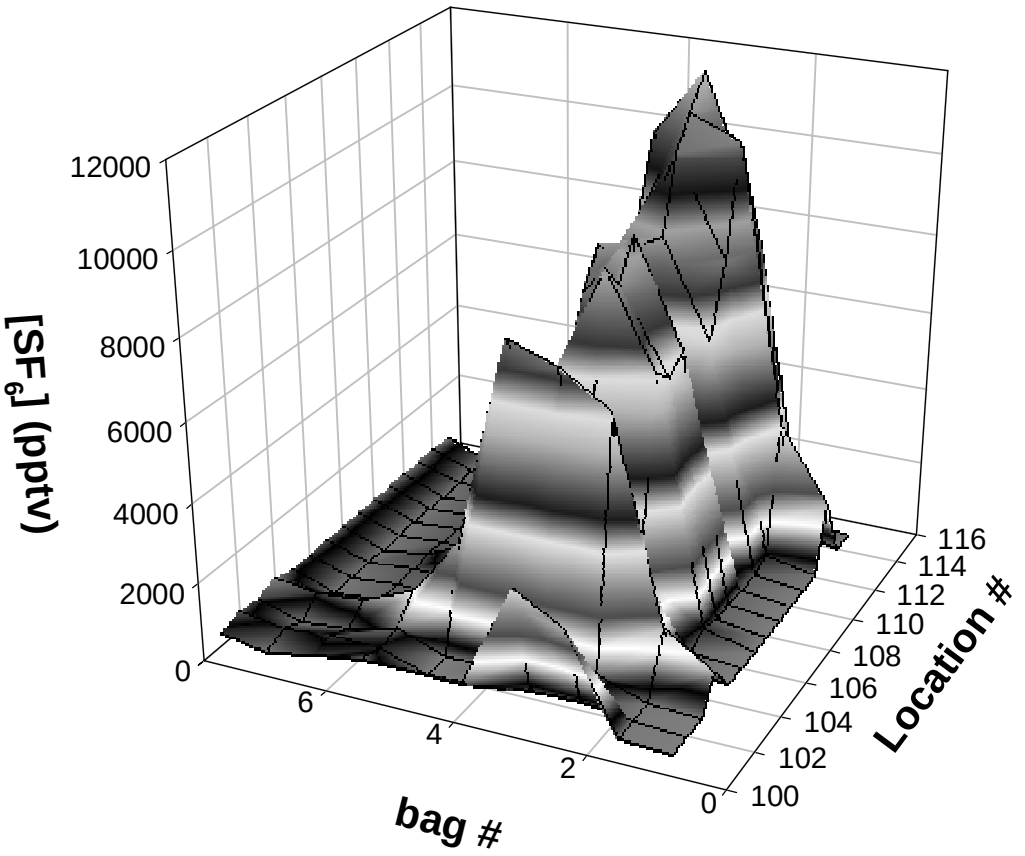

Figure E1. Whole air sampler data for Test 5, Line 1.

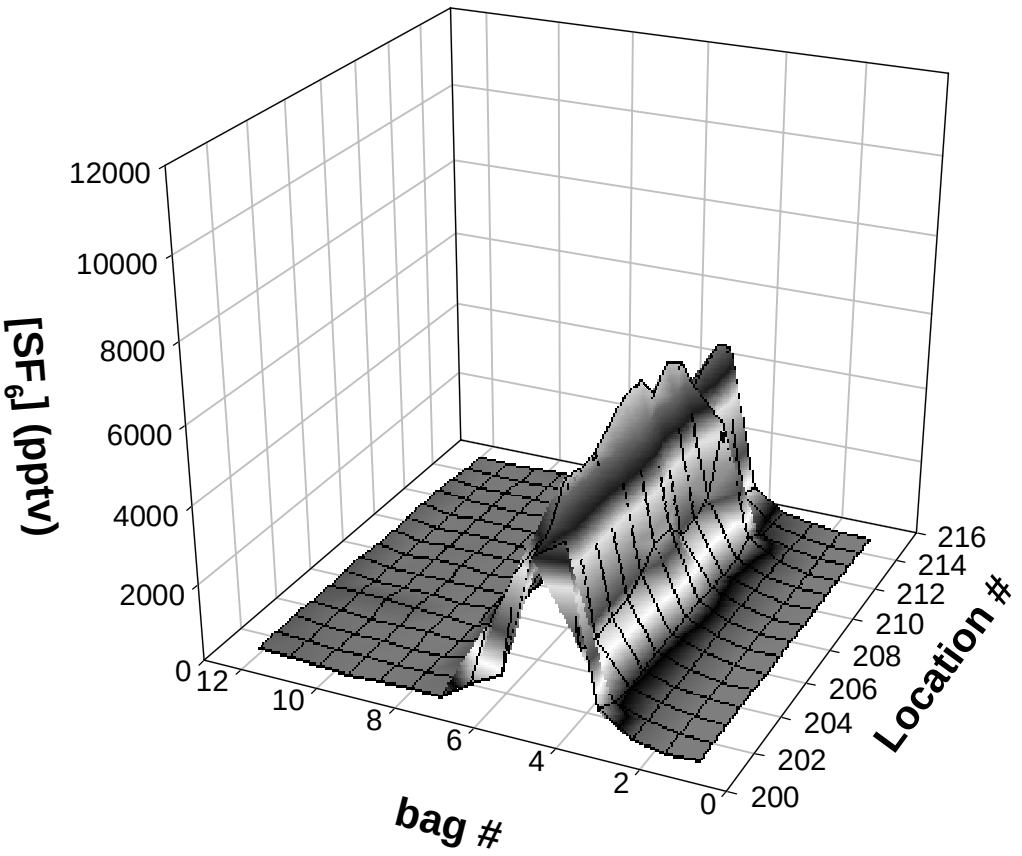

Figure E2. Whole air sampler data for Test 5, Line 2.

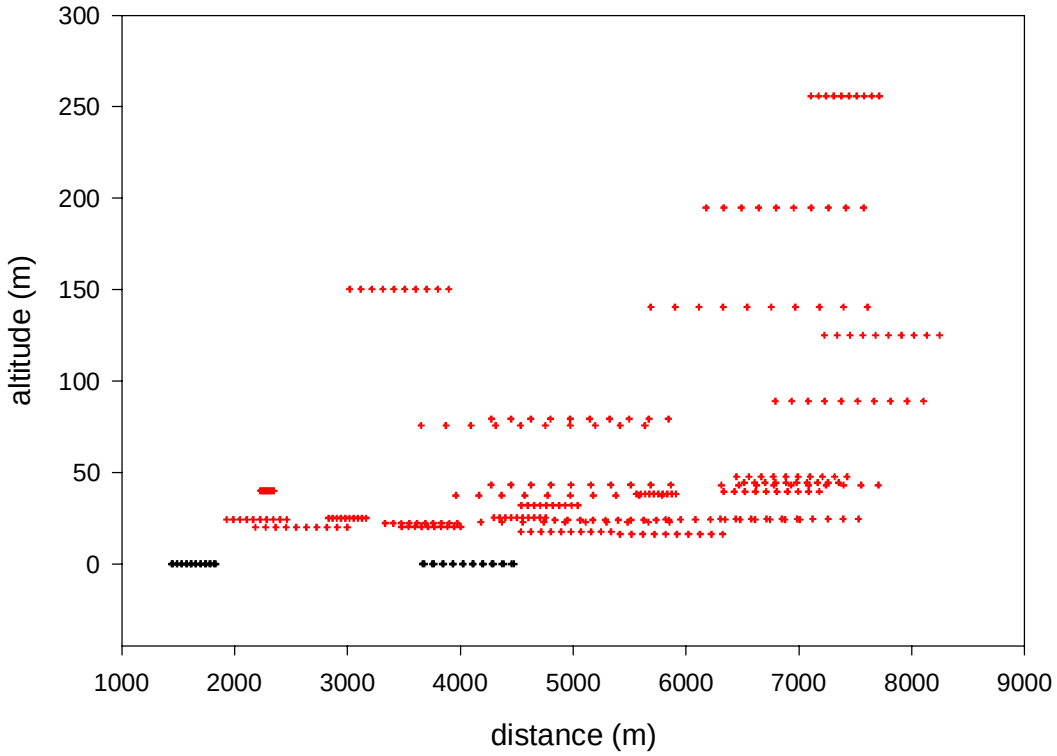

Figure E3. Test 5 continuous analyzer data. Altitude versus downwind distance. The red crosses are aircraft measurements. The black crosses are ground measurements at sampling Lines 1 and 2. The width is ± 1σ from the position of peak concentration.

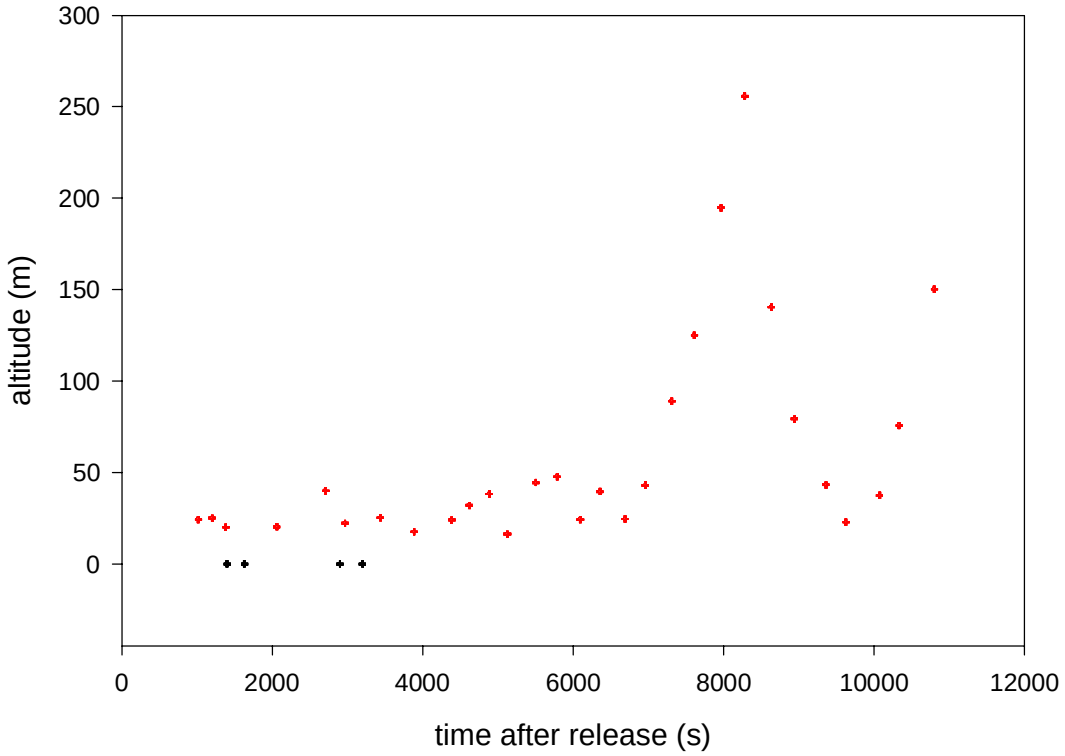

Figure E4. Test 5 continuous analyzer data. Altitude versus time after release. The red crosses are aircraft measurements. The black crosses are ground measurements at sampling Lines 1 and 2.

Table E1. Test 5 sampling line SF_6 concentration variability.

ID	WS ($m\ s^{-1}$)	σ_{ws} ($m\ s^{-1}$)	θ (deg)	σ_θ (deg)	mrsd	σ_{mrsd}	N
Line 100	1.1	0.3	128	12	1.4	1.0	7
Line 200	0.9	0.4	128	17	0.5	0.3	12
Line 300					0.5	0.4	12
All					0.7	0.7	31
0 - 100 pptv					0.7	0.6	19
100 - 500 pptv					0.4	0.2	6
> 500 pptv					1.0	1.2	6

Table E2. Test 5 sampling line SF_6 concentration variability by line for each sampling bag.

Line 100				Line 200				Line 300			
Bag	Mean SF_6 (pptv)	σ_{SF6} (pptv)	rsd	Bag	Mean SF_6 (pptv)	σ_{SF6} (pptv)	rsd	Bag	Mean SF_6 (pptv)	σ_{SF6} (pptv)	rsd
1	12	16	1.4	1	5	0	0.2	1	5	1	0.2
2	65	78	1.2	2	5	0	0.1	2	5	0	0.1
3	7543	4849	0.6	3	13	18	1.4	3	6	6	0.9
4	6099	3300	0.5	4	1835	1144	0.6	4	7	10	1.3
5	769	2660	3.5	5	4837	1423	0.3	5	5	1	0.1
6	69	141	2.0	6	2718	1204	0.4	6	21	15	0.7
7	32	20	0.6	7	231	160	0.7	7	78	23	0.3
8				8	34	13	0.4	8	176	37	0.2
9				9	19	6	0.3	9	284	114	0.4
10				10	14	4	0.3	10	333	72	0.2
11				11	40	37	0.9	11	207	57	0.3
12				12	138	54	0.4	12	48	46	0.9

Table E3. Test 5 SF_6 transport parameters from ground-based continuous analyzers.

	Location					
	101	115	201	215	301	315
WS ($m\ s^{-1}$)	1.1		0.9			
σ_{ws} ($m\ s^{-1}$)	0.3		0.4			
θ (deg)	128		128			
σ_{θ} (deg)	12		17			
V_{SF6} ($m\ s^{-1}$)	1.2	1.0	1.3	1.4		
Error Limit V_{SF6} ($m\ s^{-1}$)	0.1	0.1	0.02	0.05		
σ_x (m)	430	410	900	860		
Error Limit σ_x (m)	42	44	90	260		
SF_6 Transport Time (s)	1400	1630	3200	2900		
Error Limit SF_6 Transport Time (s)	95	95	60	95		
SF_6 Peak (pptv)	17300	19300	6165	4420		
Error Limit SF_6 Peak (pptv)	1140	1850	570	1100		

Table E4. Test 5 SF_6 transport parameters from aircraft continuous analyzer.

	Pass							
	1	2	3	4	5	6	7	8
SF_6 Speed ($m\ s^{-1}$)	2.1	2.4	1.8	1.7	0.8	1.2	1.3	1.2
Error SF_6 Speed ($m\ s^{-1}$)	0.03	0.08	0.00	0.04	0.00	0.06	0.06	0.03
σ_x (m)	590	370	910	580	130	710	510	890
Error σ_x (m)	730	410	670	90	120	620	310	800
Peak Detection Time (s)	1020	1200	1380	2060	2710	2970	3440	3890
Error Peak Detection Time (s)	11	11	11	11	11	11	11	11
Peak Concentration (pptv)	1500	260	1180	1010	690	3320	3200	4900
Error Peak Concentration (pptv)	840	190	520	140	350	2500	2090	2400
Altitude (m)	20	30	20	20	40	20	30	20
Downwind Distance (m)	2200	3000	2500	3700	2300	3600	4500	4900
Error Downwind Distance (m)	30	100	100	100	100	200	200	100

Table E4. Test 5 SF_6 transport parameters from aircraft continuous analyzer (continued).

	Pass							
	9	10	11	12	13	14	15	16
SF_6 Speed ($m\ s^{-1}$)	1.2	1.0	1.1	1.1	1.2	1.1	1.0	1.0
Error SF_6 Speed ($m\ s^{-1}$)	0.10	0.04	0.02	0.03	0.07	0.02	0.08	0.01
σ_x (m)	1120	560	390	1010	930	1090	1320	940
Error σ_x (m)	640	560	390	500	800	900	740	120
Peak Detection Time (s)	4390	4620	4890	5130	5500	5790	6100	6360
Error Peak Detection Time (s)	13	11	11	11	12	11	13	11
Peak Concentration (pptv)	3300	1170	280	3220	1480	1200	1540	1190
Error Peak Concentration (pptv)	1260	940	300	1180	1140	660	570	90
Altitude (m)	20	30	40	20	40	50	20	40
Downwind Distance (m)	5300	4800	5700	5800	6900	6900	6300	6700
Error Downwind Distance (m)	500	200	100	200	400	200	500	100

Table E4. Test 5 SF_6 transport parameters from aircraft continuous analyzer (continued).

	Pass							
	17	18	19	20	21	22	23	24
SF_6 Speed ($m\ s^{-1}$)	1.0	0.9	1.0	1.0	0.8	0.8	0.7	0.5
Error SF_6 Speed ($m\ s^{-1}$)	0.07	0.02	0.06	0.01	0.08	0.06	0.08	0.10
σ_x (m)	1360	1550	1460	1130	1550	670	2130	1740
Error σ_x (m)	680	770	780	680	820	630	1000	1140
Peak Detection Time (s)	6700	7000	7300	7600	7970	8280	8640	8940
Error Peak Detection Time (s)	13	11	13	11	15	14	15	20
Peak Concentration (pptv)	920	680	530	390	310	420	230	180
Error Peak Concentration (pptv)	310	230	210	150	120	530	90	120
Altitude (m)	20	40	90	130	190	260	140	80
Downwind Distance (m)	6900	6900	7400	7700	6800	7400	6500	5000
Error Downwind Distance (m)	500	200	500	100	700	600	800	1200

Table E4. Test 5 SF_6 transport parameters from aircraft continuous analyzer (continued).

	Pass							
	25	26	27	28	29	30	31	32
SF_6 Speed ($m\ s^{-1}$)	0.5	0.5	0.4	0.4	0.3			
Error SF_6 Speed ($m\ s^{-1}$)	0.10	0.10	0.10	0.10	0.03			
σ_x (m)	1770	1860	2030	2200	970			
Error σ_x (m)	1420	1280	1470	1160	830			
Peak Detection Time (s)	9360	9630	10100	10300	10800			
Error Peak Detection Time (s)	30	20	20	20	12			
Peak Concentration (pptv)	150	140	140	100	70			
Error Peak Concentration (pptv)	120	100	110	50	40			
Altitude (m)	40	20	40	80	150			
Downwind Distance (m)	5000	4900	4800	4500	3400			
Error Downwind Distance (m)	1800	1100	1200	1300	300			

Appendix F: Analysis of SF_6 Concentration Data for Test 6

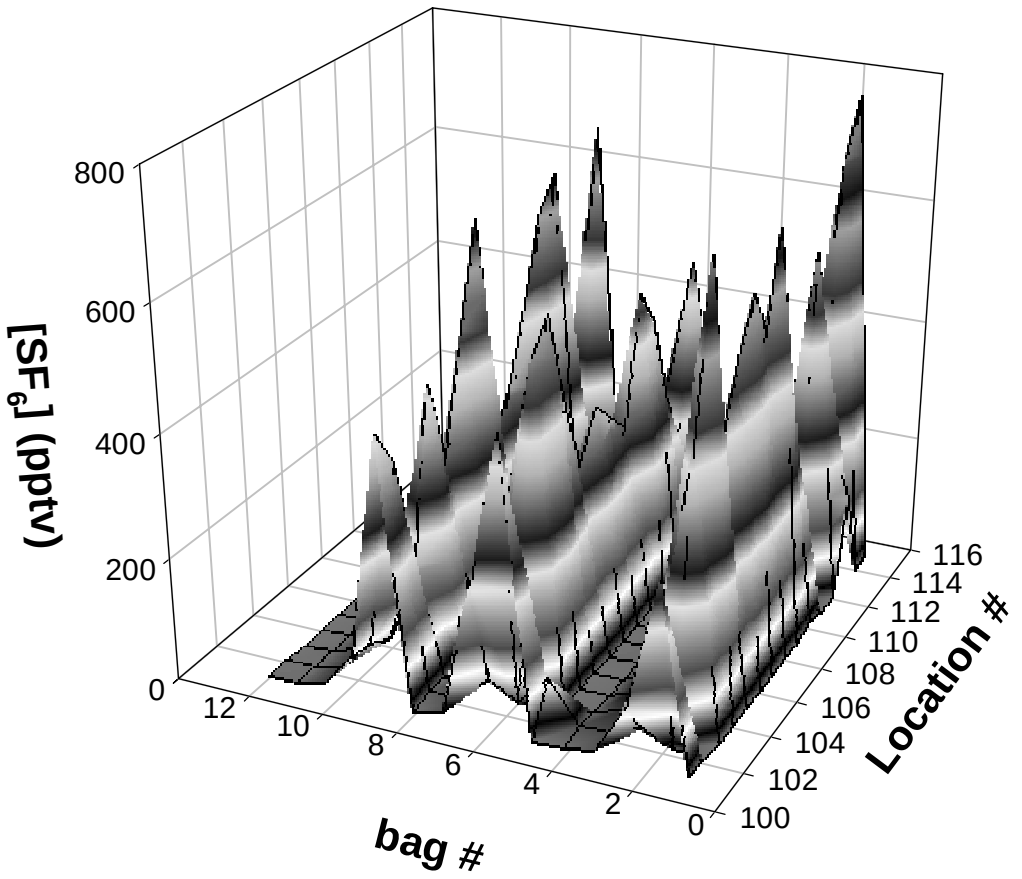

Figure F1. Whole air sampler data for Test 6, Line 1.

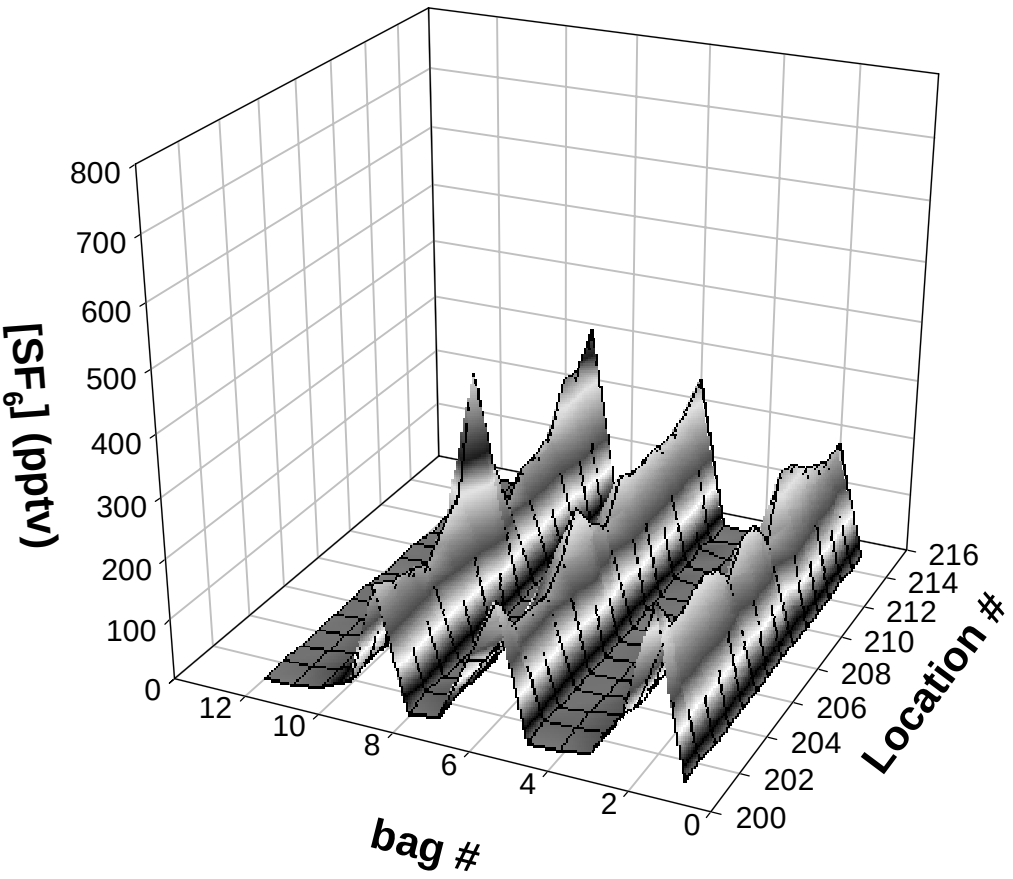

Figure F2. Whole air sampler data for Test 6, Line 2.

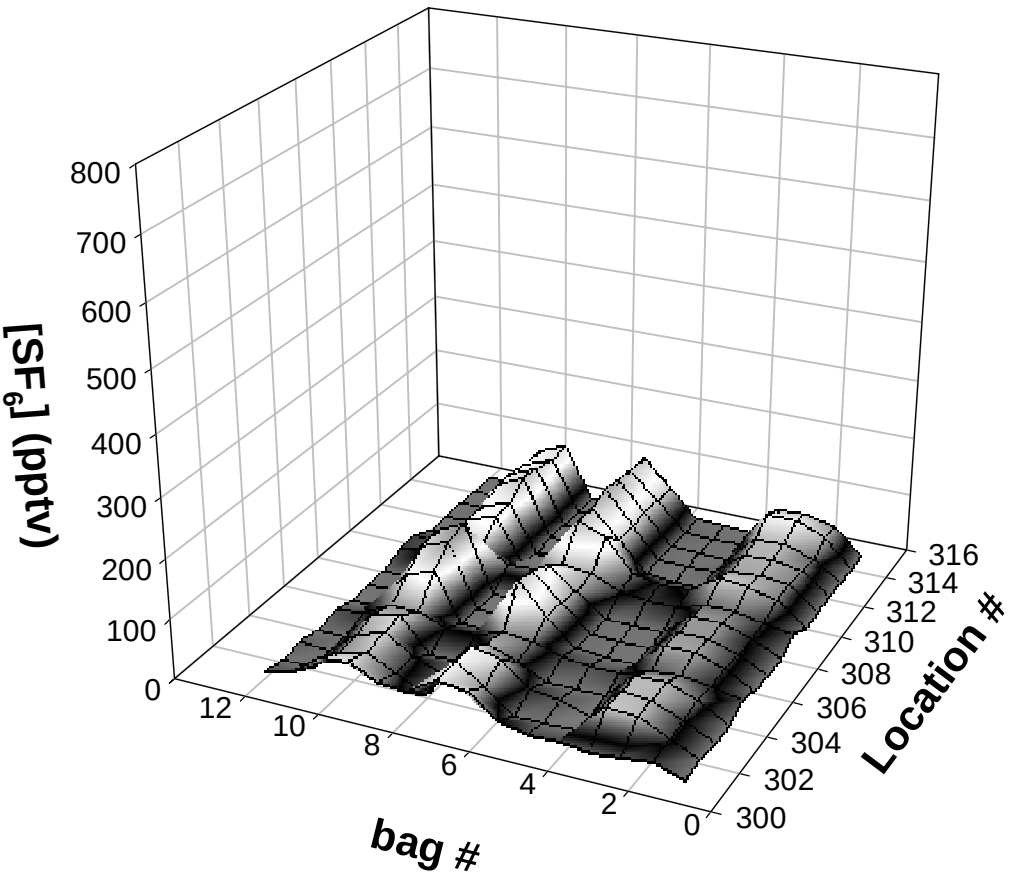

Figure F3. Whole air sampler data for Test 6, Line 3.

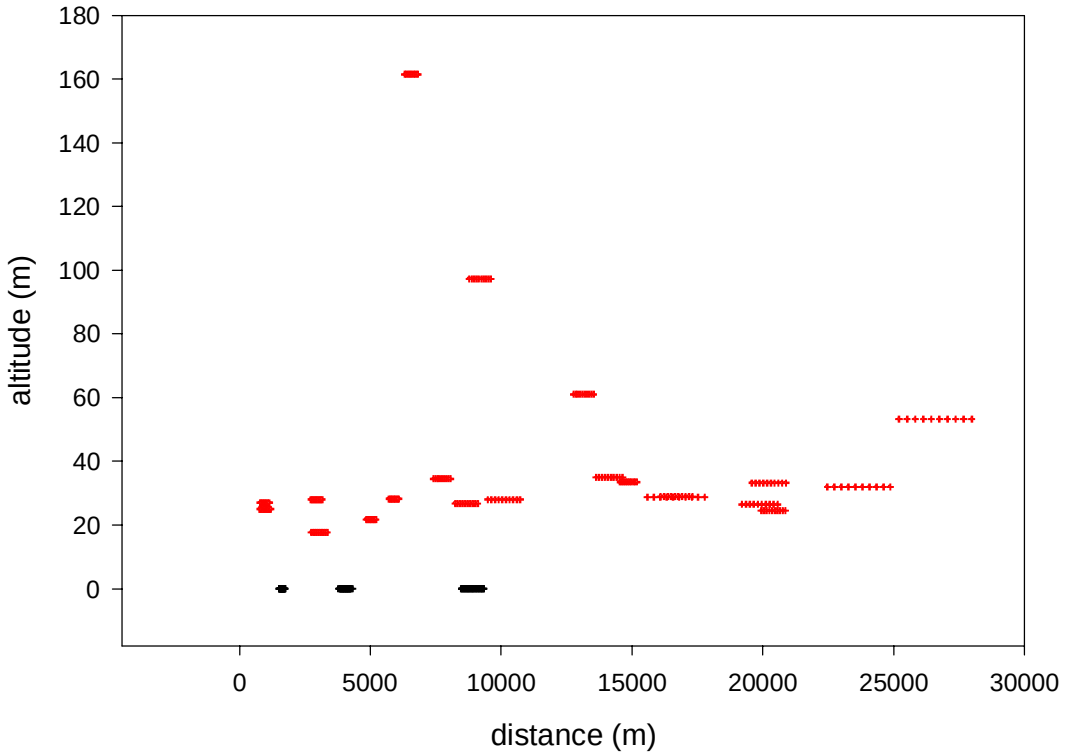

Figure F4. Test 6 continuous analyzer data. Altitude versus downwind distance. The red crosses are aircraft measurements. The black crosses are ground measurements at sampling Lines 1, 2, and 3. The width is ± 1σ from the position of peak concentration.

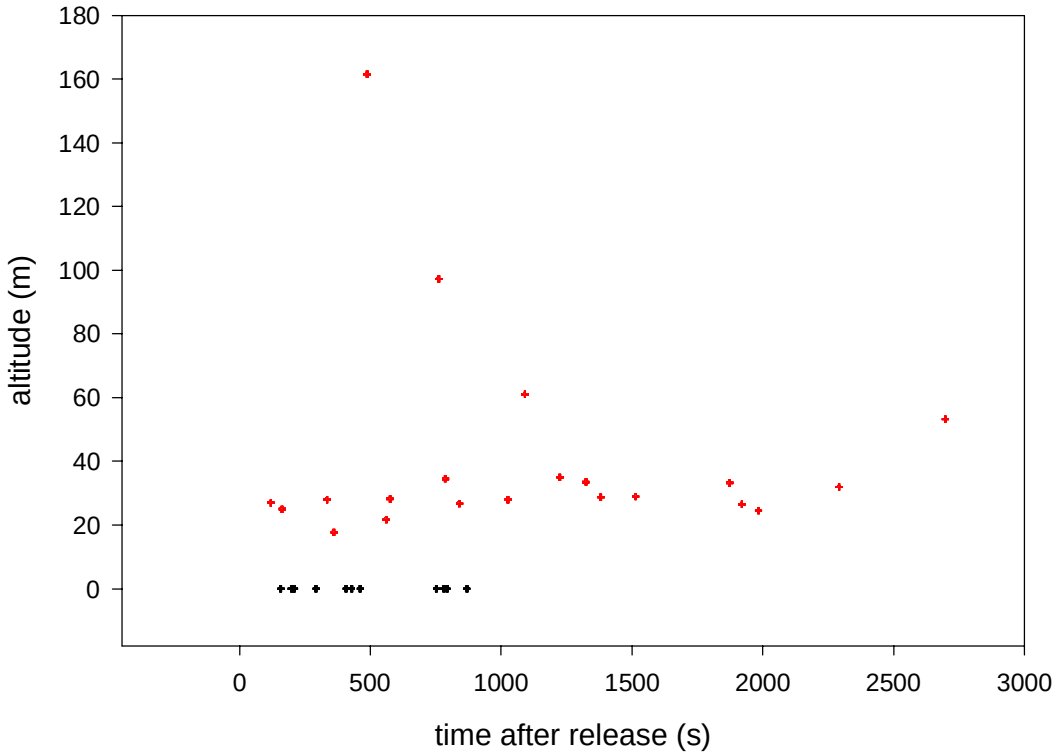

Figure F5. Test 6 continuous analyzer data. Altitude versus time after release. The red crosses are aircraft measurements. The black crosses are ground measurements at sampling Lines 1, 2, and 3.

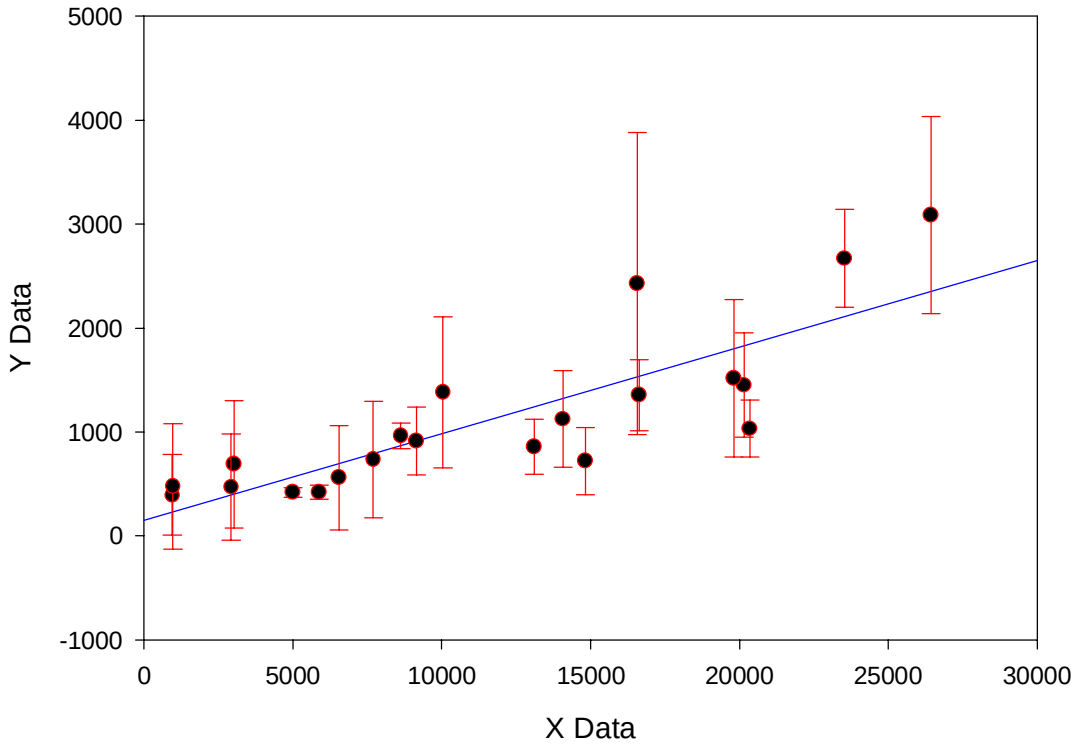

Figure F6. Test 6 σ_x versus downwind distance from aircraft continuous analyzer measurements. The blue line is a linear fit to the data with the equation $\sigma_x = (0.08 \pm 0.01)\, x + (150 \pm 20)$, $r^2 = 0.7$.

Table F1. Test 6 sampling line SF_6 concentration variability.

ID	WS ($m\ s^{-1}$)	σ_{ws} ($m\ s^{-1}$)	θ (deg)	σ_{θ} (deg)	mrsd	σ_{mrsd}	N
Line 100	5.7	0.9	133	6	0.3	0.2	12
Line 200	5.8	1.0	133	6	0.3	0.2	12
Line 300	5.7	1.0	134	6	0.3	0.2	12
All					0.3	0.2	36
0 - 100 pptv					0.3	0.2	29
100 - 500 pptv					0.3	0.1	7
> 500 pptv							

Table F2. Test 6 sampling line SF_6 concentration variability by line for each sampling bag.

Line 100				Line 200				Line 300			
Bag	Mean SF_6 (pptv)	σ_{SF6} (pptv)	rsd	Bag	Mean SF_6 (pptv)	σ_{SF6} (pptv)	rsd	Bag	Mean SF_6 (pptv)	σ_{SF6} (pptv)	rsd
1	4	1	0.2	1	4	1	0.3	1	4	1	0.2
2	520	264	0.5	2	227	31	0.1	2	34	8	0.2
3	4	1	0.1	3	4	1	0.3	3	59	20	0.3
4	5	3	0.5	4	4	2	0.4	4	4	2	0.4
5	4	1	0.2	5	4	3	0.7	5	4	1	0.1
6	430	173	0.4	6	231	40	0.2	6	3	2	0.5
7	5	1	0.1	7	5	1	0.3	7	99	23	0.2
8	5	1	0.3	8	5	2	0.4	8	5	3	0.7
9	428	182	0.4	9	226	69	0.3	9	4	1	0.2
10	5	2	0.3	10	5	2	0.3	10	106	32	0.3
11	4	2	0.5	11	4	1	0.2	11	4	2	0.4
12	5	1	0.2	12	4	2	0.5	12	4	1	0.1

Table F3. Test 6 SF_6 transport parameters from ground-based continuous analyzers for plume #1.

	Location					
	101	115	201	215	301	315
WS ($m\ s^{-1}$)	5.7		5.8		5.7	
σ_{ws} ($m\ s^{-1}$)	0.9		1.0		1.0	
θ (deg)	133		133		134	
σ_θ (deg)	6		6		7	
V_{SF6} ($m\ s^{-1}$)	10	7.8	13.8	8.8	11.8	11.2
Error Limit V_{SF6} ($m\ s^{-1}$)	1	0.2	0.3	0.1	0.7	0.7
σ_x (m)	239	213	609	379	914	933
Error Limit σ_x (m)	33	13	43	10	73	68
SF_6 Transport Time (s)	158	207	293	461	752	793
Error Limit SF_6 Transport Time (s)	16	3	7	7	48	48
SF_6 Peak (pptv)	4565	10230	1445	2506	415	407
Error Limit SF_6 Peak (pptv)	463	620	99	53	21	16

Table F4. Test 6 SF_6 transport parameters from ground-based continuous analyzers for plume #2.

	Location					
	101	115	201	215	301	315
WS ($m\ s^{-1}$)	6.1		5.7		6.4	
σ_{ws} ($m\ s^{-1}$)	1		1		1	
θ (deg)	147		133		147	
σ_θ (deg)	5.1		6		5	
V_{SF6} ($m\ s^{-1}$)	8.2	7.7	10	9.5	11.5	10.3
Error Limit V_{SF6} ($m\ s^{-1}$)	0.2	0.2	0.1	0.1	0.1	0.2
σ_x (m)	247	215	491	422	960	846
Error Limit σ_x (m)	109	23	234	50	540	316
SF_6 Transport Time (s)	198	211	408	429	781	869
Error Limit SF_6 Transport Time (s)	2	3	3	3	7	16
SF_6 Peak (pptv)	6836	10813	2440	2180	421	493
Error Limit SF_6 Peak (pptv)	2100	1141	823	240	161	136

Table F5. Test 6 SF_6 transport parameters from ground-based continuous analyzers for plume #3.

	Location					
	101	115	201	215	301	315
WS ($m\ s^{-1}$)	6.7		6.8		6.8	
σ_{ws} ($m\ s^{-1}$)	1.0		1.0		1.0	
θ (deg)	149		149		149	
σ_θ (deg)	5		5		5	
V_{SF6} ($m\ s^{-1}$)	8.5	8.3	8.9	11.2	10.9	9.9
Error Limit V_{SF6} ($m\ s^{-1}$)	0.3	0.2	0.1	0.1	0.1	0.1
σ_x (m)	182	165	476	454	750	583
Error Limit σ_x (m)	20	7	280	30	489	62
SF_6 Transport Time (s)	193	200	460	365	830	908
Error Limit SF_6 Transport Time (s)	5	2	4	4	9	12
SF_6 Peak (pptv)	7036	13862	1601	2574	354	667
Error Limit SF_6 Peak (pptv)	730	600	1061	160	161	64

Table F6. Test 6 SF_6 transport parameters (release 1) from aircraft continuous analyzer.

	Pass							
	1	2	3	4	5	6	7	8
SF_6 Speed ($m\ s^{-1}$)	13.4	11.9	12.0	11.9	10.7	10.2	9.8	
Error SF_6 Speed ($m\ s^{-1}$)	0.80	0.05	0.00	0.60	0.30	0.06	0.40	
σ_x (m)	560	910	860	2430	1450	2670	3090	
Error σ_x (m)	500	330	260	1450	500	470	950	
Peak Detection Time (s)	490	760	1090	1380	1870	2290	2700	
Error Peak Detection Time (s)	8	2	2	12	12	3	19	
Peak Concentration (pptv)	100	250	190	140	110	110	110	
Error Peak Concentration (pptv)	90	90	50	90	40	10	30	
Altitude (m)	160	100	60	30	30	30	50	
Downwind Distance (m)	6500	9100	13100	16600	20200	23500	26400	
Error Downwind Distance (m)	400	40	40	900	600	100	1100	

Table F7. Test 6 SF_6 transport parameters (release 2) from aircraft continuous analyzer.

	Pass							
	1	2	3	4	5	6	7	8
SF_6 Speed ($m\ s^{-1}$)	7.8	8.3	10.2	10.2	11.4	10.9	10.3	
Error SF_6 Speed ($m\ s^{-1}$)	0.00	0.10	0.04	0.04	0.00	0.07	0.20	
σ_x (m)	400	700	420	960	1130	1360	1520	
Error σ_x (m)	390	610	70	120	460	340	760	
Peak Detection Time (s)	120	360	580	840	1220	1510	1920	
Error Peak Detection Time (s)	2	2	2	2	2	3	9	
Peak Concentration (pptv)	5400	3180	1240	470	230	170	170	
Error Peak Concentration (pptv)	3700	1530	150	40	70	40	60	
Altitude (m)	30	20	30	30	40	30	30	
Downwind Distance (m)	900	300	2900	8600	14100	16600	19800	
Error Downwind Distance (m)	0.0	0.03	0.02	0.03	0.0	0.1	0.5	

Table F8. Test 6 SF_6 transport parameters (release 3) from aircraft continuous analyzer.

	Pass							
	1	2	3	4	5	6	7	8
SF_6 Speed ($m\ s^{-1}$)	5.9	8.7	8.9	9.7	9.7	11.1	10.2	
Error SF_6 Speed ($m\ s^{-1}$)	0.20	0.30	0.06	0.08	0.03	0.10	0.10	
σ_x (m)	480	470	420	740	1380	720	1030	
Error σ_x (m)	600	510	50	560	730	320	270	
Peak Detection Time (s)	160	340	560	790	1030	1320	1980	
Error Peak Detection Time (s)	2	3	2	3	2	4	4	
Peak Concentration (pptv)	5740	1860	2380	1000	580	220	270	
Error Peak Concentration (pptv)	3460	1000	110	450	200	80	60	
Altitude (m)	30	30	20	30	30	30	20	
Downwind Distance (m)	1000	2900	5000	7700	10000	14800	20400	
Error Downwind Distance (m)	40	130	40	70	40	170	200	

Appendix G: Analysis of SF_6 Concentration Data for Test 9

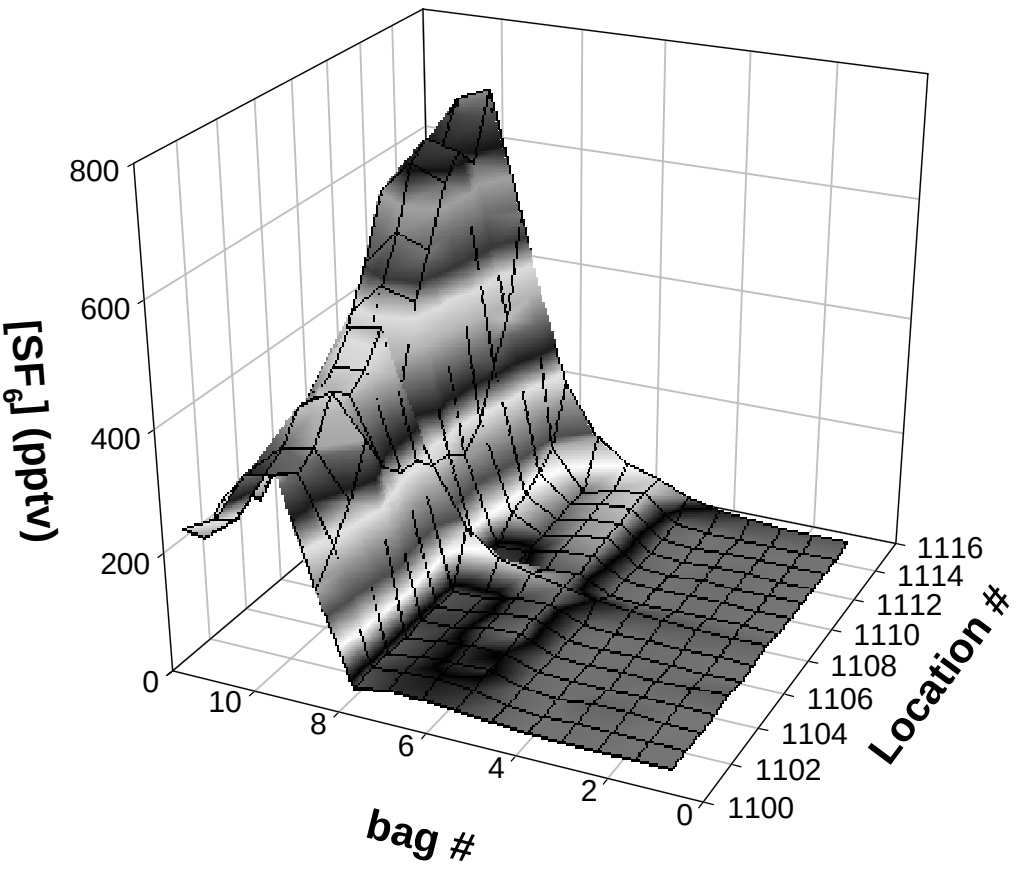

Figure G1. Whole air sampler data for Test 9, Line 1.

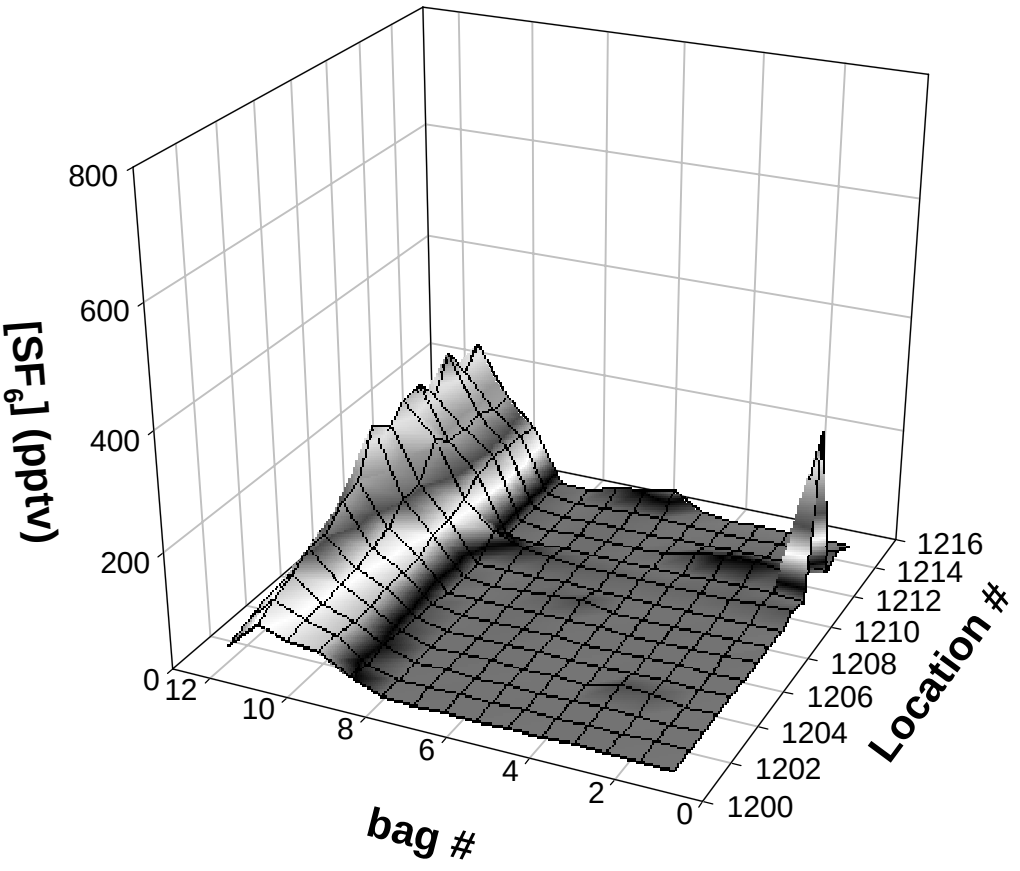

Figure G2. Whole air sampler data for Test 9, Line 2.

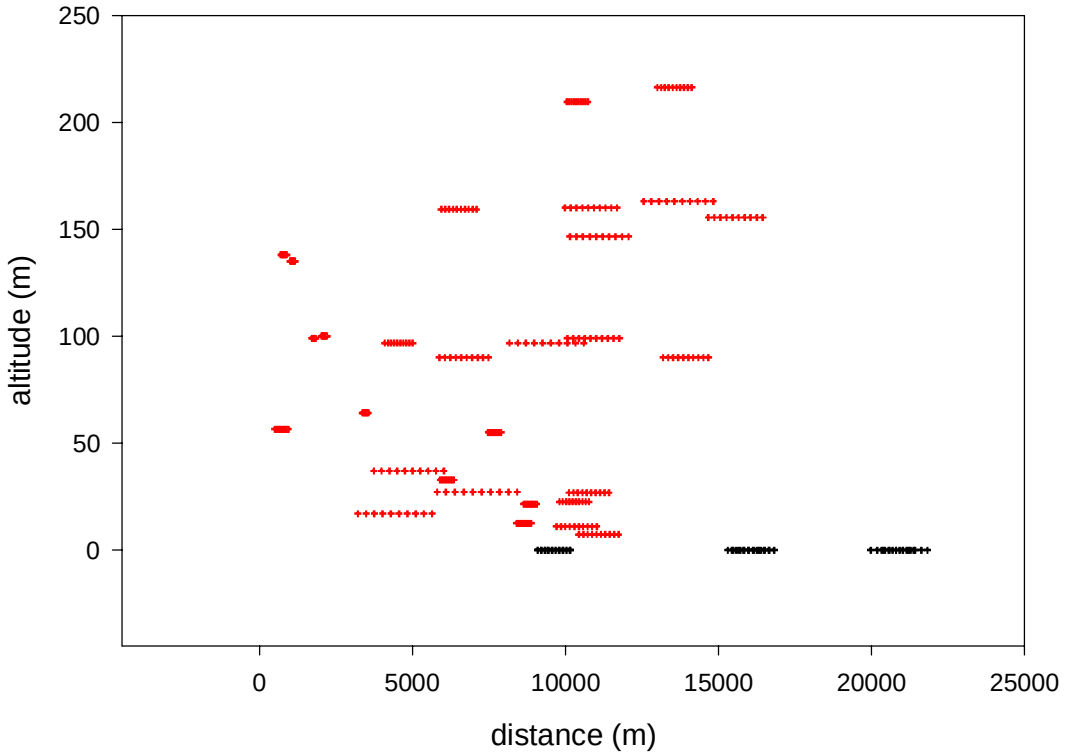

Figure G3. Test 9 continuous analyzer data. Altitude versus downwind distance. The red crosses are aircraft measurements. The black crosses are ground measurements at sampling Lines 1, 2, and 3. The width is ± 1σ from the position of peak concentration.

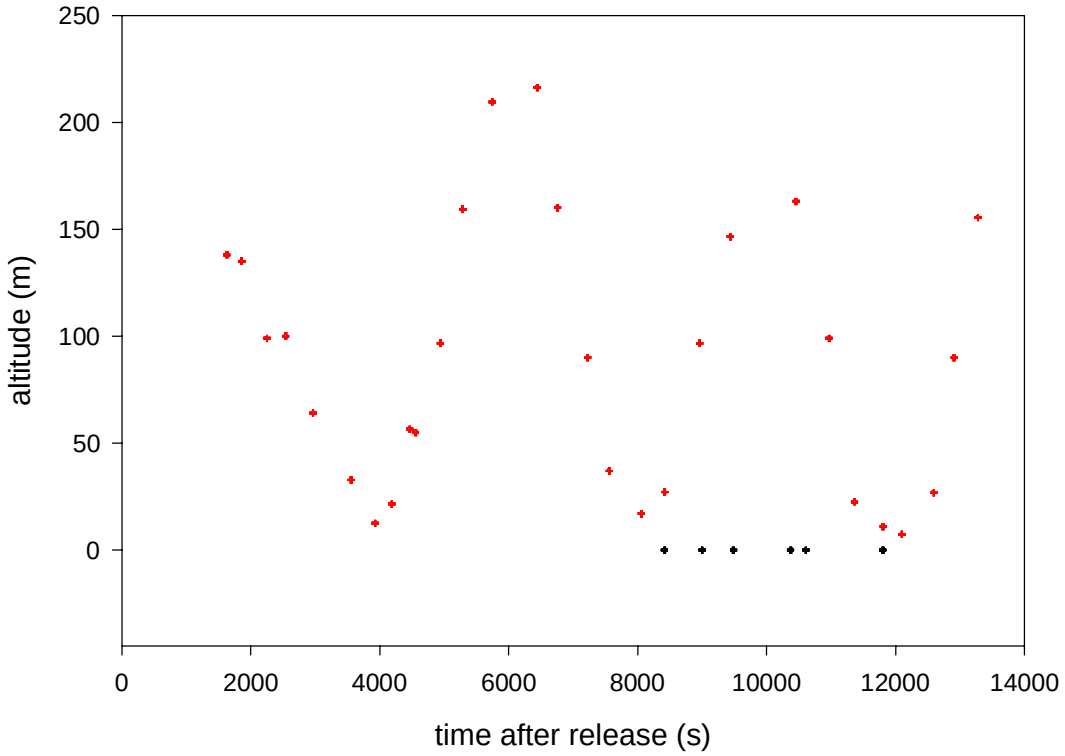

Figure G4. Test 9 continuous analyzer data. Altitude versus time after release. The red crosses are aircraft measurements. The black crosses are ground measurements at sampling Lines 1, 2 and 3.

Table G1. Test 9 sampling line SF_6 concentration variability.

ID	WS ($m\ s^{-1}$)	σ_{ws} ($m\ s^{-1}$)	θ (deg)	σ_{θ} (deg)	mrsd	σ_{mrsd}	N
Line 100	1.5	1.0	150	41	0.4	0.2	12
Line 200	1.5	1.0	150	42	0.8	0.8	12
Line 300	1.5	1.0	150	42	0.3	0.3	12
All					0.5	0.5	36
0 - 100 pptv					0.5	0.6	30
100 - 500 pptv					0.4	0.7	6
> 500 pptv							

Table G2. Test 9 sampling line SF_6 concentration variability by line for each sampling bag.

Line 1100				Line 1200				Line 1300			
Bag	Mean SF_6 (pptv)	σ_{SF6} (pptv)	rsd	Bag	Mean SF_6 (pptv)	σ_{SF6} (pptv)	rsd	Bag	Mean SF_6 (pptv)	σ_{SF6} (pptv)	rsd
1	5	2	0.4	1	24	73	3.0	1	4	0	0.1
2	5	4	0.8	2	5	3	0.6	2	4	0	0.1
3	5	2	0.4	3	7	9	1.2	3	4	0	0.1
4	4	1	0.1	4	5	4	0.8	4	5	3	0.6
5	8	1	0.1	5	4	1	0.2	5	4	1	0.2
6	36	17	0.5	6	5	4	0.7	6	4	0	0.1
7	17	4	0.2	7	4	0	0.1	7	4	1	0.3
8	35	33	0.9	8	4	0	0.1	8	6	4	0.8
9	266	95	0.4	9	12	8	0.6	9	10	6	0.6
10	546	157	0.3	10	90	33	0.4	10	36	20	0.6
11	407	153	0.4	11	190	66	0.3	11	47	16	0.4
12	210	54	0.3	12	101	47	0.5	12	19	4	0.2

Table G3. Test 9 SF_6 transport parameters from ground-based continuous analyzers.

	Location					
	1101	1115	1201	1215	1301	1315
WS ($m\ s^{-1}$)	1.5		1.5		1.5	
σ_{ws} ($m\ s^{-1}$)	1.0		1.0		1.0	
θ (deg)	150		150		150	
σ_{θ} (deg)	41		42		42	
V_{SF6} ($m\ s^{-1}$)	0.93	1.1	1.8	1.7	1.98	1.8
Error Limit V_{SF6} ($m\ s^{-1}$)	0.04	0.02	0.04	0.02	0.03	0.02
σ_x (m)	1177	1178	1348	1688	1166	2063
Error Limit σ_x (m)	208	133	386	1000	152	147
SF_6 Transport Time (s)	10375	8419	9000	9484	10607	11804
Error Limit SF_6 Transport Time (s)	503	117	196	117	164	105
SF_6 Peak (pptv)	493	985	118	168	102	117
Error Limit SF_6 Peak (pptv)	77	100	28	84	13	9

Table G4. Test 9 SF_6 transport parameters from aircraft continuous analyzer.

	Pass							
	1	2	3	4	5	6	7	8
SF_6 Speed ($m\ s^{-1}$)	0.4	0.5	0.7	0.8	1.1	1.7	2.1	2.1
Error SF_6 Speed ($m\ s^{-1}$)	0.00	0.00	0.01	0.00	0.00	0.00	0.08	0.02
σ_x (m)	210	190	130	200	220	490	530	470
Error σ_x (m)	80	80	40	20	40	200	510	140
Peak Detection Time (s)	1630	1860	2250	2540	2970	3560	3960	4190
Error Peak Detection Time (s)	1	2	2	1	1	2	4	2
Peak Concentration (pptv)	800	1150	1950	930	350	200	90	130
Error Peak Concentration (pptv)	300	350	570	20	50	70	60	30
Altitude (m)	140	140	100	100	60	30	10	20
Downwind Distance (m)	800	1100	1800	2100	3400	6100	8600	8800
Error Downwind Distance (m)	0.0	0.0	40	0.0	0.0	70	300	100

Table G4. Test 9 SF_6 transport parameters from aircraft continuous analyzer (continued).

	Pass							
	9	10	11	12	13	14	15	16
SF_6 Speed ($m\ s^{-1}$)	0.1	1.6	0.9	1.2	1.8	2.0	1.5	0.9
Error SF_6 Speed ($m\ s^{-1}$)	0.04	0.03	0.03	0.04	0.04	0.01	0.00	0.03
σ_x (m)	480	470	1010	1280	760	1250	1890	1780
Error σ_x (m)	470	250	570	830	480	160	260	970
Peak Detection Time (s)	4460	4560	4940	5290	5750	6440	6760	7230
Error Peak Detection Time (s)	3	3	3	4	4	2	1	4
Peak Concentration (pptv)	70	230	1620	800	350	320	310	1100
Error Peak Concentration (pptv)	40	80	1230	390	150	30	30	560
Altitude (m)	60	60	100	160	210	220	160	90
Downwind Distance (m)	700	7700	4500	6500	10400	13500	10700	6600
Error Downwind Distance (m)	200	200	200	300	300	90	40	230

Table G4. Test 9 SF_6 transport parameters from aircraft continuous analyzer (continued).

	Pass							
	17	18	19	20	21	22	23	24
SF_6 Speed ($m\ s^{-1}$)	0.6	0.5	0.8	1.0	1.1	1.2	0.9	0.9
Error SF_6 Speed ($m\ s^{-1}$)	0.04	0.10	0.06	0.08	0.00	0.10	0.02	0.00
σ_x (m)	2540	2690	2900	2700	2130	2520	1890	1070
Error σ_x (m)	520	890	400	560	490	560	270	120
Peak Detection Time (s)	7560	8060	8420	8960	9440	10460	10970	11370
Error Peak Detection Time (s)	4	24	7	12	1	17	4	2
Peak Concentration (pptv)	1000	930	740	310	130	190	230	140
Error Peak Concentration (pptv)	160	240	80	60	20	40	30	10
Altitude (m)	40	20	30	100	150	160	100	20
Downwind Distance (m)	4800	4300	7000	9300	11000	13600	10800	10200
Error Downwind Distance (m)	310	1610	500	800	40	1270	230	70

Table G4. Test 9 SF_6 transport parameters from aircraft continuous analyzer (continued).

	Pass							
	25	26	27	28	29	30	31	32
SF_6 Speed ($m\ s^{-1}$)	0.8	0.9	0.8	1.0	1.1			
Error SF_6 Speed ($m\ s^{-1}$)	0.03	0.01	0.09	0.00	0.00			
σ_x (m)	1460	1440	1450	1640	1970			
Error σ_x (m)	620	170	310	200	290			
Peak Detection Time (s)	11810	12100	12600	12910	13280			
Error Peak Detection Time (s)	6	2	17	2	1			
Peak Concentration (pptv)	120	130	120	100	10700			
Error Peak Concentration (pptv)	30	10	20	10	90			
Altitude (m)	10	10	30	90	160			
Downwind Distance (m)	10300	11000	10700	13900	15500			
Error Downwind Distance (m)	400	150	170	70	30			

Appendix H: Analysis of SF_6 Concentration Data for Test 10

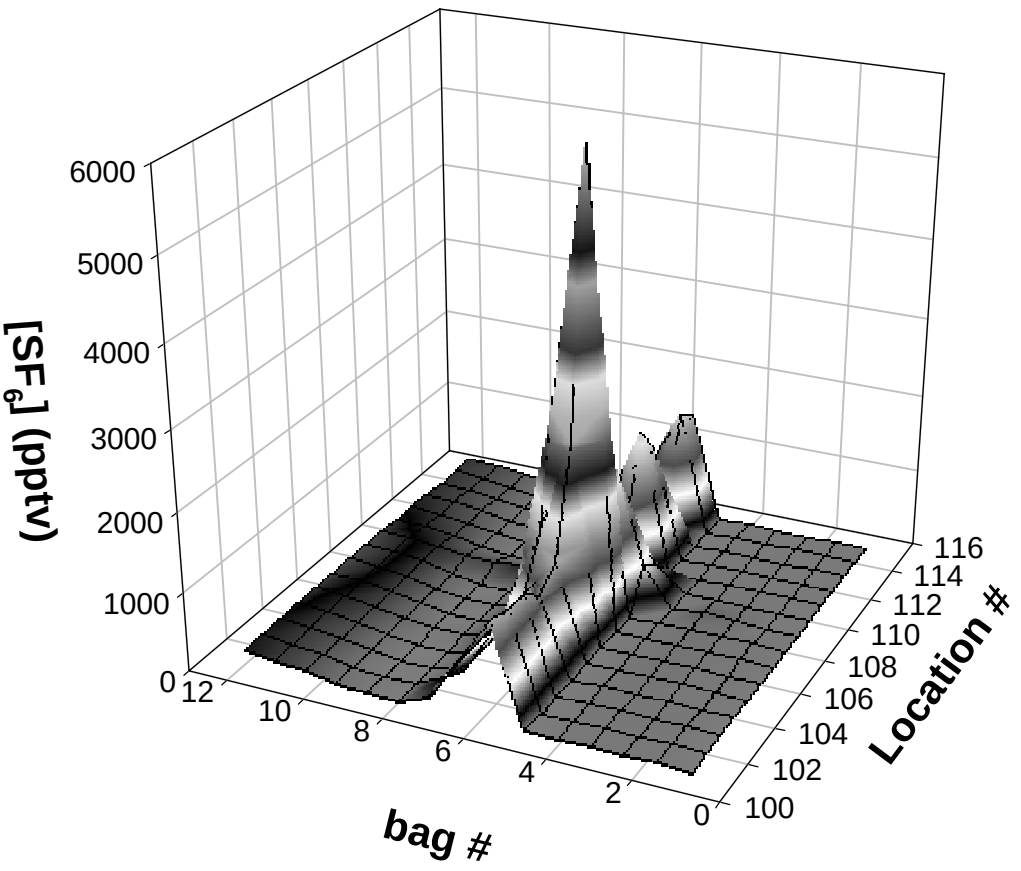

Figure H1. Whole air sampler data for Test 10, Line 1.

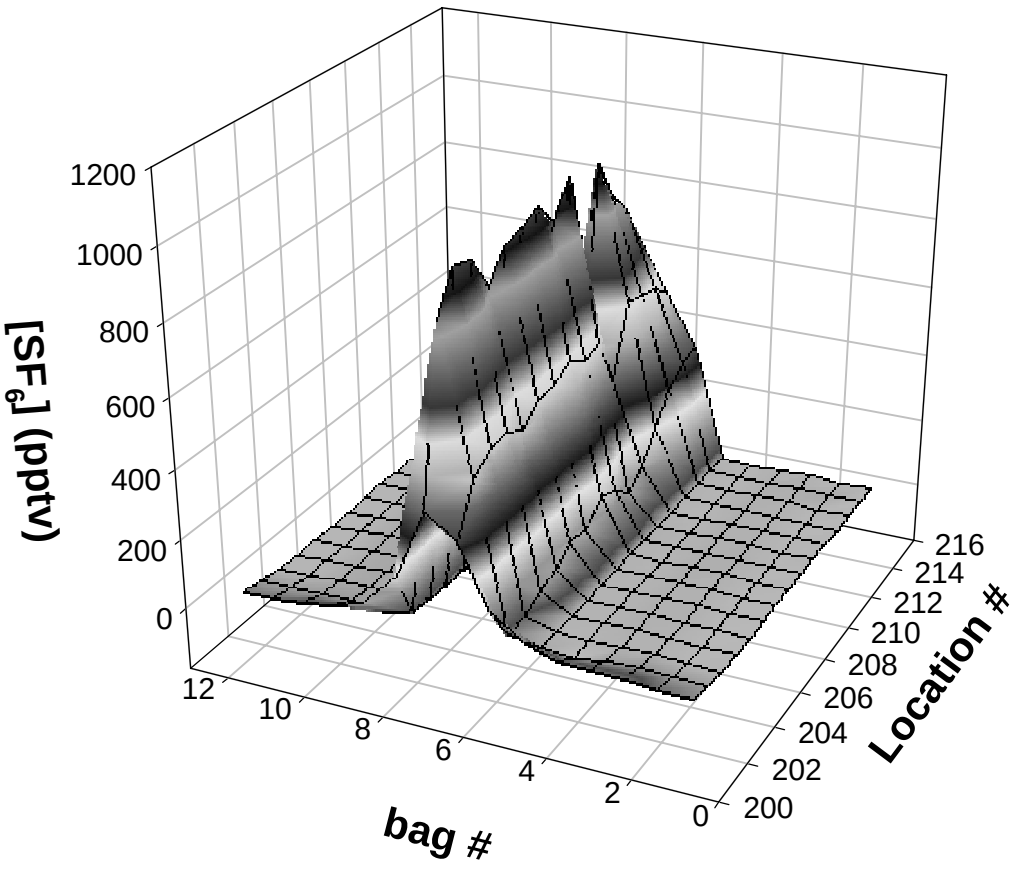

Figure H2. Whole air sampler data for Test 10, Line 2.

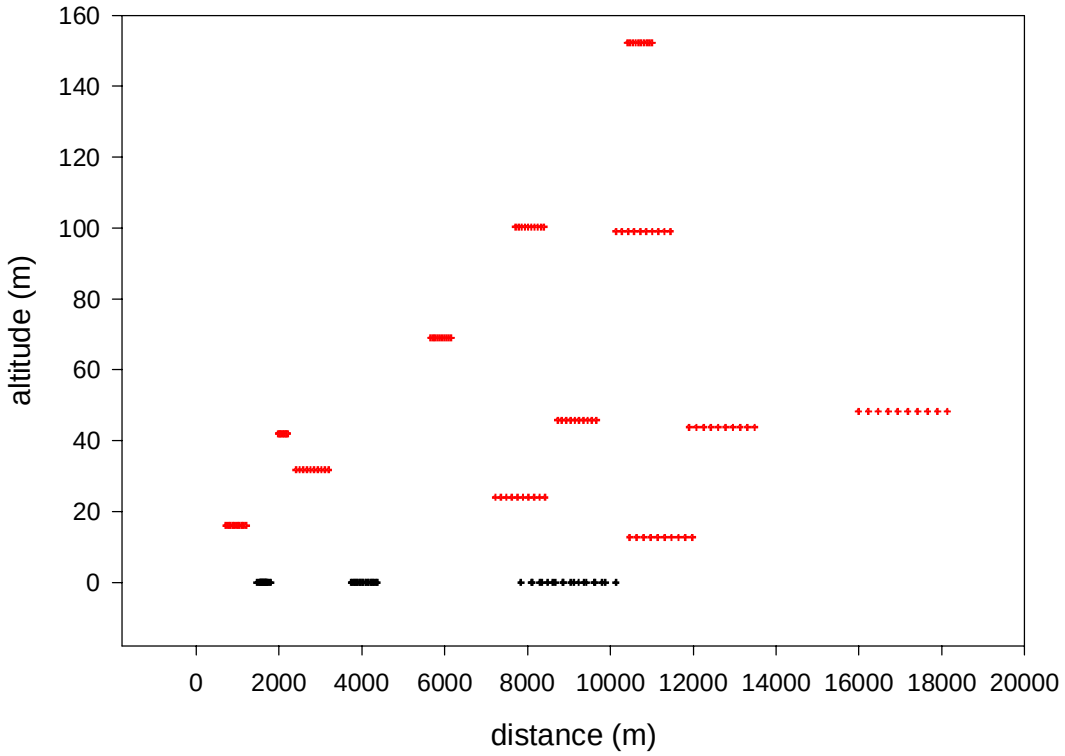

Figure H3. Test 10 continuous analyzer data. Altitude versus downwind distance. The red crosses are aircraft measurements. The black crosses are ground measurements at sampling Lines 1, 2, and 3. The width is ± 1σ from the position of peak concentration.

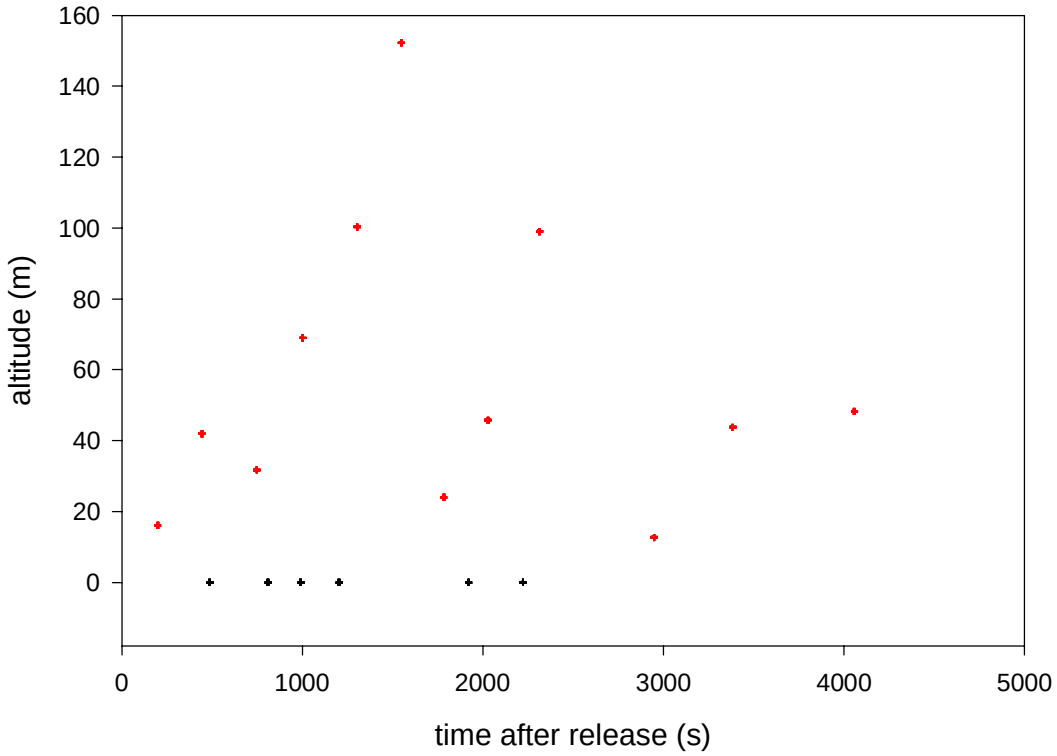

Figure H4. Test 10 continuous analyzer data. Altitude versus time after release. The red crosses are aircraft measurements. The black crosses are ground measurements at sampling Lines 1, 2, and 3.

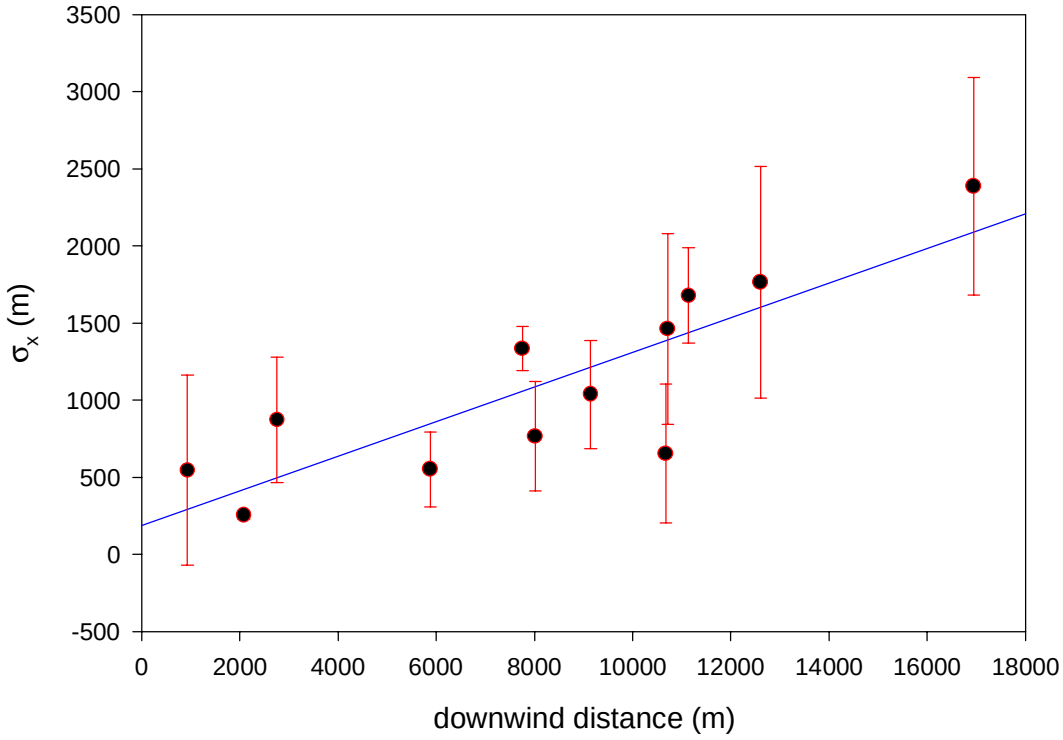

Figure H5. Test 10 σ_x versus downwind distance from aircraft continuous analyzer measurements. Data is from all altitudes. The blue line is a linear fit to the data with the equation $\sigma_x = (0.11 \pm 0.02)$ $x + (200 \pm 200)$, $r^2 = 0.7$.

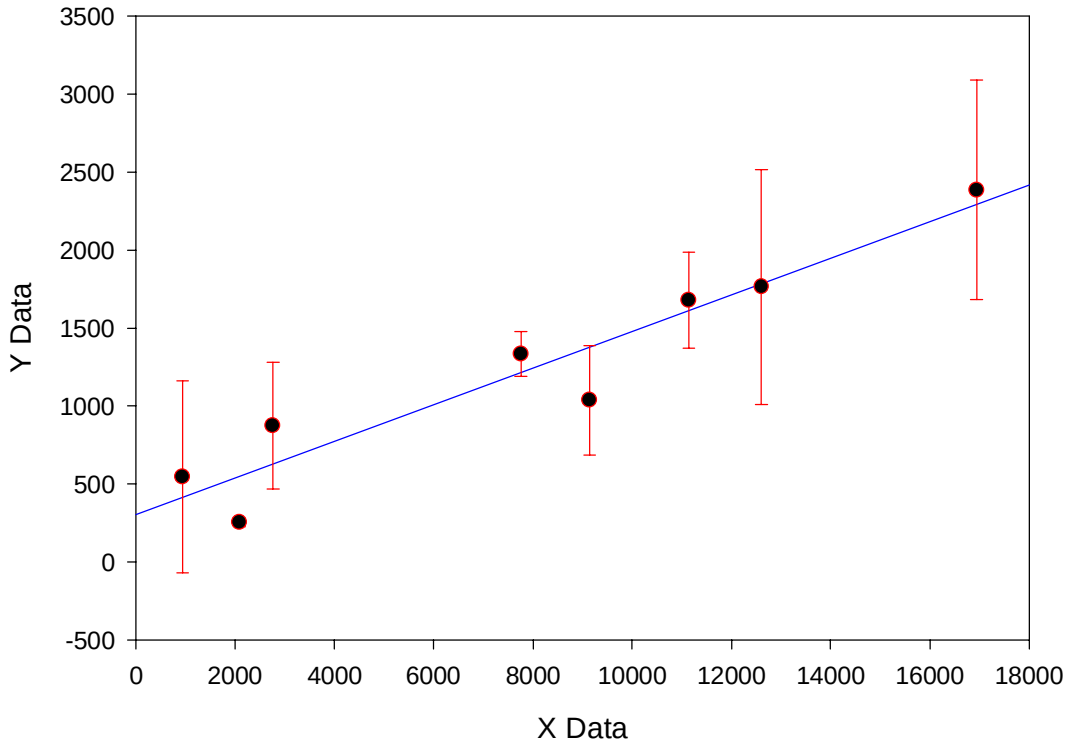

Figure H6. Test 10 σ_x versus downwind distance from aircraft continuous analyzer measurements. Data is from altitudes less than 50 m. The blue line is a linear fit to the data with the equation $\sigma_x = (0.12 \pm 0.02)\ x + (300 \pm 140)$, $r^2 = 0.9$.

Table H1. Test 10 sampling line SF_6 concentration variability.

ID	WS ($m\ s^{-1}$)	σ_{ws} ($m\ s^{-1}$)	θ (deg)	σ_{θ} (deg)	mrsd	σ_{mrsd}	N
Line 100	2.3	0.6	161	22	1.3	1.2	12
Line 200	2.2	0.8	157	30	0.4	0.3	12
Line 300	2.3	0.8	150	30	0.3	0.3	12
All					0.7	0.8	36
0 - 100 pptv					0.7	0.9	29
100 - 500 pptv					0.6	0.4	5
> 500 pptv					0.4	0.5	2

Table H2. Test 10 sampling line SF_6 concentration variability by line for each sampling bag.

Line 100				Line 200				Line 300			
Bag	Mean SF_6 (pptv)	σ_{SF6} (pptv)	rsd	Bag	Mean SF_6 (pptv)	σ_{SF6} (pptv)	rsd	Bag	Mean SF_6 (pptv)	σ_{SF6} (pptv)	rsd
1	9	3	0.4	1	5	4	0.6	1	5	1	0.3
2	16	4	0.2	2	4	0	0.1	2	4	1	0.1
3	7	2	0.2	3	4	0	0.1	3	4	0	0.1
4	13	3	0.2	4	5	1	0.3	4	4	1	0.1
5	5	1	0.2	5	8	1	0.2	5	5	1	0.2
6	2043	1573	0.8	6	139	125	1.0	6	6	1	0.2
7	47	54	1.2	7	1002	118	0.1	7	253	74	0.3
8	13	18	1.4	8	18	8	0.4	8	490	102	0.2
9	27	77	2.8	9	6	1	0.1	9	152	75	0.5
10	31	99	3.2	10	5	3	0.5	10	31	34	1.1
11	25	69	2.7	11	5	3	0.6	11	5	1	0.2
12	15	36	2.4	12	5	4	0.7	12	5	2	0.3

Table H3. Test 10 SF_6 transport parameters from ground-based continuous analyzers.

	Location					
	101	115	201	215	301	315
WS ($m\ s^{-1}$)	2.3		2.2		2.3	
σ_{ws} ($m\ s^{-1}$)	0.6		0.8		0.8	
θ (deg)	161		157		150	
σ_{θ} (deg)	22		30		30	
V_{SF6} ($m\ s^{-1}$)	2.2	3.6	3.5	4.3	4.7	4.08
Error Limit V_{SF6} ($m\ s^{-1}$)	0.3	0.7	0.2	0.3	1.2	0.7
σ_x (m)	184	370	633	697	2553	1871
Error Limit σ_x (m)	24	160	112	54	1175	1085
SF_6 Transport Time (s)	810	488	1203	991	1921	2222
Error Limit SF_6 Transport Time (s)	94	95	72	64	490	385
SF_6 Peak (pptv)	6970	6806	2344	2245	696	652
Error Limit SF_6 Peak (pptv)	395	2100	433	98	264	236

Table H4. Test 10 SF_6 transport parameters from aircraft continuous analyzer.

	Pass							
	1	2	3	4	5	6	7	8
SF_6 Speed ($m\ s^{-1}$)	4.6	4.6	3.6	5.8	6.1	6.8	4.3	4.5
Error SF_6 Speed ($m\ s^{-1}$)	0.50	0.06	0.10	0.10	0.02	0.10	0.08	0.08
σ_x (m)	550	250	870	550	770	660	1330	1040
Error σ_x (m)	620	30	410	240	360	450	140	350
Peak Detection Time (s)	200	440	750	1000	1300	1550	1780	2030
Error Peak Detection Time (s)	11	11	11	11	11	11	11	11
Peak Concentration (pptv)	6270	6210	2470	1020	230	80	790	530
Error Peak Concentration (pptv)	3520	110	840	420	120	40	30	180
Altitude (m)	20	40	30	69	100	150	20	50
Downwind Distance (m)	900	2100	2800	5900	8000	10700	7800	9100
Error Downwind Distance (m)	100	30	100	200	40	200	100	200

Table H4. Test 10 SF_6 transport parameters from aircraft continuous analyzer (continued).

	Pass							
	9	10	11	12	13	14	15	16
SF_6 Speed ($m\ s^{-1}$)	4.6	3.7	3.7	4.1				
Error SF_6 Speed ($m\ s^{-1}$)	0.13	0.09	0.00	0.03				
σ_x (m)	1460	1680	1760	2390				
Error σ_x (m)	620	310	750	700				
Peak Detection Time (s)	2310	2950	3380	4060				
Error Peak Detection Time (s)	12	11	11	11				
Peak Concentration (pptv)	320	270	200	100				
Error Peak Concentration (pptv)	110	40	80	20				
Altitude (m)	100	10	40	48				
Downwind Distance (m)	10700	11100	12600	16900				
Error Downwind Distance (m)	300	300	30	100				

Appendix I: Analysis of SF_6 Concentration Data for Test 11

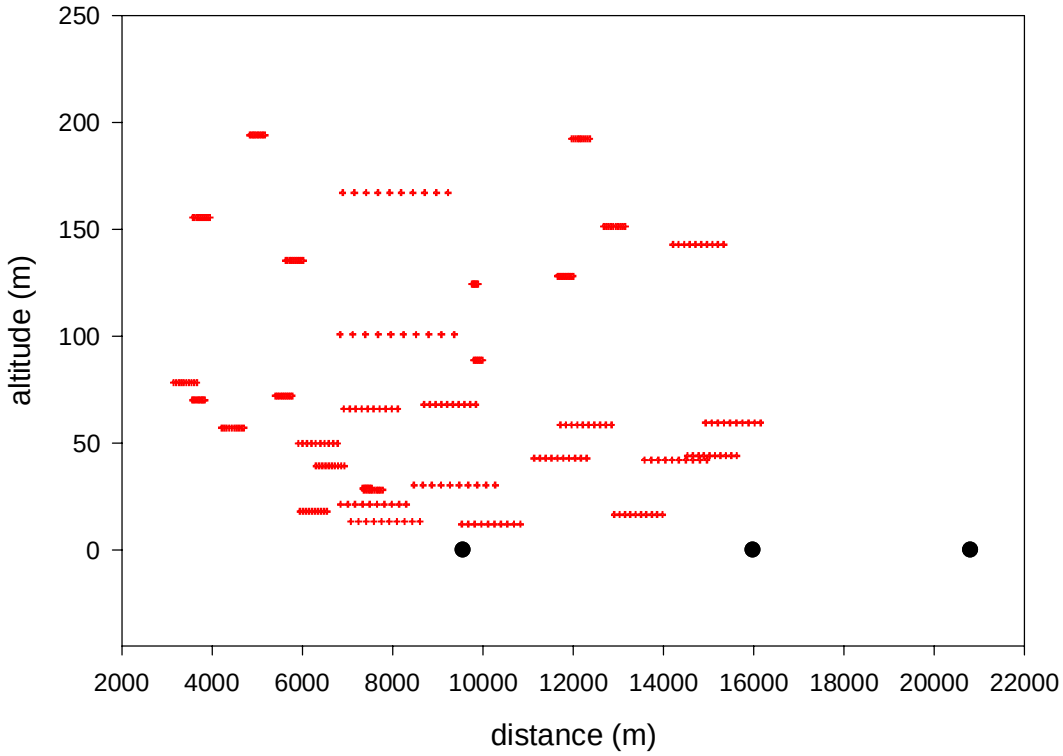

Figure I1. Test 11 continuous analyzer data. Altitude versus downwind distance. The red crosses are aircraft measurements. The black circles are the positions of sampling Lines 1, 2, and 3. The width is ± 1σ from the position of peak concentration.

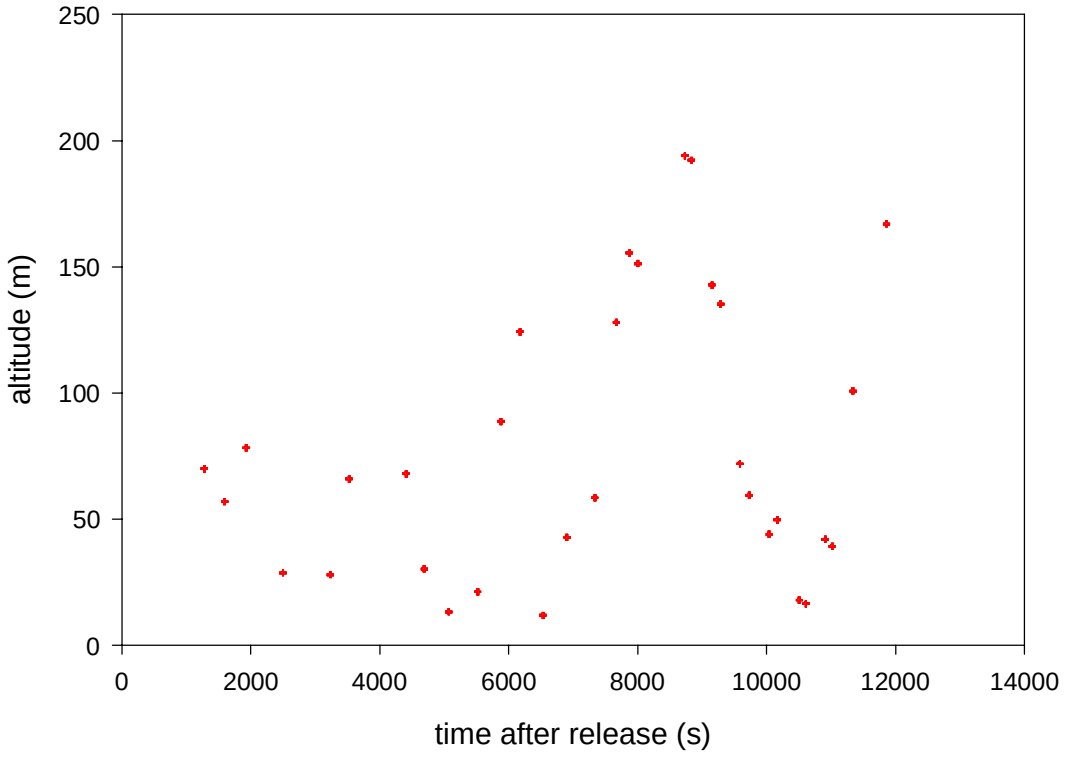

Figure I2. Test 11 continuous analyzer data. Altitude versus time after release. The red crosses are aircraft measurements.

Table I1. Test 11 SF_6 transport parameters from aircraft continuous analyzer.

	Pass							
	1	2	3	4	5	6	7	8
SF_6 Speed ($m\ s^{-1}$)	2.8	2.7	1.7	2.9	2.3	2.1	2.0	1.9
Error SF_6 Speed ($m\ s^{-1}$)	0.00	0.04	0.07	0.01	0.00	0.20	0.10	0.20
σ_x (m)	300	550	570	210	460	1330	1280	2000
Error σ_x (m)	110	80	530	130	160	1230	800	2030
Peak Detection Time (s)	1280	1600	1930	2500	3240	3530	4400	4700
Error Peak Detection Time (s)	22	22	22	22	22	26	24	27
Peak Concentration (pptv)	6620	12500	9120	5730	14000	10340	6620	13480
Error Peak Concentration (pptv)	2260	1390	5680	2830	4030	11000	3440	15040
Altitude (m)	70	60	80	30	30	70	70	30
Downwind Distance (m)	3700	4400	3400	7400	7600	7500	9200	9300
Error Downwind Distance (m)	0.0	0.07	0.13	0.03	0.0	0.9	0.7	1100

Table I1. Test 11 SF_6 transport parameters from aircraft continuous analyzer (continued).

	Pass							
	9	10	11	12	13	14	15	16
SF_6 Speed ($m\ s^{-1}$)	1.5	1.3	1.6	1.5	1.5	1.6	1.6	1.5
Error SF_6 Speed ($m\ s^{-1}$)	0.40	0.20	0.00	0.01	0.10	0.00	0.03	0.00
σ_x (m)	1700	1620	220	150	1450	1300	1260	390
Error σ_x (m)	1540	1550	40	60	1160	340	260	160
Peak Detection Time (s)	5080	5520	5880	6180	6530	6900	7340	7670
Error Peak Detection Time (s)	36	27	22	22	30	22	22	22
Peak Concentration (pptv)	1120	3030	3380	130	7130	4000	3400	350
Error Peak Concentration (pptv)	1280	2950	530	40	8610	1000	600	110
Altitude (m)	10	20	90	120	10	40	60	130
Downwind Distance (m)	7800	7500	9900	9800	10100	11700	12200	11800
Error Downwind Distance (m)	2000	1100	40	100	1300	30	300	0

Table I1. Test 11 SF_6 transport parameters from aircraft continuous analyzer (continued).

	Pass							
	17	18	19	20	21	22	23	24
SF_6 Speed ($m\ s^{-1}$)	0.4	1.6	0.5	1.3	1.6	0.6	0.5	1.5
Error SF_6 Speed ($m\ s^{-1}$)	0.01	0.02	0.00	0.00	0.03	0.00	0.00	0.09
σ_x (m)	410	520	380	450	1250	440	400	1360
Error σ_x (m)	220	350	140	580	720	130	70	530
Peak Detection Time (s)	7870	8000	8730	8840	9160	9290	9590	9730
Error Peak Detection Time (s)	22	22	22	22	22	22	22	25
Peak Concentration (pptv)	390	110	860	1000	2200	670	450	1920
Error Peak Concentration (pptv)	200	70	330	570	940	200	60	570
Altitude (m)	160	150	190	190	140	140	70	60
Downwind Distance (m)	3700	12900	5000	12100	14700	5800	5600	15500
Error Downwind Distance (m)	100	200	80	30	300	0.06	0	0.8

Table I1. Test 11 SF_6 transport parameters from aircraft continuous analyzer (continued).

	Pass							
	25	26	27	28	29	30	31	32
SF_6 Speed ($m\ s^{-1}$)	1.4	0.6	0.5	1.2	1.3	0.5	0.7	0.6
Error SF_6 Speed ($m\ s^{-1}$)	0.08	0.00	0.01	0.01	0.00	0.00	0.10	0.10
σ_x (m)	1210	970	660	1190	1530	690	2810	2590
Error σ_x (m)	940	600	110	460	720	130	1970	1550
Peak Detection Time (s)	10040	10170	10510	10610	10910	11020	11340	11860
Error Peak Detection Time (s)	25	22	22	22	22	22	32	32
Peak Concentration (pptv)	2580	400	460	810	530	690	450	430
Error Peak Concentration (pptv)	2230	170	60	240	180	110	330	300
Altitude (m)	40	50	20	20	40	40	100	170
Downwind Distance (m)	15000	6300	6200	13400	14200	6600	8000	7900
Error Downwind Distance (m)	0.8	0.03	0.1	0.1	0.0	0.03	1.6	1.6

Appendix J: Analysis of SF_6 Concentration Data for Test 12

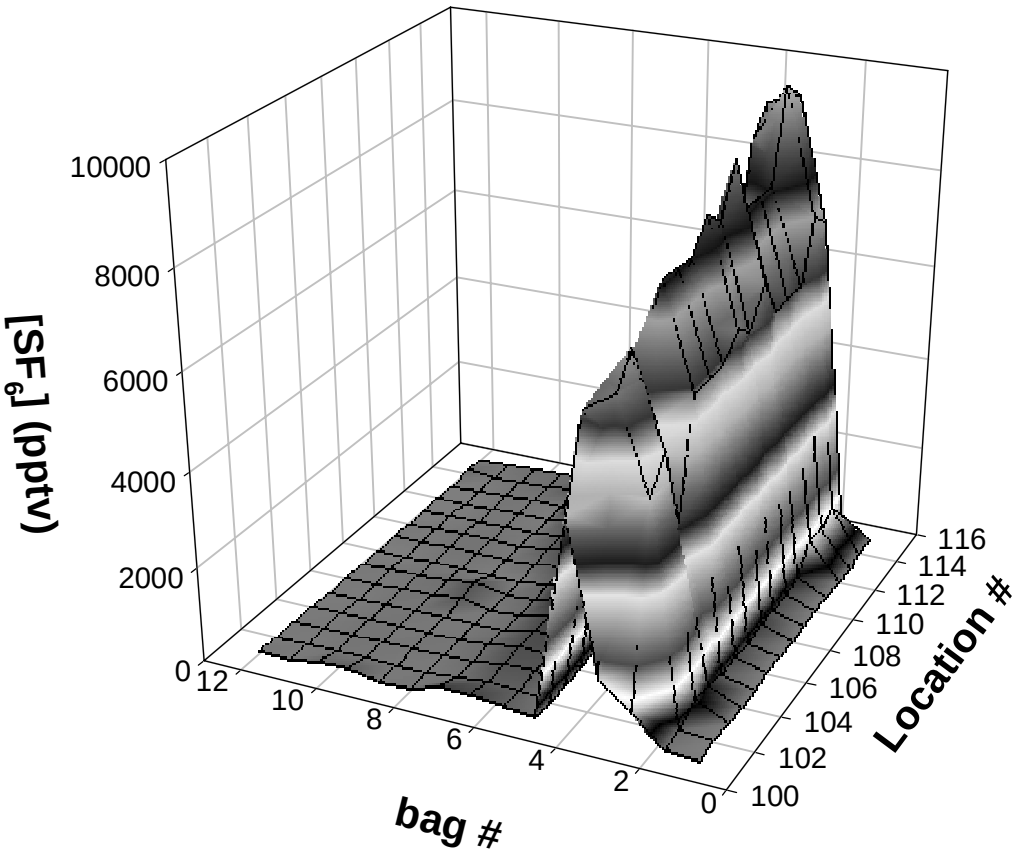

Figure J1. Whole air sampler data for Test 12, Line 1.

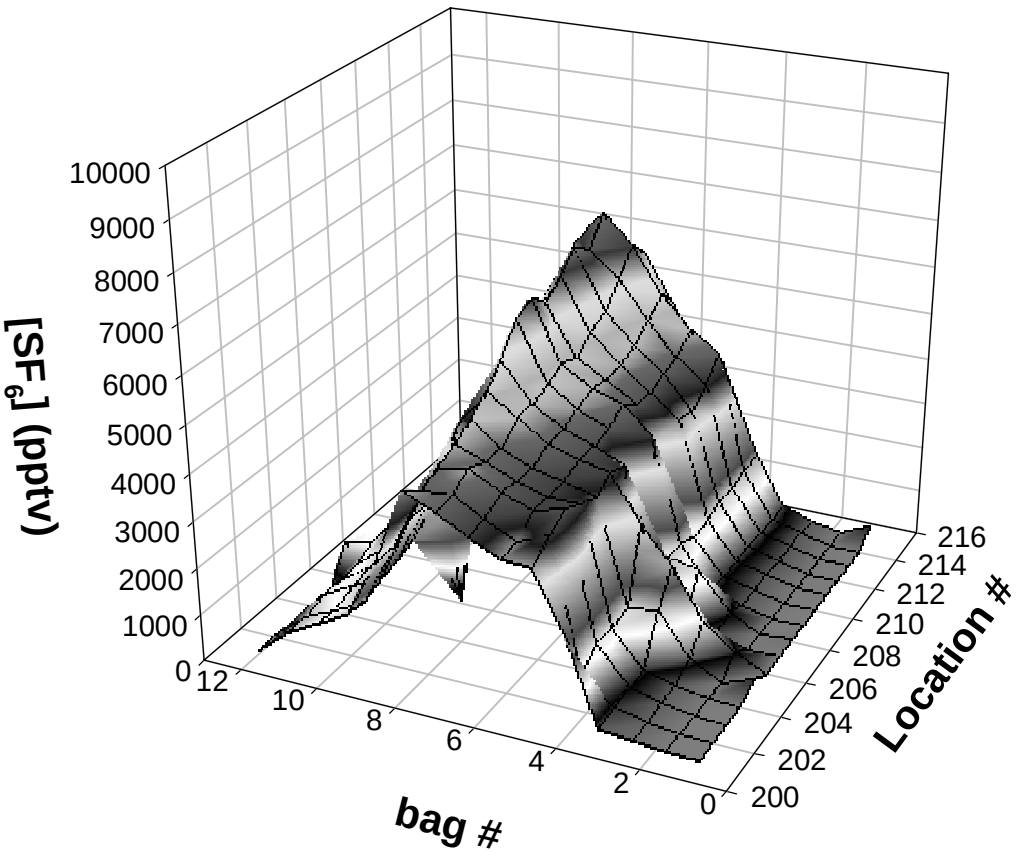

Figure J2. Whole air sampler data for Test 12, Line 2.

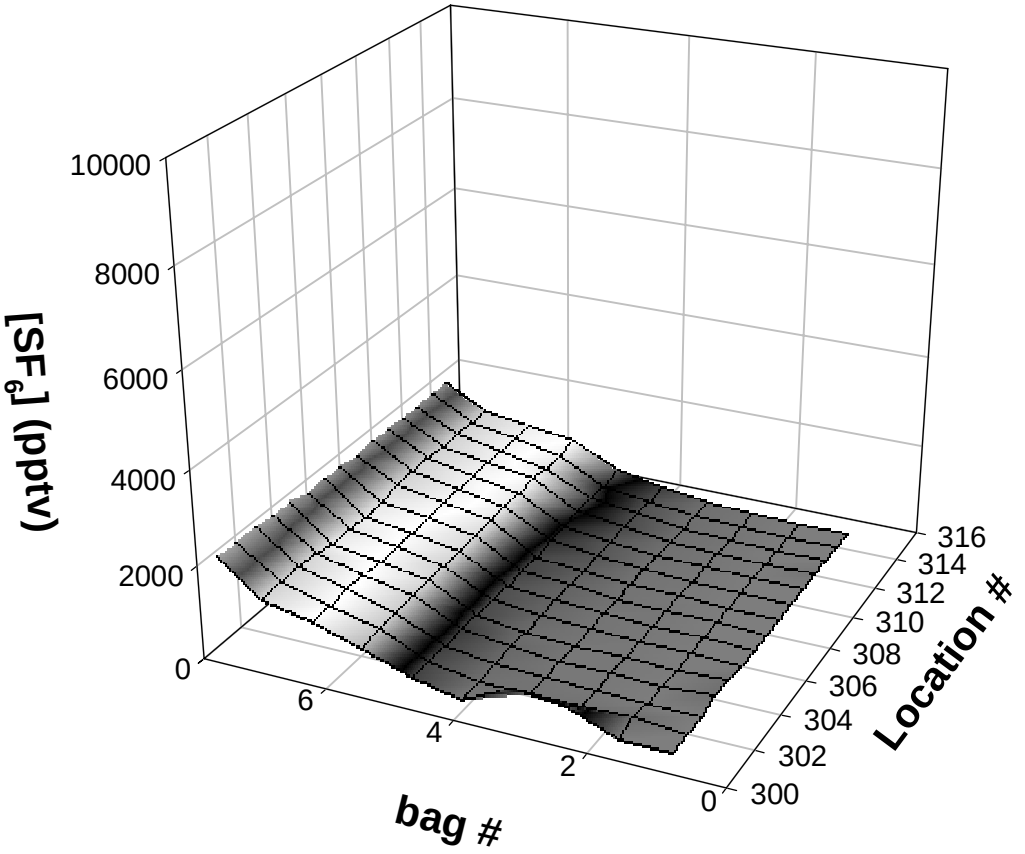

Figure J3. Whole air sampler data for Test 12, Line 3.

Table J1. Test 12 sampling line SF_6 concentration variability.

ID	WS ($m\ s^{-1}$)	σ_{ws} ($m\ s^{-1}$)	θ (deg)	σ_{θ} (deg)	mrsd	σ_{mrsd}	N
Line 100	0.9	0.4	142	41	0.9	0.4	12
Line 200	0.9	0.4	138	47	0.4	0.2	12
Line 300	0.9	0.4	139	45	0.5	0.9	12
All					0.6	0.6	36
0 - 100 pptv					0.8	0.4	10
100 - 500 pptv					1.1	0.9	7
> 500 pptv					0.3	0.3	19

Table J2. Test 12 sampling line SF_6 concentration variability by line for each sampling bag.

Line 100				Line 200				Line 300			
Bag	Mean SF_6 (pptv)	σ_{SF6} (pptv)	rsd	Bag	Mean SF_6 (pptv)	σ_{SF6} (pptv)	rsd	Bag	Mean SF_6 (pptv)	σ_{SF6} (pptv)	rsd
1	6	4	0.6	1	6	3	0.5	1	12	18	1.5
2	232	269	1.1	2	5	1	0.1	2	5	1	0.2
3	8447	2688	0.3	3	22	15	0.7	3	55	172	3.1
4	6219	1247	0.2	4	1223	494	0.4	4	131	55	0.4
5	1304	1632	1.3	5	3250	794	0.2	5	261	67	0.3
6	651	816	1.3	6	3819	334	0.1	6	823	88	0.1
7	232	252	1.1	7	4655	638	0.1	7	1116	70	0.1
8	124	132	1.1	8	5263	899	0.2	8	1808	83	0.1
9	47	53	1.1	9	4064	1194	0.3	9	2435	661	0.3
10	30	40	1.3	10	2346	1115	0.5	10	1698	490	0.3
11	17	12	0.7	11	1032	317	0.3	11	1448	167	0.1
12	16	13	0.8	12	148	122	0.8	12	1108	196	0.2

Table J3. Test 12 SF_6 transport parameters from ground-based continuous analyzers.

	Location					
	101	115	201	215	301	315
WS ($m\ s^{-1}$)	0.9		0.9		0.9	
σ_{ws} ($m\ s^{-1}$)	0.4		0.4		0.4	
θ (deg)	142		138		139	
σ_{θ} (deg)	41		47		45	
V_{SF6} ($m\ s^{-1}$)	0.7	0.8	0.7	0.7	1.04	0.96
Error Limit V_{SF6} ($m\ s^{-1}$)	0.3	0.1	0.2	0.1	0.02	0.005
σ_x (m)	215	422	1014	1101	724	1782
Error Limit σ_x (m)	35	146	166	195	141	240
SF_6 Transport Time (s)	2303	2134	5547	5586	8521	9244
Error Limit SF_6 Transport Time (s)	110	200	148	85	146	48
SF_6 Peak (pptv)	15530	30466	4640	5900	2891	2897
Error Limit SF_6 Peak (pptv)	2270	8269	861	1098	659	433

Appendix K: Whole Air Sampling System

K.1 Operational Description

Keeping track of the large number of samples involved in a typical tracer field program is a difficult process requiring careful record keeping. The samples must be tracked through the analysis process and the results associated with the correct time and place. The logistics of this process are complex and errors can easily occur. We have developed an integrated Whole Air Sampling System that uses barcodes, computer data storage, and a relational database to keep track of samples, sample cartridges, analytical results, and cartridge history. The steps required to operate the equipment collect data on sample time and location and automatically associate this with the analysis results. All of the data is transferred electronically.

The following eight steps explain the operation of the system. They have been kept simple with the intent of providing an overview. The various components are explained in more detail below.

1. The process begins with the location of the sampling sites. A location number is assigned to the site. A bar code tag with the number on is left at the site, typically attached to a post. The latitude and longitude is measured by differential GPS and recorded on a laptop computer. The operator enters the location number for each site into the computer as the samplers are placed. The location information is uploaded to the system computers. It becomes part of the "history files". These files are an electronic log of all operations performed on the samplers or sampler bags.

2. Before sampling begins, an operator programs sampling information into a TimeWand II. This is a handheld computer with a built-in bar code reader manufactured by Videx, Inc. The TimeWand II's are used to operate the samplers. The sampling information includes start time, sampling time for each bag, and a test and project ID.

3. A TimeWand II is taken to each sampler site. The operator installs a cartridge in the sampler. The TimeWand II is connected to the sampler with a RS232 cable and the operator scans the bar code labels on the sampler, cartridge, and location tag. The TimeWand II then downloads the sampling information into the sampler.

4. After the sampling is complete, the cartridges are removed from the samplers. The TimeWand II's are used to record the cartridge serial number and the pickup time.

5. When the cartridges are brought back into the analysis laboratory, the data from the TimeWand II's are uploaded into the history files.

6. The sample cartridges are then analyzed on a gas chromatograph (GC). A cartridge is connected to the GC and the serial number scanned into the computer operating the GC. The

computer then queries the history files and retrieves the location information (including the latitude and longitude), the sampling time and duration, and the test and project identifications. It then analyzes the samples and stores the results along with the position and sampling information in a raw data file.

7. Once the cartridges are analyzed, the data are extracted from the raw data file on each GC and stored in a relational database. Information about samples that were not analyzed is extracted from the history files directly.

8. The relational database is then used to generate data reports and statistics. It can also generate performance reports on the GCs, individual samplers, or operators.

Once the data is stored in the relational database, it can be manipulated, sorted, and analyzed in many different ways. All the information is in one place and can be readily accessed. Since it has all arrived electronically, the chances for human error are very low.

The operators keep hand written logs during every step of the process. In the event of an equipment failure or operator error, these are used to hand enter the data into the system. The relational database can usually be used to identify these problems by searching for missing or inconsistent data points.

K.2 Component Descriptions

K.2.1 Sampler and Cartridges

The samplers are a waxed cardboard box containing a single circuit board with a Motorola 68HC811A2 microcontroller, a power supply, and 12 miniature air pumps. A single D size battery powers the sampler. The circuit board is mounted in a waxed corrugated cardboard box, which provides an inexpensive weatherproof housing. Rubber tubing serves as inlet hoses for the pumps and allows easy connection of the sample bags.

The cartridge is a slightly smaller cardboard box designed to slip inside the sampler box. An aluminum frame across the top holds the 12 Tedlar bags attached to rubber tubes. Plastic clips on the tubes seal the bags when they are not connected to the sampler. The cartridge allows easy transport and handling of the sample bags and protects them from damage. The entire system is lightweight, relatively inexpensive, and has been used successfully in a wide range of weather conditions.

K.2.2 TimeWand II

The TimeWand II accomplishes two functions simultaneously. First, it downloads the operating parameters into the microcontroller on the sampler. It also collects data on the operation of the samplers in the field. It is a hand held computer with a built-in bar code wand and an RS232

port. To download the sampler, the RS232 port is connected to the sampler with a cable. The operator then uses the bar code wand to scan the sampler serial number, the cartridge serial number, and the location number. Once the TimeWand II has these three numbers, it sends the operating parameters to the sampler. It also stores the numbers, the time, and the sampling parameters in memory to be uploaded to the history files later. When the cartridge is analyzed on a GC, its serial number is matched with a location, sampler, and sampling time using this information collected by the TimeWand II.

Videx, Inc manufactures the TimeWand II. It has 128K bytes of memory and is powered by rechargeable batteries. It is designed for field use and has proven to be rugged and reliable. Hard drops onto concrete and steel have caused the only failures.

Connecting them to the RS232 port of a computer and running the setup software programs the TimeWand II. The sampling parameters are entered from the keyboard and then transmitted to the TimeWand II. Usually, several TimeWand II's are programmed and each one is used for part of the samplers in the test. This reduces the time needed for sampler servicing by allowing several operators to work simultaneously.

The TimeWand II has the ability to hold up to four sets of sampling parameters. The location number determines the set that is downloaded to the sampler. Numbers between 0 and 999 receive the first set; 1000 to 1999 receive the second set; 2000 to 2999 the third set; and 3000 or over receive the fourth set. By numbering the locations correctly, the project may be designed so that an operator with a single TimeWand II can service samplers with several sampling times.

K.2.3 Gas Chromatograhs

The gas chromatographs were designed and built by FRD for use with this system. Typically they are configured for measuring SF6, but may be configured to measure other gases. For SF6, they use packed columns and an ECD detector. What sets these GC's apart is the sample handling system that allows them to automatically analyze all 12 bags in a cartridge.

The GC and sample handling system are completely computer controlled. The cartridge is connected to the GC and its serial number is scanned into the computer with a bar code reader. The computer then retrieves the sampling and location information from the history files. Once it has this, it uses a multiport rotary valve to sequentially pull air from each sample bag and inject it into the GC. The output from the detector is digitized with a 20-bit analog-to-digital converter and automatically integrated and converted to concentration.

Once the GC has analyzed the cartridge, it records that the bag has been analyzed in the history files and stores the data in a binary raw data file. All the information collected by the TimeWand II's about the cartridge is stored with the data, eliminating the need to match data values with locations and times.

K.2.4 Relational Database

The purpose of developing a database was to improve the collection and facilitate the use of the data acquired from the whole air samplers. The Access relational database from Microsoft was chosen as the storage format. This database supports Structured Query Language (SQL), has a built-in report generator, macro language, forms support, and various administrative tools. The database, or any queried portion, can be saved in a variety of other database or text formats such as comma delimited or fixed length. This database format is also easily manipulated though the Visual Basic programming language, also from Microsoft, which speeds the development of Windows based applications.

Using a Visual Basic developed application; data is captured from binary files that are generated through the automated analysis routines that run the gas chromatographs. The capture program has built-in viewing of control charts and statistics for each GC, generating virtually real-time feedback on the status of the instruments

Using SQL any number of ad-hoc reports can be generated quickly to satisfy the needs of the principals of the test. The fields that are stored in the Access database are as follows:

RecordIndex	Internal use field for assuring uniqueness of records
FileName	The binary file from which the data originates
Record Number	The record number within the binary file implied by sequence
Date	The date the sample was run on the GC
Time	The time of day that the sample was run on the GC
GC	The GC number on which the sample was run
CartridgeSerial	The cartridge number of the sample
SamplerSerial	The sampler number that was used to fill the sample cartridge
LocationSerial	The location number (fixed location) where the sample was taken
Latitude	The latitude associated with the location number
Longitude	The longitude associated with the location number
SampleType	Type of sample (0=Sample, 1=Spike, 2=Blank, 3=Replicate,4=Cal)
ProjectID	Identifier for this test (i.e., OLAD)
TestNumber	The number of the test
StartDate	The day when the pump started taking this sample
StartTime	The time when the pump started taking this sample
Seconds	The number of seconds the pump ran while taking this sample
Bag	The number of the bag that constitutes this sample
GCPressure	The pressure registered by the GC while analyzing this sample
GCTemperature	The oven temperature registered while running this sample
GCRetentionTime	The retention time the sample was on the GC column
PeakArea	The area under the curve of the chromatogram
PeakHeight	The maximum height of the curve of the chromatogram
PeakCorrectedArea	The area corrected to Standard Temperature and Pressure (STP)

Concentration	The concentration of the sample in pptv
BadAnalysis	Flag set to determine the status of this sample (1=flat, 2=clipped, 4=suspect, 5=clipped but used anyway, 6= sample failure, 7=clips closed, 8=battery pulled, 9=exclude analysis)
CheckStatus	Flag for use with the check-in function
AnalysisCount	Keeps track of how many times a sample was analyzed
Attenuation	The attenuation of the ECD at the time the sample was analyzed